N-alkyl Quaternary Chitosan Derivatives for Permeation Enhancement in Bronchial Epithelia

Berglind Eva Benediktsdóttir

Thesis for the degree of Philosophiae Doctor

Faculty of Pharmaceutical Sciences

School of Health Sciences

November 2012

UNIVERSITY OF ICELAND

N-alkyl Quaternary Chitosan Derivatives for Permeation Enhancement in Bronchial Epithelia

Berglind Eva Benediktsdóttir

Thesis for the degree of Philosophiae Doctor

Faculty of Pharmaceutical Sciences

School of Health Sciences

University of Iceland

November 2012

Efnasmíði á *N*-alkýl-fjórgildum kítósan afleiðum og ákvörðun á gegndræpisaukandi áhrifum þeirra í berkjuþekju

Berglind Eva Benediktsdóttir

Ritgerð til doktorsgráðu
Lyfjafræðideild
Heilbrigðisvísindasvið
Háskóli Íslands
Nóvember 2012

Author's address   Faculty of Pharmaceutical Science
                              School of Health Sciences
                              University of Iceland

Supervisors   Professor Már Másson
                              Faculty of Pharmaceutical Science
                              School of Health Sciences
                              University of Iceland

                              Ólafur Baldursson MD, Ph.D.
                              Department of Pulmonary Medicine
                              Landspitali – The National University Hospital of
                              Iceland

Doctoral Committee   Professor Knud J. Jensen
(Other than supervisors)   Center for Carbohydrate Recognition and Signaling
                              Faculty of Science
                              University of Copenhagen

                              Associate Professor Sesselja Ómarsdóttir
                              Faculty of Pharmaceutical Science
                              School of Health Sciences
                              University of Iceland

                              Associate Professor Þórarinn Guðjónsson
                              Biomedical Center
                              School of Health Sciences
                              University of Iceland

Opponents   Dr. Ben Forbes
                              Reader, Institute of Pharmaceutical Science
                              King's College London

                              Dr. Jón Valgeirsson
                              Vice-President R&D Iceland
                              Actavis Group

ÁGRIP

Gegndræpisaukandi efni hafa verið í þróun um nokkurt skeið til að auka aðgengi peptíð- og próteinlyfja í gegnum slímþekjur líkamans. *N*-fjórgildar kítósanafleiður eru vatnsleysanlegar óháð sýrustigi og hafa verið rannsakaðar m.t.t. þess að auka gegndræpi þessara lyfja. Verkunarmáti þessara fjölliða er ekki vel þekktur en þó hafa bein áhrif á þéttitengi verið talin hugsanlegur möguleiki. Með því að lengja *N*-alkýl keðjuna í þessum *N*-fjórgildu kítósanafleiðum eykst yfirborðsvirkni þeirra og það gæti ýtt undir gegndræpisaukandi virkni þeirra. Til þess að það sé mögulegt að rannsaka þessa nálgun er þörf fyrir sértækar efnasmíðaleiðir sem leiða af sér afleiður með hátt hlutfall *N*-fjórgildra sethópa sem einnig auðveldar byggingarákvörðun þeirra. Ennfremur er mikilvægt að prófa þessar *N*-fjórgildu kítósanafleiður á þekju sem hefur vel skilgreind og virk þéttitengi.

Markmið þessa doktorsverkefnis var að þróa efnasmíðaaðferðir fyrir kítósanafleiður með hátt hlutfall *N*-fjórgildingar, skilgreina vel byggingu þeirra og jafnframt að ákvarða samband á milli lengdar *N*-alkýlhóps og aukins gegndræpis í berkjuþekjufrumulíkani.

Efnasmíðaaðferðir sem byggðu á notkun dí-*tert*-bútýldímetýlsilýl verndaðs kítósans voru þróaðar og notaðar til að smíða *N*-metýl-, *N*-própýl-, *N*-bútýl- og *N*-hexýl-*N*,*N*-dímetýl kítósan (TMC, QuatPrópýl, QuatBútýl og QuatHexýl) án *O*-metýleringar. Oxím efnasmíðaaðferð var notuð til að innleiða flúrljómandi efni sértækt inn á afoxandi enda TMC. Með því að staðfesta tilvist þessa myndefnis gefst möguleiki á frekari þróun oxím hvarfa fyrir aðra virka hópa. VA10 berkjuþekjufrumulínan gat líkt eftir eðlilegum þekjuvefstálma, gegndræpi og svipgerð og var því talin vera viðeigandi til að kanna samband á milli byggingar *N*-alkýl fjórgildu afleiðanna og gegndræpisaukandi áhrifa þeirra. Þær niðurstöður sýndu að aukin yfirborðsvirkni afleiðanna leiddi til aukins gegndræpis, riðlunar þéttitengja og minni lífvænleika í röðinni QuatHexýl ≈ QuatBútýl > QuatPrópýl > TMC. Þessar niðurstöður sýna jafnframt að aukið gegndræpi er ekki einungis háð katjónísku hleðslunni heldur einnig lengd *N*-alkýl keðju fjórgildu kítósanafleiðunnar. Þar sem að TMC var virkt í tiltölulega lágum styrk og dró ekki úr lífvænleika með langvarandi hætti, er hún talin vera sú fjölliða sem gæti einna helst verið áhugaverð til frekari þróunar í innöndunarlyfjaformum.

Lykilorð: Kítósan, TMC, oxím, berkjuþekjufrumulína, gegndræpisaukandi efni.

ABSTRACT

Permeation enhancers have been studied to increase the bioavailability of peptide and protein based drugs through mucosal membranes. *N*-quaternary chitosan derivatives are water soluble, independent of the pH and have been investigated as such permeation enhancers. The precise mechanism explaining this effect is unknown but an interaction with tight junction (TJ) proteins has been suggested. Before initiating the PhD project, it was hypothesized that by increasing the *N*-alkyl length of *N*-quaternary chitosan derivatives, more degree of amphiphilicity could be achieved, augmenting further the permeation enhancement effect. This approach would require specific synthetic strategies for the production of highly *N*-quaternized derivatives, enabling detailed structure determination. In order to test the hypothesis, it is also important to use a differentiated epithelium with established TJ structure and function for the investigation.

Therefore, the aim of this PhD project was to develop strategies for the synthesis of highly *N*-quaternized chitosan derivatives with well defined structures and determine the relationship between their *N*-alkyl chain length and their permeation enhancement in a bronchial epithelial cell model.

The synthesis was done with the aid of di-*tert*-butyldimethylsilyl hydroxyl protected chitosan, which resulted in highly quaternized *N*-methyl-, *N*-propyl-, *N*-butyl- and *N*-hexyl-*N,N*-dimethyl chitosan derivatives (TMC, QuatPropyl, QuatButyl and QuatHexyl respectively), without *O*-methylation. A fluorophore was regioselectively conjugated to the reducing end of TMC by oxime formation and visualized in bronchial epithelial cells. This provided an important proof of concept for further reducing-end oxime modifications of chitosan derivatives with other functional groups. It was shown that the VA10 bronchial epithelial cell line was able to model the native bronchial epithelial integrity, permeability and morphology and can, therefore, be considered suitable to elucidate the relationship between the structure of *N*-quaternary chitosan derivatives and their activity as permeation enhancers. Those results demonstrated that increased amphiphilicity of the *N*-quaternary chitosan derivatives caused increased permeation, TJ disassembly and decreased viability in the order of QuatHexyl ≈ QuatButyl > QuatPropyl > TMC at pH 7.4, showing that the permeation is not only affected by the degree of quaternization but also by the degree of *N*-alkylation. The TMC homopolymer

possesses promising permeation enhancer properties, being effective in low concentrations without causing prolonged adverse effects and should therefore be considered as a promising candidate for the development of future respiratory dosage forms.

ACKNOWLEDGEMENTS

ABBREVIATIONS

A - surface area (cm^2)

ACN - acetonitrile

ALI - air-liquid interface

ASL – airway surface liquid

ATCC - American type culture collection

ATP – adenosine triphosphate

CSLM – confocal scanning laser microscopy

DA – degree of acetylation

DCl – deuterium chloride

DCM – dichloromethane

DMF – dimethyl formamide

DMS - dimethylsulfate

DMSO - dimethylsulfoxide

DQ – degree of quaternization

DS – degree of substitution

EA – elemental analysis

EDANS-O-NH$_2$ - 5-(2-((aminooxyacetyl) amino)ethylamino) naphthalene-1-sulfonic acid

ER -Permeation enhancement ratio

FBS – fetal bovine serum

FCS – fetal calf serum

FD - fluorescein isothiocyanate labeled dextran

FDA - Food and Drug Administration

FITC – fluorescein isothiocyanate

Flu-Na - fluorescein sodium

FT-IR – fourier transform infrared spectroscopy

hAEpc – human alveolar epithelial cells

HBSS - Hanks balanced salt solution

HPV-16 - human papilloma virus-16

KI – potassium iodide

LCC - liquid-covered culture

LDH - lactate dehydrogenase

MALDI-TOF - matrix assisted laser desorption/ionization time-of-flight

MeI – methyl iodide

MTT – (4,5-dimethylthiazol-2-yl)-2,5-diphenyltetrazolium bromide

MW – molecular weight

NaI - sodium iodide

NaOH – sodium hydroxide

NHBE - normal human bronchial epithelial

NMP – *N*-methyl-2 pyrrolidone

NMR – nuclear magnetic resonance

NR - not reported

P$_{app}$ - apparent permeability

P-gp - P-glycoprotein

PLC – phospholipase C

PLD – phospholipase D

PKC – protein kinase C

PSA – polar surface area

QuatPropyl – *N*-propyl-*N*,*N*-dimethyl chitosan

QuatButyl – *N*-butyl-*N*,*N*-dimethyl chitosan

QuatHexyl – *N*-hexyl-*N*,*N*-dimethyl chitosan

Rb - retinoblastoma tumor suppressor protein

Rh123 - rhodamine 123

RT – room temperature

SEM - scanning electron microscopy

sER – secretory efflux ratio

STAB-H – sodium triacetoxyborohydrate

TBAF – tetrabutylammonium fluoride

TBDMS - *tert*-butyldimethylsilyl

TER - transepithelial electrical resistance

TJ – tight junctions

TMC – *N*,*N*,*N*-trimethyl chitosan

TMS – trimethylsilyl

Trityl – triphenylmethyl

UG – Ultroser-G

3D - three-dimensional

TABLE OF CONTENTS

LIST OF FIGURES

LIST OF TABLES

LIST OF SCHEMES

LIST OF ORIGINAL PAPERS

I. Benediktsdóttir, B.E., Gaware, V.S., Rúnarsson, Ö.V., Jónsdóttir, S., Jensen, K.J., Másson, M. Synthesis of *N,N,N*-trimethyl chitosan homopolymer and highly substituted *N*-alkyl-*N,N*-dimethyl chitosan derivatives with the aid of di-*tert*-butyldimethylsilyl chitosan. *Carbohydrate Polymers* **86**, 1451-1460, 2011.

II. Benediktsdóttir, B.E., Sørensen, K.K., Thygesen, M.B., Jensen, K.J., Gudjónsson, T., Baldursson, Ó., Másson, M. Regioselective Fluorescent Labeling of *N,N,N*-Trimethyl Chitosan via Oxime Formation. *Carbohydrate Polymers* **90**, 1273-1280, 2012.

III. Benediktsdóttir, B.E., Arason, A.J., Halldórsson, S., Gudjónsson, T., Másson, M., Baldursson, Ó. Drug delivery characteristics of the progenitor bronchial epithelial cell line VA10. Pharmaceutical Research, in Press.

IV. Benediktsdóttir, B.E., Gudjónsson, T., Baldursson, Ó. Másson, M., *N*-alkylation of highly quaternized chitosan derivatives affects the permeation enhancement in bronchial epithelia *in vitro.* Submitted manuscript.

INTRODUCTION

1. CHITOSAN

1.1. Structure and physiochemical properties

Chitosan is a naturally occurring linear β-(1→4) glucosamine polymer. This polymer can be found in certain fungi (Kurita, 2006) but is usually derived from chitin by deacetylation. Chitin (Figure 1.A) is one of the most abundant polysaccharides found in nature, second only to cellulose (Kurita, 2006).
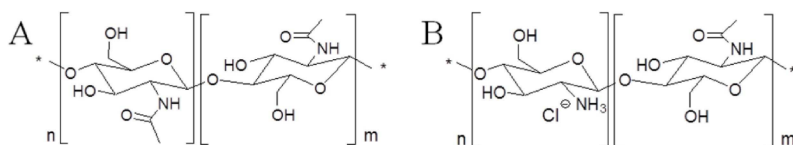
Figure 1. Structure of chitin (A) and chitosan (B).

Chitosan (Figure 1.B), produced from chitin, is partially acetylated and has a varying degree of acetylation (DA), usually less than 50% of the entire polymer structure, as well as different average molecular weight (MW) and these factors have been known to affect the bioactivity of the polymer. Chitosan has a pKa value of 6.5-6.6 (Anthonsen and Smidsrod, 1995, Strand et al., 2001), resulting in solubility at acidic conditions when the amino groups at the C-2 position (Figure 1.C) are protonated. Chitosan has greater reactivity than chitin due to these free amino groups, introducing a variety of possible modifications.

1.2. Chitosan in biomedical applications

Interest in chitosan can be attributed to the unique chemical properties and various biological activities of this biopolymer. Chitosan can be polycationic and this contributes to its mucoadhesive properties (Lehr et al., 1992) and its potential use in gene delivery (Merkel et al., 2012), in vaccines (Illum et al., 2001), as an antimicrobial agent (Kong et al., 2010) and use as a permeation enhancer (Artursson et al., 1994). The structure of chitosan partially resembles glycosaminoglycans, which are an important component of

the connective tissue. As such, chitosan has been investigated for use in tissue engineering (Mathews et al., 2011, Muzzarelli et al., 2012). The mucoadhesive and regenerative properties of chitosan have been utilized to develop chitosan based wound dressings which have been approved by the Food and Drug Administration (FDA) (Wedmore et al., 2006). Furthermore, chitosan has been marketed as a form of dietary supplement for weight control (Schiller et al., 2001).

Good biocompatibility and biodegradability of chitosan (Baldrick, 2010) is the basis for its varied applications in the pharmaceutical field. Degradation of chitosan in human tissues is thought to be facilitated by lysozymes although chitinases and acid hydrolysis may also affect the degradation process (Muzzarelli, 1997, Vårum et al., 1997). Chitosan and the chitosan derivative N,N,N-trimethyl chitosan (TMC) are degraded at similar rates (Verheul et al., 2009). Low DA in these polymers has been reported to make them more resistant towards lysozyme degradation (Verheul et al., 2009).

2. SYNTHESIS OF QUATERNARY CHITOSAN DERIVATIVES

Low solubility of chitosan at physiological pH values (generally above pH 6) limits its use for many applications and reduces the biological activity. More water soluble chitosan derivatives are therefore attractive. Introducing quaternary betainate on the free amino group or converting the amino group into N,N,N-trimethyl ammonium, creates a permanent positive charge that contributes to good aqueous solubility independent of pH.

2.1. Challenges in characterization of chitosan products

Synthesis of chitosan derivatives can be cumbersome. Due to size and charge of the chitosan derivative, chromatography cannot be used to follow the progress of the reaction. Thus, it is often necessary to run the reaction for a long time or follow the progress of the reaction by isolating small sample for analysis. Scientists working with chitosan derivatives have mostly relied on infrared (IR) spectroscopy and ^{1}H nuclear magnetic resonance (^{1}H NMR) techniques for structure characterization. However, structure elucidation based solely on ^{1}H NMR is difficult. Peaks are often broad, overlapped and seldom show sharp signals for coupling constant determination. By using

other NMR techniques available, such as 2D NMR ^{1}H-^{1}H COSY and ^{13}C-^{1}H HSQC, more detailed structure information can be obtained. However, there are relatively few examples in literature where these methods have been used to determine the structure of chitosan derivatives (Holappa et al., 2005, Runarsson et al., 2008a, Sajomsang et al., 2009).

2.2. Different synthesis methods for TMC and other *N*-quaternized chitosan derivatives

Various *N*-methylation methods have been used to synthesize TMC as can be seen in Table 1. Given the fact the *O*-methylation is a known side-reaction in TMC production, it is interesting that reports on its presence are scarce. Due to incomplete trimethylation reaction, the formation of a complex heteropolymer takes place that is nearly impossible to fully analyze by ^{1}H NMR alone as can be seen in Figure 2.
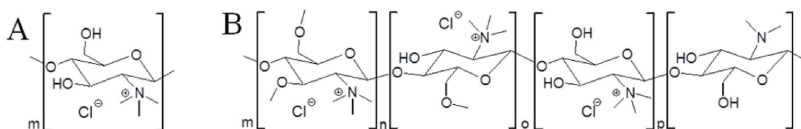
Figure 2. *N,N,N*-trimethylated chitosan.
A. The desired structure of the polymer after trimethylation reaction. B. Heterogeneous products often isolated after trimethylation reaction.

One of the most commonly used methods was originally reported by Domard and coworkers (Domard et al., 1986). It uses methyl iodide (MeI) as the reagent, sodium hydroxide (NaOH) as the base and potassium iodide (KI) as catalyst in 1-methyl-2-pyrrolidine (NMP). This method yields a heterogeneous *N,N,N*- trimethyl, *N,N*- dimethyl and *O*-methyl substituted chitosan as confirmed by Sieval and colleagues (Sieval et al., 1998). Later, Runarsson and co-workers (Dr. Ögmundur V. Rúnarsson was a PhD student supervised by Professor Már Másson) made improvements of this method to include the use of *N,N*-dimethylformamide (DMF)/H$_2$O mixture as solvent, with no *O*-methylation observed and 86% trimethylation (Runarsson et al., 2008a).

Table 1: Trimethylation reactions (highest trimethylation reported)

Type of reaction	Reagents and conditions	DA (%)	N-(CH$_3$)$_3$ (%)	N-(CH$_3$)$_2$ (%)	O-3/O-6 CH$_3$ (%)	Structure characterization	Ref
Reductive amination followed by reaction with MeI	AcOH, CH$_2$O (rt, 12 h) pH 3.2; NaBH$_4$ (8 h); ACN, MeI (35°C, 30 h)	42	60	25	NR	EA, IR, ^{13}C NMR	1
	AcOH, CH$_2$O (rt, 30 min) pH 4.5; NaBH$_4$ (1 h); NMP (rt, 12 h), MeI, NaOH, NaI (12 h, 50°)	2	63	NR	NR	EA, IR, ^{13}C NMR, potentiometry	2
	AcOH, CH$_2$O (rt, 1 h) pH 4.5; NaBH$_4$ (1.5 h); NMP (rt, 12 h), MeI, NaOH, NaI (12 h, 50°)	4	91	NR	NR	Potentiometry, IR	3
	CHO$_2$H, CH$_2$O (70°C, 118 h); NMP, MeI (40°C, 70 h)	3	73	NR	No	^{1}H NMR	4
MeI, NaJ, NaOH in NMP	60°C, 60 min	12	53[a]	NR	No	^{1}H NMR[a]	5
	Step 1: 60°, 60 min. Step 2: 60°, 30 min Addition step: 60°, 60 min	7	85	NR	Yes	^{1}H and ^{13}C NMR	6
	Step 1: 60°, 45 min. Step 2: 60°, 30 min. Addition step: 60°, 45 min. Step 3: 60°, 30 min	7	59	Yes	Yes	^{1}H NMR	7
	Step 1: 60°, 1.5 h. Step 2. 60°, 1.5 h Addition step: 160°C, 5h	3	91	Yes	Yes (83/99)	^{1}H NMR	8
MeI, NaI, NaOH in DMF/H$_2$O	Step 1: rt, 48h, Addition: same as step 1, repeated three times	5	86	11	No	^{1}H, ^{1}H-^{1}H COSY and ^{1}H-^{13}C HSQC NMR, IR	9
DMS	DMS, NaOH, NaCl in DMS/H$_2$O, rt, 6 h	4	53	Yes	Yes	^{1}H NMR, solid state ^{13}C NMR, IR	10

NR: not reported; rt: room temperature; EA: elemental analysis. [a]2.95 ppm is assigned as the trimethyl peak. **Ref 1**: (Muzzarelli and Tanfani, 1985), **2**: (Kim et al., 1997), **3**: (Jia et al., 2001), **4**: (Verheul et al., 2008), **5**: (Ledung et al., 1994), **6**: (Sieval et al., 1998), **7**: (Snyman et al., 2002), **8**: (Polnok et al., 2004), **9**: (Runarsson et al., 2008a), **10**: (de Britto and Assis, 2007).

An alternative trimethylation method uses formaldehyde and sodium borohydrate in acidic water to produce *N,N*-dimethyl chitosan followed by reaction of MeI in acetonitrile (Muzzarelli and Tanfani, 1985). However in this case the, 60% trimethylated polymer was insoluble in water, suggesting considerable *O*-methylation or possibly lower degree of trimethylation than the authors reported. This method was later refined to give no *O*-methylation with around 76% trimethylation (Verheul et al., 2008). Other methylating agents such as dimethylsulfate (DMS) have given around 50% trimethylation with some *O*-methylation also reported (de Britto and Assis, 2007).

Table 2 summarizes conditions that have been used for the synthesis of various *N*-alkyl and *N*-aryl quaternized chitosan derivatives. The usual synthetic strategy starts with reductive alkylation, followed by quaternization with MeI or other alkyl iodides. *N*-butyl-*N,N*-dimethyl chitosan is a good example of derivative prepared with this procedure. The reported degree of *N*-alkylation was 78% and degree of quaternization (DQ) 58%, according to elemental analysis (Kim et al., 1997). Later, Bayat and coworkers synthesized *N*-ethyl-*N,N*-dimethyl chitosan following similar reaction scheme, with 52% DQ reported (Bayat et al., 2006). Detailed structure analysis was not done in order to determine the extent of *O*-methylation, *N*-monomethylation or *N,N*-dialkylation, all of which can occur under the reported reaction conditions.

2.3. Protection groups in chitosan chemistry

Most reported chitosan modifications are performed in organic solvents, nevertheless the polymer is only partially soluble or insoluble in such solvents (Runarsson et al., 2008a). Low solubility of the polymer could be one of the reasons that only partial modification (e.g. quaternization) can be obtained. Protection groups have been used in the synthesis of chitosan derivatives, not only to allow more selective modifications but also to enhance the solubility of the polymer in organic solvents. The protected polymers *N*-phthaloyl chitosan and *O*-6-triphenylmethyl (*O*-6 trityl) chitosan are most commonly used in the selective synthesis of chitosan derivatives (Holappa et al., 2004, Kurita et al., 2001). Nishimura and Kurita were the first to use protection groups in synthesis of chitosan derivatives (Nishimura et al., 1991). They have reported procedure where *N*-phthaloylation is achieved by reaction of chitosan with phthalic anhydride in 95:5 DMF/H$_2$O (Kurita et al., 2001).

Table 2: Different *N*-quaternization reactions of chitosan

Chitosan derivative	Reagents and conditions	DA (%)	Quat (%)	$(CH_3)_2$ (%)	O-3/O-6 CH_3(%)	Characterization	Ref
N-methyl-*N,N*-diethyl chitosan	• AcOH, formaldehyde (rt, 1 h) pH 4.5, $NaBH_4$ (1.5 h) • NMP, CH_3CH_2I, NaOH, NaI, (5h, 60°)	6	79	NR	NR	^{1}H NMR, IR	**1**
N-ethyl-*N,N*-dimethyl chitosan	• AcOH, ethyl aldehyde (rt, 1.5 h) pH 4.5, $NaBH_4$ (2 h) • NMP (rt, 5 h), MeI, NaOH, NaI (5h, 60°)	5	52	NR	NR	^{1}H NMR, IR	**2**
N,N,N-triethyl-chitosan	• NMP (4 h, rt), CH_3CH_2I, NaOH, NaI, (60°C, 6 h)	6	66	NR	NR	^{1}H NMR, IR	**3**
N-propyl-*N,N*-dimethyl chitosan	• AcOH, propyl aldehyde (rt, 1 h), pH 4.5, $NaBH_4$ (1.5 h) • NMP (rt, 12 h), MeI, NaOH, NaI (12 h, 50°)	4	92	NR	NR	IR	**4**
N-butyl-*N,N*-dimethyl chitosan	• AcOH, butyl aldehyde (rt, 30 min), pH 4.5, $NaBH_4$ (1 h) • NMP (12 h at rt), MeI, NaOH, NaI (12 h, 50°)	2	58	NR	NR	EA, potentiometry, FT-IR, ^{13}C NMR	**5**
N-benzyl-*N,N*-dimethyl chitosan	• H_2O, benzaldehyde (rt, 2 h), $NaBH_4$ (2 h) • NMP (rt, 12 h), MeI, NaOH, NaI (20 h at 50°)	3	81	NR	NR	EA, IR	**6**
N-(4-*N,N*-dimethylamino-benzyl)-*N,N*-dimethyl chitosan	• AcOH, 4-*N,N*-dimethylaminobenzyl aldehyde (rt, 1h), pH 5, $NaCNBH_3$ (rt, 24 h) • NMP (rt, 12 h), MeI, NaOH, NaI (5 h, 50°)	6	42	Trace	Trace/ 17	^{1}H NMR, IR	**7**

NR: not reported; rt: room temperature; EA: elemental analysis; **Ref 1**: (Avadi et al., 2004), **2**: (Bayat et al., 2006), **3**. (Avadi et al., 2003), **4**: (Jia et al., 2001), **5**: (Kim et al., 1997), **6**: (Guo et al., 2007). **7**: (Sajomsang et al., 2008).

Subsequent selective *O*-6 tritylation can then be carried out by reaction with triphenylmethyl chloride. Finally, the phthaloyl group can be removed by reaction with hydrazine giving *O*-6 protected chitosan (Figure 3.A). Trityl chitosan has been used in the synthesis of various derivatives such as chitosan *N*-betainates (Holappa et al., 2004), quaternary piperazine chitosan derivatives (Holappa et al., 2006) and *N*-acyl chitosan derivatives (Holappa et al., 2005). Although the nucleophilic *O*-3 group is less reactive than the *O*-6 group it can react with various electrophiles. Thus, Runarsson and co-workers observed that *N,N,N*-trimethylation of *O*-6 trityl chitosan also lead to *O*-3 methylation (Runarsson et al., 2007).
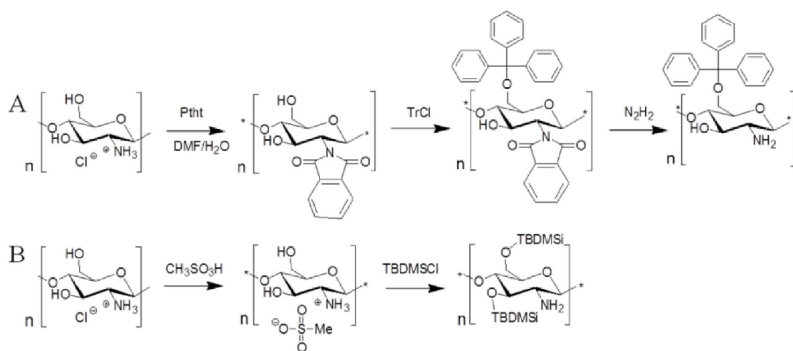
Figure 3. Synthetic protection strategies for chitosan.

A. The phthalic-trityl protection strategy for *O*-protection of chitosan. B. di-TBDMS protection strategy for *O*-protected chitosan.

It is therefore preferable to fully protect the hydroxyl groups on the chitosan backbone. Hydroxyl groups can be protected by conversion to silyl ethers and the silylation is *O*-selective in the presence of amines. The reason for their popularity can partially be attributed to the fact that the reactivity for the protection and deprotection step can be controlled by the selection of the substituents on the silicon atom (Wuts and Greene, 2007). Kurita and co-workers have reported trimethylsilylation (TMS) of chitosan, with the modification improving the solubility of the polymer in organic solvents (Kurita et al., 2004). However, the TMS group is not ideal as protection group since it is one of the most labile silyl group under acidic conditions (Wuts and Greene, 2007) and is therefore not compatible with slightly acidic reaction conditions.

Other silyl groups are more stable under acidic conditions and of particular interest is the di-*tert*-butyl dimethylsilyl (di-TBDMS) protecting group. This protection group is stable under a variety of reaction conditions but can still be easily removed without affecting other functional groups (Wuts and Greene, 2007). Recently, Runarsson and co-workers developed a procedure for *O*-3 and *O*-6 protection of chitosan. Chitosan hydrochloride was converted into the mesylate salt to increase its solubility in DMSO, followed by reaction with *tert*-butyldimethylsilyl (TBDMS) chloride as reagent and imidazole as a catalyst in DMSO (Figure 3.B). This TBDMS protection strategy gave 100% *O*-protected material for both *O*-3 and *O*-6 groups, achieved in one step at or below room temperature (Runarsson et al., 2008b, Song et al., 2010). This compares favorably to the three step procedure and reaction temperature of 100-120°C required for *O*-6 tritylation (Holappa et al., 2004). Furthermore, the TBDMS protection resulted in high solubility in a wide variety of organic solvents such as dichloromethane (DCM), NMP and ethanol (Runarsson et al., 2008a). This compares favorably to the solubility of *N*-phthaloyl and *O*-trityl protected chitosan derivatives (Binette and Gagnon, 2007, Nishimura et al., 1991). Consequently, the TBDMS protection method gives rise to new possibilities in employing various chemical reactions aimed at modifying the amino group on the chitosan backbone such as the trimethylation reaction.

3. FLUORESCENT CHITOSAN DERIVATIVES

3.1. Synthesis of fluorescent chitosan derivatives

Chitosan and chitosan derivatives have been used as drug carriers (Dünnhaupt et al., 2012), to aid cellular uptake of siRNA (Malmo et al., 2012) and DNA (Zheng et al., 2009), as permeation enhancers (Illum et al., 1994) and in regenerative medicine (Jiang et al., 2008). This has prompted search for appropriate methods to determine localization of these polymers *in vitro*. To clarify the mode of action, labeling the polymer backbone with a fluorophore such as fluorescein isothiocyanate (FITC, Figure 4.A) has been the standard approach (Onishi and Machida, 1999, Qaqish and Amiji, 1999).
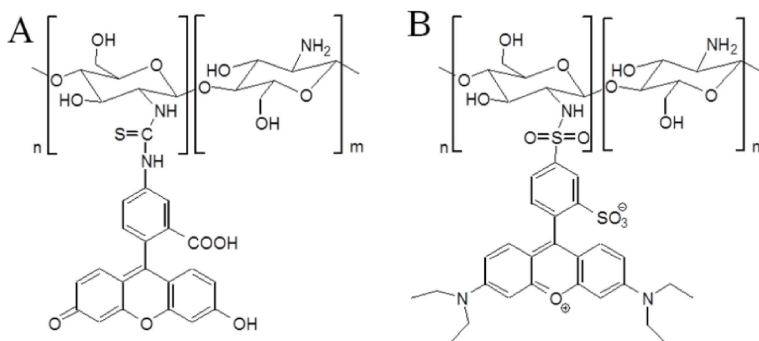
Figure 4. Fluorescent chitosan derivatives.

A. FITC-labeled chitosan. B. Lissamine-rhodamine-labeled chitosan.

Studies focused on visualizing the FITC-labeled chitosan *in vitro* have revealed that chitosan in solution usually adheres to the cellular membrane while chitosan nanoparticles are taken up by the cells (Huang et al., 2002, Jia et al., 2009). In addition to FITC, other fluorophores have been randomly introduced to the amino group of chitosan, such as lissamine-rhodamine (Schipper et al., 1997) (Figure 4.B) and Cy5.5 conjugated to glycol modified chitosan (Nam et al., 2010). Reports of structure characterization of these fluorescently labeled chitosan derivatives have been scarce but it is suggested that the fluorophore is linked through the amino group (Jia et al., 2009).

Incorporating these fluorophores randomly into the chitosan backbone has become a widely used application to visualize the localization of the polymer *in vitro*. However, this introduction could have some effects on the spatial structure of the polymer, thereby possibly altering its biological properties (Fei and Gu, 2009). The size distribution of fluorescent chitosan nanoparticles formed can also be affected (Huang et al., 2004). Furthermore, these random labeling techniques utilize the free amino group on the polymer backbone and are therefore not applicable to chitosan derivatives, such as TMC, where the amino group is blocked by methylation.

4. PULMONARY DRUG DELIVERY

4.1. Anatomy and morphology of the lungs

The human lung is a complex organ which has the vital function of oxygen/CO_2 exchange. The lung can be divided into the upper- and lower conducting airways that branch between 20-25 times before reaching the alveolar region (Figure 5). The upper airways, extending from the nasal cavity to the bronchi, contain a pseudostratified epithelium. Consequently, all cells are in contact with the basal lamina but not all reach the luminal surface. The region is mainly composed of basal, ciliated, undifferentiated and goblet cells (Crystal et al., 2008). Ciliated cells are around 50% of the cells in this region and serve as an integrate member of the mucociliary clearance mechanism along with the mucus producing goblet cells (Knight and Holgate, 2003). Basal cells occupy around 30% of the cells in the bronchial epithelial lining (Boers et al., 1998, Mercer et al., 1994) and are considered to be the progenitor cells of mucosal and ciliated epithelial cells (Boers et al., 1998, Rock et al., 2009).

The lower airways form a monolayer of cuboidal and columnar cells that are smaller than the upper conducting epithelial cells with secretory clara cells appearing instead of goblet cells (Patton, 1996). The alveolar region consists of extremely thin type I and type II cells that are heavily populated with macrophages (Stone et al., 1992).The lungs have evolved to protect the body from inhaled pathogens and foreign material. Efficient mucociliary clearance, present in the upper airways, is the forefront of this defense mechanism and is maintained by secretory- and ciliated cell. Other defenses of the airway epithelium include tight junctions, cough reflex, dendritic network and the secretion of enzymes, inflammatory mediators and antimicrobial peptides (Nicod, 1999).

4.2. The tight junction complex

The expression of tight junction (TJ) proteins in the bronchial epithelium is an important part of the innate defense of the lungs. The TJs are membrane bound proteins that produce apical to basolateral polarity (Schneeberger and Lynch, 2004) and form a paracellular permeability barrier that limits the permeation to small, uncharged solutes (Watson et al., 2001) that is dependent on both ion concentration and pH (Tang and Goodenough, 2003, Yu et al., 2003).
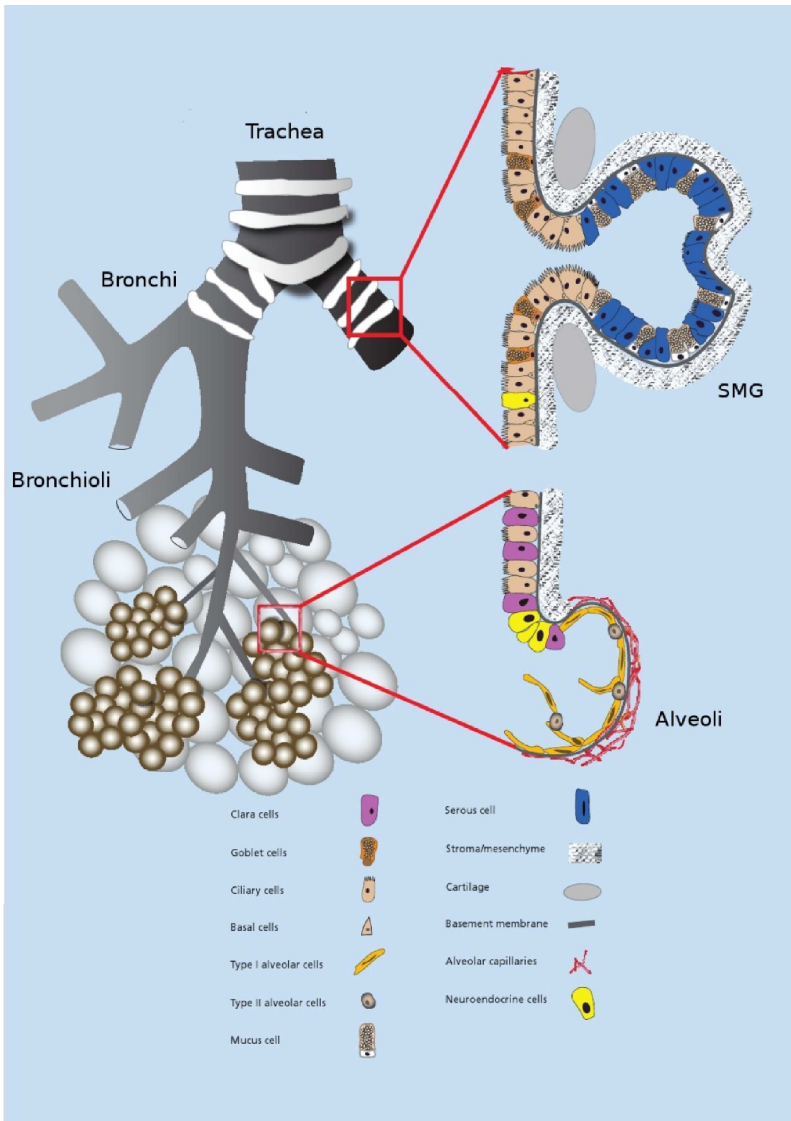
Figure 5. The morphology and cell type composition of the lungs

(Magnusson et al., 2011).

The bronchial epithelia express a variety of TJ proteins such as JAM-A which has one membrane spanning domain and claudins, occludins and tricellulin that have four transmembrane domains (Schneeberger and Lynch, 2004). Intracellularly, there are TJ associated proteins such as the members of the ZO family (ZO-1, ZO-2, ZO-3) that connect to the actin cytoskeleton (Figure 6).

The "tightness" of the TJs can be measured with the transepithelial electrical resistance (TER). Thus, when an epithelium is intact *in vivo,* the TER value is, generally speaking, relatively high. However, the TER of different epithelial surfaces is variable, both between organ systems and within the same organ, depending on functional requirements. This can be best described in the kidneys where the TER ranges from ~10 $\Omega*cm^2$ in the proximal tube to as high as 40.000 $\Omega*cm^2$ in the urinary bladder (Cereijido et al., 2007). Tight junctions in the airways, as determined with primary bronchial epithelial cells, generate TER around 800 to 1300 $\Omega*cm^2$ (Jakiela et al., 2008, Lin et al., 2007b) and are consequently considered to have medium paracellular permeation properties compared to other epithelial surfaces of the body.
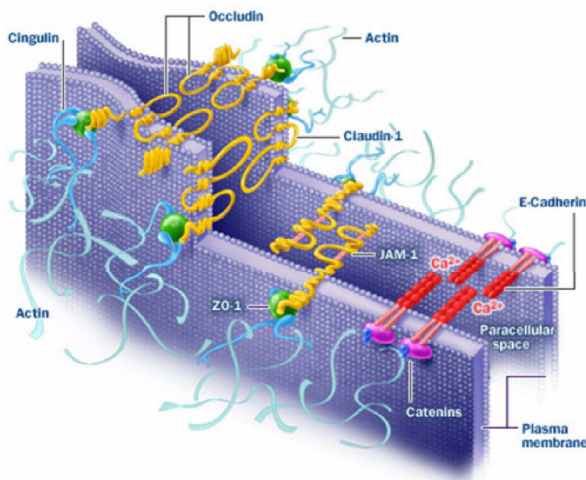
Figure 6. The tight junction (TJ) complex.

The TJ complex is made of membrane spanning occludin, claudins and JAM-A in addition to the ZO scaffolding proteins that link the membrane spanning proteins to the actin filaments in the cytoskeleton (Tight Junction Biology, 2007).

4.3. Mechanism of drug absorption in the airways

Small molecules, hydrophobic drugs in particular, are generally rapidly absorbed in the lungs through passive diffusion (Rabinowitz et al., 2004) and have similar bioavailability as by the injection route (Dershwitz et al., 2000). Consequently, the onset of action is fast, which is important for certain conditions such as pain, anxiety and nausea. The lung epithelium is more permeable to macromolecules than other epithelia used for non-invasive drug delivery (Patton, 1996, Tronde et al., 2003b). For macromolecules below 40 kDa, the diffusion-limited, paracellular pathway through the tight junction belt is considered to be the dominant pathway (Patton and Byron, 2007).

There is no general consensus about the optimal drug disposition site in the lungs for systematic delivery of macromolecules. The distal airways have lower TER than the proximal airways (Boucher et al., 1981), which is advantageous for systemic drug delivery. However, due to the large surface area of the alveolar region (Weibel, 1963), as well as its extremely thin epithelium has attracted attention of scientists as a possible drug disposition site. With ongoing progress in drug formulation, scientists have been able to formulate drug candidates in such a way that they can be delivered to the small airways and the alveoli where the surface area is at its greatest, as was done with the inhaled insulin drug Exubera^{TM} (Patton, 2005). Targeting the alveolar region is however less ideal for the delivery of larger proteins (> 300 kDa) due to their low bioavailability. This can be attributed to slow absorption of these proteins. Thus, they can aggregate and be cleared by macrophages (Perry et al., 1997, Stone et al., 1992). The upper conducting airways are free of macrophage scavenging, are more readily targeted and have leakier epithelium compared to the alveolar region number (Ehrhardt et al., 2008, Patton, 1996) and can, hence, be considered an attractive alternative to alveolar drug delivery.

4.4. Models for airway drug delivery

Choosing the right system to model the drug permeation and disposition depends on the drug developing stage. *In vivo* models are most relevant to study the fate of inhaled compounds. Typically small rodents are used (Sakagami, 2006), advancing into bigger animals such as dogs, sheep and monkey for determining inhalation pharmacokinetics and formulation efficiency (Adjei et al., 1990, Bitonti et al., 2004, Schreier et al., 1994).

Although these *in vivo* models are clearly necessary and relevant to the drug development process they are less suitable for use at the early stages of drug development (Sakagami, 2006).

Studies using *in vitro* human cell models have emerged as a more convenient method to investigate drug permeability due to their relative simplicity, small amount of test compounds required and because sacrifice of animals is not needed (Sakagami, 2006). These cell models, which can be primary cultured cells or continuous cell lines, allow for a detailed study at the cellular level; enable characterization of drug transport and assessment of toxicity and metabolism of a new drug entity. Primary cells are directly isolated from the lung and consequently have the advantage of representing closely the target organ. However, isolating primary cells is time consuming and these cells have a finite lifespan and the results are often poorly reproducible. Lung epithelial cell lines on the other hand are continuous and have better reproducibility, making their use the standard technique for apparent permeability (P_{app}) determination and enabling high-throughput screening of compound libraries. The use of monolayer epithelial cultures to classify permeability of certain new drugs absorbed in the gastrointestinal tract has been recommended by both the FDA and the European Agency for the Evaluation of Medicinal Products (CDER/FDA, 2000, Note for guidance on the investigation of bioavailability and bioequivalence, December 2000), thereby highlighting the importance of valid *in vitro* cell models.

Continuous airway cell lines can have cancerous origin or be immortalized from the normal lung. Common airway cancerous cell lines include the bronchial Calu-3 (Fogh et al., 1977) and the alveolar A549 (Giard et al., 1973). Transfection of primary cells with either SV40 large T antigen virus or human papilloma virus has been commonly used to generate immortalized cells. Transformed cell lines include the bronchial 16HBE14o- (Cozens et al., 1994), BEAS-2B (Reddel et al., 1988) and NuLi-1 (Zabner et al., 2003) and are further listed, along with the cancerous cell lines, in Table 3. There it can be seen that a variety of lung epithelial cell lines exists. Since it is important that the cell line forms a tight polarized epithelium for the appropriate assessment of drug transport (Sakagami, 2006), it narrows down the options to a few representative respiratory cell lines that are suitable for modeling epithelial integrity and drug permeation (Forbes and Ehrhardt, 2005, Sakagami, 2006, Sporty et al., 2008).

The conducting airways are the major disposition site for pharmaceutical aerosols on the market today (Forbes, 2000). The two cell lines commonly used to study upper airway drug permeation *in vitro* are Calu-3 and 16HBE14o- bronchial epithelial cell lines. The Calu-3 cell line is the prominent cell line found in the literature. Its availability from the American type culture collection (American Type Culture Collection Catalog: HTB-55, 2012) certainly aids in its distribution as compared to the non-commercial availability of 16HBE14o-. Both Calu-3 and 16HBE14o- have functional barrier properties (Cozens et al., 1994, Shen et al., 1994, Wan et al., 2000) and their permeability characteristics correlate with *ex vivo* (Manford et al., 2005) or *in vivo* models (Mathias et al., 2002). The difference in the origin of these two cell lines translates into morphological differences as listed in Table 3. 16HBE14o- cells have basal cell phenotype (Dorscheid et al., 1999, Zhu et al., 1999), generate microvilli protrusions, form 1-5 layers of cells when grown in liquid-covered culture (LCC) and 10-16 cell layers in air-liquid interface (ALI) culture (Ehrhardt et al., 2002b, Pohl et al., 2009) consistent with squamous metaplasia. Calu-3 cells form either a monolayer in culture (Fiegel et al., 2003, Florea et al., 2003, Shen et al., 1994) or cell layers (Grainger et al., 2006, Stentebjerg-Andersen et al., 2011) and produce mucus (Finkbeiner et al., 1993, Haghi et al., 2010). Ciliate-like structures have been reported (Grainger et al., 2006) that have been observed to disappear with increasing passage number (Ehrhardt et al., 2008). However, this cell line does not have the phenotypic traits of normal epithelial cells. Its serous origin in the submucosal glands could have different attributes than its ciliated luminal counterparts (Mathias et al., 2002) and different expression levels of metabolizing enzymes due to cancerous origin (Ehrhardt et al., 2008, Mathias et al., 2002). This raises some questions about its relevance as a suitable airway epithelial model. Moreover, debates regarding cross-contamination of previously established cell lines have emerged (Nardone, 2007, Rojas et al., 2008), prompting the need to confirm the identity of the Calu-3 cell line (Otton, 2009). This also compromises the use of this cell line to model the native bronchial epithelia. Therefore, drug evaluation at the cellular level calls for consideration of alternative cell lines that capture more closely the phenotypic traits of the *in vivo* bronchial epithelium.

Table 3. Characteristics of human epithelial lung cell lines[1].

	Cell line	Derivation	Phenotype	Remarks	Ref
Cancerous	Calu-3*	Adeno-carcinoma from serosal gland	Non-ciliated, columnar, monolayer or cell layers with mucus secretion	Medium TER, Sparse cilia that disappear with increasing passage number	1
	A549*	Adeno-carcinoma	Similar to type II alveolar cells	Low TER	2
Transfected	16HBE14o-	SV40 large T-antigen virus	Non ciliated, cuboidal cells with basal cell markers	Medium TER, no mucus, multilayered	3
	NuLi*	hTERT, E6/E7 from HPV-16	Adherent epithelial cells	Medium TER	4
	BEAS-2B*	Adeno-SV40 hybrid virus	Squamous	No tight junctions, cilia or mucus	5

* Available from the American Type Culture Collection. **Ref. 1**: (Ehrhardt et al., 2008, Finkbeiner et al., 1993, Grainger et al., 2006, Haghi et al., 2010, Shen et al., 1994), **2**: (Blank et al., 2006, Giard et al., 1973), **3**: (Cozens et al., 1994, Ehrhardt et al., 2002b, Forbes et al., 2003, Pohl et al., 2009), **4**: (Zabner et al., 2003), **5**: (Ke et al., 1988, Reddel et al., 1988).

4.5. The human bronchial epithelial VA10 cell line

Figure 7. VA10 cell layer in air-liquid interface culture (20x).

The human bronchial epithelial cell line VA10 (Figure 7) was recently established from primary bronchial cells by retroviral transfection with E6 and E7 oncogenes from human papilloma virus-16 (HPV-16) (Halldorsson et al., 2007) that targets and inactivates p53 and the retinoblastoma tumor suppressor protein (Rb), respectively. This cell line has all the major hallmarks of epithelial origin. VA10 generates active TJs in both LCC and ALI culture as evidenced by high TER (Halldorsson et al., 2007). Additionally, this cell line has basal cell phenotype when cultured under LCC and has non-malignant growth (Halldorsson et al., 2007). VA10 can capture both bronchial and bronchioalveolar-like

[1] This list only contains some of the many cell lines observed in the literature

16

epithelial histology, depending on cell culture conditions, thereby showing stem cell properties (Franzdottir et al., 2010). The fact that VA10 can produce *in vivo* like phenotype in 3D culture and form high TER in ALI makes this cell line a potential candidate for studying bronchial epithelial integrity and response to drug delivery. VA10 may provide a unique opportunity to study absorption enhancers and their mechanism of action.

5. PERMEATION ENHANCERS

5.1 Inhalation of macromolecules for systemic delivery

The inhalation route has been used for many years to treat bronchial symptoms in disease such as asthma, cystic fibrosis and chronic obstructive pulmonary disease. Systemic delivery of compounds through inhalation has, however, been restricted to anesthetics, nicotine and illegal substances (Gonda, 2006). This appears to be changing. New biotechnology drugs are emerging and they generally have unfavorable physiochemical properties for delivery, such as high molecular weight, hydrophilicity and lability (Uchenna Agu et al., 2001). These properties limit their use to the parenteral route, which reduces patients' compliance and convenience. The inhalation route for systemic delivery of these macromolecules has been considered as an attractive alternative due to higher bioavailability compared to other non-invasive routes.

The increased bioavailability can be attributed to low surface volume, large surface area in the lower airways and the alveoli, avoiding hepatic first pass metabolism and relatively low enzymatic activity compared to the gastrointestinal tract (Patton and Byron, 2007). Although much development has been focused on the pulmonary delivery of peptide and protein based drugs (Scheuchi et al., 2007, Thipphawong, 2006), there is not a single inhaled product for systemic action commercially available. Exubera[TM], the inhaled insulin, was an exception. It was approved for treatment of diabetes (Lenzer, 2006) but after less than two years on the market, the drug was discontinued. Failure to get acceptance from the health insurance providers and prescribing physicians was claimed to be the main reason. This could have been attributed to the inconvenient dosing units, large inhalation device, relatively high cost and the fact that the glycemic control was not superior compared to subcutaneous insulin (Mathieu and Gale, 2008).

Safety concerns regarding possible carcinogenic- and immunogenicity potential, which is a concern with peptide and protein drugs (Patton et al., 2004, Patton and Platz, 1992), always haunted this new inhalation therapy (Mathieu and Gale, 2008).

The failure of Exubera™ has encouraged pharmaceutical companies to reconsider their strategy regarding inhaled therapeutics for systemic action, as it has also shown the limitations of this delivery route. Beside the above mentioned concerns, the possible irritation and toxicity of the drug must also be considered. Additional safety issues include stability problems, risk of insufficient dosing or unfavorable pharmacodynamics which can be detrimental diseases such as for diabetes. More fundamental research to improve understanding of the parameters affecting the safety and efficiency of this delivery route is therefore needed.

5.2 The use of permeation enhancers

Peptide and protein drugs are both relatively large and hydrophilic, rendering the paracellular pathway the optimal absorption route. The passage of these macromolecular drugs between the cells is limited by the TJ proteins that serve as a fence mechanism, polarizing the cell membrane and regulating paracellular epithelial permeability (Matter and Balda, 2003) as shown in Figure 8.
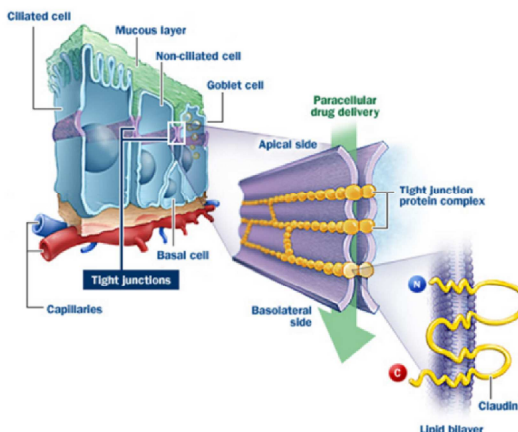
Figure 8. Tight junctions in the epithelium.

TJs are the most apical of all junctional proteins and serve as a fence mechanism, only allowing certain molecules to pass between the cells (Tight Junction Biology, 2007).

Permeation enhancers have been studied to circumvent this gating mechanism. The enhancer must exert its action upon the cells without inducing serious adverse effects to the cell membrane.

A variety of different permeation enhancers are available (Table 4) with compounds such as the unsaturated fatty acid of oleic acid and the bile salt sodium taurocholate being proposed to increase the lung permeation of macromolecular drugs (Hussain et al., 2004). Despite many published *in vitro* and *in vivo* studies showing their convincing enhancing properties (Deli, 2009), few of them have been registered as such. This can be due to concerns related to their direct toxicity to the epithelium and indirect toxicity by opening the barrier for pathogens (Maher et al., 2009). The medium chain fatty acid sodium caprate has been used as a permeation enhancer in Doktacillin® rectal suppositories, formerly marketed in Sweden and Japan (Lindmark et al., 1997). Permeation enhancers are essentially either of low molecular weight or high molecular weight. Due to the polymeric and cationic nature of the high molecular weight chitosan and poly-L-lysine, they are mucoadhesive, thereby, prolonging their residence time at the site of action.

Table 4. Permeation enhancers and their proposed mode of action

	Enhancers	Possible mode of action	Ref
Surface-active reagents	Bile salts and acids	F-actin relocalization, opening of TJ, removal of epithelial cells	1
	Fatty acids and non-ionic surfactants	↑Intracellular Ca^{2+}, PLC, ↓ATP, redistribution and opening of TJ, membrane perturbation	2
Poly-cations	Chitosan and derivatives	Opening of TJ: further reported in Table 5	3
	Poly-L-lysine	PLD activation	4
	Poly-L-arginine	TJ redistribution, PLD activation, PKC	5
Miscellaneous	Alkylglycosides	Opening of TJ	6
	EDTA	Depletion of extracellular Ca^{2+} thereby activating PKC	7
	Dimethyl-β-cyclodextrin	Extraction of membrane lipids and proteins	8

Abbreviation: ATP: adenosine triphosphate; PLC: Phospholipase C; PLD: Phospholipase D; PKC: protein kinase C. **Ref 1:** (Hersey and Jackson, 1987, Johansson et al., 2002, Lin et al., 2007a), **2:** (Lindmark et al., 1998, Machida et al., 2000, Tomita et al., 1996, Tomita et al., 1992), **3:** (Ranaldi et al., 2002), **4:** (Ohtake et al., 2003a) **5:** (Ohtake et al., 2003a, Ohtake et al., 2003b), **6:** (Ahsan et al., 2003, Pillion et al., 1994), **7:** (Tomita et al., 1996). **8:** (Monnaert et al., 2004, Shao et al., 1994).

5.3 Permeation enhancing effects of chitosan

Chitosan has been intensively investigated as a polymeric permeation enhancer for macromolecular delivery through mucosal membranes. Early reports showed that chitosan increased the nasal delivery of insulin in rats and sheep (Illum et al., 1994). Although relatively high doses of chitosan were used (2-5 mg/ml) at pH 4.4, these data suggested the possibility of chitosan induced permeation enhancement. This sparked numerous investigations, with the widely used human colorectal cancer cell line Caco-2, aimed at studying the permeation enhancing effects of chitosan. Table 5 summarizes several studies carried out for chitosan to further determine the extent of the permeation enhancement. All studies show that treatment with chitosan solutions decreases epithelial TER and increases paracellular permeability of inert markers under acidic conditions. However, direct comparison between the studies of the permeation enhancing effect of chitosans can be difficult due to difference in experimental conditions, DA and MW as is evident in Table 5.

The concentration of chitosan required to produce enhanced permeation in the Caco-2 cell line varied greatly, from as low as 0.05 mg/ml (Schipper et al., 1996) to as high as 15 mg/ml (Florea et al., 2006, Kotze et al., 1999a). If chitosan in the range of 0.05 mg/ml induces increased permeation then doses 300 times larger seem to be hardly applicable since the aim should always be for as low dosage as possible for drugs and excipient. The permeation enhancement ratio (ER) obtained after chitosan treatment depends on the MW of the permeation markers. ER of 10-30 has been reported for ^{14}C mannitol (0.184 kDa) (Kotze et al., 1999a, Schipper et al., 1997, Schipper et al., 1996), while ER of 3-10 for fluorescein isothiocyanate labeled dextrans (FD) 4 kDa (FD4) was observed (Kudsiova and Lawrence, 2008, Schipper et al., 1997, Vllasaliu et al., 2010). Limited increase in permeability after chitosan treatment for 20-40 kDa dextrans has been reported (Kudsiova and Lawrence, 2008, Schipper et al., 1997), indicating a size selective opening of the TJ. This size restriction of the paracellular passage is important, as it may limit unwanted permeation of bacterial antigens and other immunoreactive molecules that could produce adverse effects *in vivo*. Recently, a detailed study showed that insulin co-administered with chitosan could penetrate the intestinal mucosa to the systematic circulation without lipopolysaccharide entry (Sonaje et al., 2011), thereby showing size dependent opening of TJ after chitosan treatment.

The chitosans evaluated for their permeation enhancement have differed in DA, MW and salt form and the pH used for the tests has also varied between studies. Chitosan has a pK$_a$ value of 6.5-6.6 (Anthonsen and Smidsrod, 1995, Strand et al., 2001) and in order to be efficient as permeation enhancer it must remain positively charged (Artursson et al., 1994, Kotze et al., 1999a, Rosenthal et al., 2012). Consequently, if the pH is higher than the pK$_a$ the polymer has lower charge density and the structure coils, leading to lower water solubility and ultimately precipitation. The importance of charge density has, for example, been shown by adding negatively charged heparin to the chitosan solution, resulting in no net increase of permeation (Schipper et al., 1997).

The degree of acetylation also has a significant impact on the charge density of chitosan and its derivatives. Less DA means more free amino groups that can become positively charged (Schipper et al., 1996). Previous studies have shown that chitosan with DA 35-49% and low MW (12-22 kDa) had less permeation enhancing effect and limited or no mucoadhesion compared to chitosan with lower DA (Schipper et al., 1997). However, chitosan with DA of 35-49% and high molecular weight (98-170 kDa) had similar permeation enhancing effect as chitosans with lower DA and less cellular toxicity (Schipper et al., 1996). Comparable results have been obtained for TMC where the polymer, with DQ of~45% and DA ~50%, did not decrease TER (Verheul et al., 2009). There appears to be different permeation enhancing effect depending on the chitosan salt form. There are, however, inconsistencies in these studies. For example, chitosan HCl has been reported to be both more efficient (Kotze et al., 1998) and less efficient (Opanasopit et al., 2007) in paracellular permeation enhancement than chitosan glutamate. Although MW has also been reported to affect the permeation enhancing effect of chitosan (Schipper et al., 1996), the effect seems to be less pronounced than DA.

Table 5 shows that studies using bronchial epithelial cell lines are scarce compared to studies using the Caco-2 cell line. Studies using chitosan for nasal or pulmonary administration show adequate permeation enhancing ratio when acidic buffers (pH ≤ 6) are used (Kudsiova and Lawrence, 2008, Vllasaliu et al., 2010). The airway surface liquid (ASL) has a pH of ~ 6.8 (Walters, 2002) which is slightly acidic, not favoring the dissolution of chitosan formulations into the liquid..

Table 5. Effects of chitosan in solution on permeability *in vitro*.

Ref	Effects on tight junctions and morphology	Viability	Model (pH)	Salt	DA (%) /MW (kDa)	Conc. (mg/ml)	Permeation marker	ER	TER reduction[a]/ TER recovery[a]
1	Subtle effects on ZO-1, occludin and F-actin. Large intracellular vacuoles observed. Swollen endoplasmic reticulum	LDH: Dose dependent decrease in viability from 0.1 mg/ml. Trypan blue: 98% viability	Caco-2 (6-6.5)	HCl	20/NR	0.1 1 5	^{14}C Mannitol	4.3 15.1 18.7	25/100 NR NR
2	(1/31) (1/170) resulted in discontinuities and reduced number of microvilli. Chitosans with high MW and/or low DA necessary for absorption enhancement activity	MTT: 1/31 and 1/170 decreased the viability in 0.05 mg/ml	Caco-2 (5.5)	HCl	1/31 1/170 15/4.7 15/190	0.01 0.05 0.25 0.01 0.05 0.25 0.01 0.05 0.25 0.01 0.05 0.25	^{14}C Mannitol	1.2 4.5 10.0 1.2 3.6 10.9 1.0 3.2 15.4 1.9 6.3 11.2	NR
3	Disbandment of F-actin and some areas were absent of ZO-1. Permeation enhancement is due to charge dependent mechanism	PI : Increased staining at 0.05 mg/ml for both 1/31 and 35/170	Caco-2 (5.5)	HCl	1/31 35/170 1/31 35/170 1/31 35/170	0.05 0.05 0.05 0.05 0.05 0.05	^{14}C Mannitol ^{14}C Mannitol FD-4 FD-4 FD-20 FD-20	3.1 11.2 4.2 3.0 1.3 1.7	60/NR 60/NR
4	Disbandment of F-actin, occludin and ZO-1	NR	Caco-2 (6.0$_{ap}$, 7.4$_{bl}$)	HCl	22/NR	0.02 0.1	^{14}C Inulin	NR NR	29/94 14/36

22

Table 5 (contd.). Effects of chitosan in solution on permeability *in vitro*

Ref	Effects on tight junctions and morphology	Viability	Model (pH)	Salt	DA (%)/MW (kDa)	Conc. (mg/ml)	Permation marker	ER	TER reduction[a]/TER recovery[a]
5	Decrease in TER and increase in P_{app} only at pH 6.2. No significant difference between chitosan concentrations. TER recovery not evident	Tryptan blue: no change	Caco-2 (6.2)	HCl Gluta-mate	17/NR 17/NR	5 15 5 15	[14]C Mannitol	32.3 36.3 19.7 25.4	11/NR 8/NR 31/NR 17/NR
6	No effects on F-actin expression. Redistribution of ZO-1 and occludin into the cytoskeleton	Tryptan blue: no change	Caco-2 (6.3)	Gluta-mate	15/128	0.5 1 5	HRP	4.3 15.1 18.7	88/NR 46/100 17/80
7	Actin not affected. TER decrease due to both decreases in paracellular and transcellular resistance. Activity due to chloride-bicarbonate exchanger	LDH: effect from 0.05 mg/ml	HT-29 (6.5)	NR	75-85/ 50-190	0.05 0.1	Mannitol FD4 FD10	$\sim3^{b}$ $\sim9^{b}$ $\sim6^{b}$	17/100 5/100
8	NR	MTT: 30% decrease	Calu-3 (5.5)	NR	7/ 100-500	15	Octreotide	21	60/93
9	Loss in continued staining for ZO-1	MTS/LDH, Effect from 0.06 mg/ml	Calu-3 $(6.0_{ap}, 7.4_{bl})$	HCl	14/113	0.015 0.03 0.06	FD-4, FD-10	NR 10.1 NR	NR <10/84 <10/<10
10	pH 6 decreased TER and viability in 16HBE14o-	MTT: Decrease in viability at and above 0.1 mg/ml	16HBE14o- (6.0)	NR	15/150	0.05 0.1 0.1 0.1 0.5 1.0	[14]C Mannitol FD-40 FD-250 FD-250 FD-250	NR 10.7 4.4 3.0 3.1 2.5	8/20 NR NR NR
		MTT:Decrease in viability observed with 4 mg/ml	Caco-2 (6.0)	NR	15/150	0.05 0.1 0.5 1.0		NR NR NR NR	57/100 ~55/100 ~55/100 45/100

23

Table 5 (contd.). Effects of chitosan in solution on permeability *in vitro*

Ref	Effects on tight junctions and morphology	Viability	Model (pH)	Salt	DA(%)/MW(kDa)	Conc. (mg/ml)	Permeation marker	ER	TER reduction[a]/ TER recovery[a]
11	Weaker staining for F-actin and actin disbandment was observed	NR	Caco-2 (6.0)	Gluta-mate	11/162	1 2.5 5	^{14}C Mannitol	2.1 2.5 3.2	NR
12	NR	Trypan blue: no change	Caco-2 (7.4)	Gluta-mate	NR	5 10 15	^{14}C Mannitol	NR NR ~1	No effect No effect 60/60
13	NR. Treatment with chitosan at pH of 7.4 did not result in any decrease in TER or increase in ER	Trypan blue: no change	Caco-2 (6.2)	HCl	17/NR	2.5 5.0 10.0 15.0	^{14}C Mannitol/ FD-4	34/27 32/26 36/39 36/48	16/NR NR NR 8/NR
				Gluta-mate	17/NR	2.5 5.0 10.0 15.0		25/10 20/11 29/14 25/11	40/NR NR NR 17/NR
14	NR	NR	Caco-2 (5.6)	Gluta-mate	NR	4 10		NR NR	71/NR 45/NR
15	NR	NR	Caco-2 (5.5ap, 7.4bl)	HCl	1/31 35/170	0.05 0.05	Atenolol	14.7 10.8	NR NR
16	Possible action through the PKC signaling pathway	Trypan blue: no change	Caco-2 (6.3)	Gluta-mate	15/128	5		No effect	17/ recovered

NR: not reported, ER: permeation enhancement ratio, ap: apica,. bl: basolateral, HRP: horseradish peroxidases, [a](% initial value), [b]Values obtained from figure and are not accurate. **Ref. 1**: (Dodane et al., 1999), **2**: (Schipper et al., 1996), **3**: (Schipper et al., 1997), **4**: (Ranaldi et al., 2002), **5**: (Kotze et al., 1999a), **6**: (Smith et al., 2004), **7**: (Rosenthal et al., 2012), **8**: (Florea et al., 2006), **9**: (Vllasaliu et al., 2010), **10**: (Kudsiova and Lawrence, 2008), **11**: (Artursson et al., 1994), **12**: (Borchard et al., 1996), **13**: (Kotze et al., 1998), **14**: (Luessen et al., 1997), **15**: (Schipper et al., 1999), **16**: (Smith et al., 2005).

Table 6. Effects of chitosan on permeability *in vivo*

	Ref	Toxicity, TJ and morphology	Salt	Model (pH)	DA (%)/ MW (kDa)	Conc. (mg/ml)	ER
Airways	1	Cilia present, nasal epithelium more disordered than control	Gluta-mate	Sheep, Rats (4.4)	NR	Sheep: 5 Rat: 2	5.6[a]
	2	High levels of neutrophil infiltration and severe damage to the pulmonary tissue	NR	Rats (5.5)	7/100-500	15	2.4[b]
	3	No apparent adverse effects, toxicity not investigated directly	Gluta-mate	Sheep (4.0)	NR	5	3[c]
	4	NR	HCl	Rats (6.7)	NR	15	51[d]
	5	NR	NR	Rats (6.0)	15/50	5	1.3[e]
					15/100	5	1.5[e]
	6	NR	Non-salt form	Rats (4.0)	15/100	5	11.0[a]
						10	12.8[a]
						15	17.3 [a]
Intestinal	7	LDH: no effect. Epithelial layer separated from underlying tissue, microvilli not clearly present after treatment	HCl	Rats (5.5)	1/31	0.025	1.5[f]
					35/170	0.025	0.8[f]

NR: not reported; ER: permeation enhancement ratio; [a]insulin, [b]octreotide, [c]calcitonin, [d]buserelin, [e]2,3,5,6-tetramethylpyrazine, [f]atenolol. **Ref**. **1**: (Illum et al., 1994), **2**:(Florea et al., 2006), **3**: (Hinchcliffe et al., 2005), **4**: (Luessen et al., 1996), **5**: (Mei et al., 2008), **6**: (Yu et al., 2004), **7**: (Schipper et al., 1999).

The feasibility of using acidic solutions can be debated, since the bronchial epithelial cell lines 16HBE14o- and Calu-3, incubated at or below pH 6.5 and 5.0 respectively, showed decreased viability (Kudsiova and Lawrence, 2008, Scherließ, 2011). The ASL can compensate for changes in pH *in vivo* (Jayaraman et al., 2001) but is not present in these cell lines, leading to the abovementioned decreased viability.

Interestingly, many of the *in vitro* studies focus on the permeation enhancing effects of chitosan in the intestinal Caco-2 cell line whereas *in vivo* studies predominantly focus on intranasal and intratracheal delivery (Table 6). The ER in these *in vivo* studies ranged from 0.8 for atenolol (Schipper et al., 1999) to 17.3 for insulin (Yu et al., 2004). However, one study showed that chitosan produced an ER of 51 for buserelin after intranasal administration in rats (Luessen et al., 1996). With both the studies done by Yu et al. and Luessen et al., the chitosan concentration was 15 mg/ml and the morphology of the epithelial tissue was not studied after the permeation enhancement. *In vitro* and *in vivo* studies using chitosan at pH of 7.4 have given poor

permeation enhancing results (Borchard et al., 1996, Kotze et al., 1998). As discussed above, *N*-modified derivatives of chitosan have been synthesized to improve the solubility properties of chitosan at physiological pH and, consequently, their permeation enhancing effects. These include *N,N,N*-trimethylation (Florea et al., 2006), *N*-arylation (Kowapradit et al., 2011), *N*-carboxymethylation (Thanou et al., 2001a) and *N*-thiolation (Zambito et al., 2009) of chitosan.

5.4. TMC as a permeation enhancer

There is increasing interest in TMC as a permeation enhancer for intestinal, pulmonary and ocular drug delivery (Sahni et al., 2008) and has been reported to have mucoadhesive properties (Snyman et al., 2003). This current review focuses on the application of TMC, strictly as a permeation enhancer but it has also been used to formulate nanoparticles to improve delivery of insulin (Sandri et al., 2010) and ovalbumin (Amidi et al., 2006). Studies with solubilized TMC use mainly Caco-2 as *in vitro* cell model as can be seen in Table 7. The concentration to produce enhanced permeation varies from 0.5 mg/ml (Thanou et al., 2000b) to as high as 25 mg/ml (Kotze et al., 1997a), with permeation enhancement generally more prominent for small molecules than for macromolecules. With TMC at pH ~7.4, the degree of quaternization (DQ) comes into play as a major factor influencing the permeation enhancement (Jonker et al., 2002). In general, higher DQ will give higher ER (Kotze et al., 1999b, Thanou et al., 2000b). In contrast, one study reports that TMC with low DQ but high concentration (15-25 mg/ml) has given ER of 373 for FD4 (Kotze et al., 1997b) which seems remarkably high compared to other studies. It has also been observed that with concomitant increase in DQ there is a general decrease in mucoadhesion, attributed to the excessive polymer hydration (Sahni et al., 2008).

In vivo studies aimed at investigating the permeation enhancing effects of TMC have been carried out with both airway and intestinal models (Table 8). Concentrations needed to obtain an increased permeation enhancement varied, from 1.25 to 50 mg/ml, showing increased permeation as the DQ increased. Most previous synthesis methods for TMC have also produced unwanted *O*-methylation. An example of possible *O*-methylation affecting *in vivo* results can be shown with a study by Hamman and co-workers.

Table 7. Permeation enhancing effects of TMC in cell models at pH 7.4*

Ref	TJ, morphology, remarks	Viability	Model	DQ (%)	DA (%)	Conc. (mg/ml)	Permeation marker	ER	TER reduction[d]/ TER recovery[d]
1	NR	Trypan blue: no staining	Caco-2	12	25	10		NR	No effect
						15	Mannitol/ FD-4	32/167	~80/NR
						20		48/274	~50/NR
						25		60/373	~20/NR
2	NR	Trypan blue: no staining	Caco-2 (pH 6.2)	12	25	2.5	Mannitol/ FD-4	11/4	76/NR
						15		10/5	35/NR
						20		17/7	28/NR
						25		21/9	15/NR
3	NR	Trypan blue: no staining	Caco-2	39	7	10	Buserelin	21.2	NR
				63		10		60.0	NR
4	NR	Trypan blue: no staining	Caco-2 (pH 6.8)	13	17	15	Mannitol/ FD-4	19/4	~90/NR
						20		35/4	64/NR
						25		51/1	38/NR
				20	7	15		28/5	~80/NR
						20		56/7	47/NR
						25		97/17	32/NR
5	Complete recovery from TER was not observed	Trypan blue and propidium iodide: no staining	Caco-2	39	7	0.5	Mannitol	10.4	50/NR
						1		11.7	51/NR
						2.5		13.0	37/NR
						5		24.3	31/NR
						10		27.1	24/NR
				65	7	0.5		25.9	61/NR
						1		26.4	59/NR
						2.5		27.0	53/NR
						5		33.0	45/NR
						10		39.0	41/NR

Table 7 (contd.). Permeation enhancing effects of TMC in cell models at pH 7.4 *

Ref	TJ, morphology, remarks	Viability	Model	DQ (%)	DA (%)	Conc. (mg/ml)	Permeation marker	ER	TER reduction[d] /TER recovery[d]
6	Gel-phase formulation	MTT: no effects	Calu-3	20	7	15	Octreotide	16	89/100
				60	7	15		30	52/88
7	NR	MTT and LDH: Effect of TMC[a] (DQ 43%) above 0.1 mg/ml	Caco-2	43	17[a]	2.5		NR	~30/~50
				45	11[b]	2.5		NR	~70/~100
				44	55[c]	2.5		NR	No effect
8	O-CH$_3$ and N-(CH$_2$)$_2$ present	Trypan blue: staining	Caco-2	12	25	0.5	Mannitol	ND	No effect
						1		ND	No effect
						2.5		ND	No effect
						5		1	No effect
						10		2	No effect
						15		2	No effect
				61	25	0.5		31	65/65
						1		30	57/57
						2.5		32	54/54
						5		43	31/31
						10		48	40/40
						15		32	37/37
9	NR	Trypan blue: no staining	Caco-2 (pH 6.2)	12	25	15	Buserelin	34.5	45/NR
						25		68.5	26/NR
10	F-actin, occludin and claudin-1 were not altered	NR	Caco-2 (pH 7.2)	60	NR	10	Octreotide	4.5	30/64

* Unless otherwise stated. ND: not detected, ER: permeation enhancement ratio, [a]O-CH$_3$ free, 40% N-(CH$_2$)$_2$, [b]16-25% O-CH$_3$, 44% N-(CH$_2$)$_2$, [c]O-CH$_3$ free, [d]% initial value. Ref. **1**: (Kotze et al., 1997b), **2**: (Kotze et al., 1998), **3**: (Thanou et al., 2000a), **4**: (Kotze et al., 1999c), **5**: (Thanou et al., 2000b), **6**: (Florea et al., 2006), **7**: (Verheul et al., 2009), **8**: (Kotze et al., 1999b), **9**: (Kotze et al., 1997a), **10**: (Dorkoosh et al., 2004).

Table 8. Permeation enhancing effects of TMC in other models

	Ref	TJ, morphology and viability	Model (pH)	DQ (%)	Conc. (mg/ml)	ER
Airways	1	NR	Rats (7.4)	12	5	1.3[a]
				36	5	2.7[a]
				59	5	2.9[a]
	2	NR	Rats (6.0)	40	5	1.6[b]
	3	20% DQ caused neutrophil infiltration, 60% DQ showed mild irritation	Rats (7.4)	20	15	2.5[c]
				60	15	3.9[c]
Intestinal	4	NR	Rats (7.4)	22	0.625	1.17[a]
					1.25	1.27[a]
					2.5	1.44[a]
					5	1.78[a]
				49	0.625	1.30[a]
					1.25	2.04[a]
					2.5	3.41[a]
					5	4.20[a]
	5	NR	Pigs (7.4)	60	50	7.7[c]
					100	14.5[c]
	6	NR	Rats (7.2)	39	10	7.9[d]
				63	10	16.3[d]

NR: not reported, ER: permeation enhancement ratio. [a] Mannitol, [b] 2,3,5,6-tetramethylpyrazine, [c] octreotide, [d] buserelin. Ref. **1**: (Hamman et al., 2002), **2**: (Mei et al., 2008), **3**: (Florea et al., 2006), **4**: (Jonker et al., 2002), **5**: (Thanou et al., 2001b), **6**: (Thanou et al., 2000a).

They concluded that the maximal permeation enhancing effect could be reached with TMC having DQ of 48%, with no added effect with 59% DQ (Hamman et al., 2002). Yet, the degree of *O*-methylation was not reported. TMC with 59% DQ was produced with additional methylation step compared to the TMC with 48% DQ (Hamman et al., 2002). Since this methylation process has been reported to yield more *O*-methylation with more reaction steps, which lowers its solubility in aqueous solutions (Polnok et al., 2004) in addition to diminishing the permeation enhancing properties of TMC (Verheul et al., 2008, Verheul et al., 2009). Therefore, the absence of permeation enhancement for the more quaternized derivatives in this study could therefore be due to increased *O*-methylation.

In addition to TMC, other *N*-alkyl quaternary chitosan derivatives have been synthesized and tested as possible permeation enhancers. TMC proved to be more

efficient in increasing the permeation in Caco-2 cells and was in the order of *N,N,N*-trimethyl > *N*-ethyl-*N,N*-dimethyl > *N*-methyl-*N,N*-diethyl > *N,N,N*-triethyl chitosan (Sadeghi et al., 2008). Other *N*-quaternized chitosan derivatives such as *N*-piperazine, *N*-betainate (Korjamo et al., 2008) and *N*-aryl (Kowapradit et al., 2011) chitosan derivatives have also been reported to act as efficient permeation enhancers.

5.5. Safety of chitosan permeation enhancers

Increased permeability and decreased TER may be due to reduced viability of the cell layer rather than an effect on the TJ barrier. A variety of assays such as 3-(4,5-dimethylthiazol-2-yl)-2,5-diphenyltetrazolium bromide (MTT), lactate dehydrogenase (LDH) and trypan blue have been used to assess the effects of chitosan and its derivatives on viability. However, these assays are not in agreement regarding the effects of chitosan and its derivatives on viability. All trypan blue staining for cytotoxicity of chitosan and TMC are negative, indicating that viability is not affected (Table 5 and 7).Since trypan blue only assess if the cell is dead or alive, it might not be the best marker to assess reduced viability where chitosan could have adverse effects on cells that take longer time to emerge.

MTT is a convenient high throughput assay that measures metabolic activity of the cell by spectrophotometry. This assay can be considered as a more relevant assay since there is a linear response between the cell activity and the absorbance readout. MTT has also been reported to be more sensitive than neutral red assay and more reliable than LDH for evaluating acute toxicity of excipients in the Calu-3 cell line (Scherließ, 2011). This assay showed that the viability was affected from as low as 0.05 mg/ml chitosan (Schipper et al., 1996) to as high as 4 mg/ml (Kudsiova and Lawrence, 2008) in the Caco-2 cell line (Table 7) with low DA reported to decrease the viability (Schipper et al., 1996).

As can be seen in Table 6, not many studies have focused on reporting the morphology after chitosan treatment *in vivo*. Where reported, the epithelium appears to be disordered or separated from the underlying tissue (Illum et al., 1994, Schipper et al., 1999), with sights of neutrophil infiltration after intratracheal administration (Florea et al., 2006). This shows the importance of characterizing the impact on the epithelium, which could be due to adverse effects on the epithelial structure and function. The

majority of the permeation studies have been done with Caco-2 cells, thus aiming for the oral drug delivery.

There are also disparities in the reports of TMC cytotoxicity as Table 7 shows. Treatment with partially trimethylated chitosan (DQ ~45%) resulted in decreased viability above 0.1 mg/ml (Verheul et al., 2009) as determined with MTT and LDH viability assays. Introducing partial *O*-methylation or increasing the DA abolished this effect (Verheul et al., 2008, Verheul et al., 2009). Another study showed that TMC with DQ of 20 and 60% did not show any effect on the viability at a concentration of 15 mg/ml (Florea et al., 2006) as determined with MTT. In general, *in vivo* TMC studies have not been done to investigate the effects of DQ on morphological changes. Nevertheless, one study showed some level of neutrophil infiltration in the investigated trachea (Florea et al., 2006).

5.6. Possible mechanism of chitosan permeation enhancement

The permeation enhancing effect of chitosan and TMC have been well documented in the decrease of TER and increase in the permeability of inert markers of paracellular permeation. Studies disagree whether the mechanism behind the permeation enhancement lies in alterations of TJs or TJ associated proteins. F-actin disbandment or redistribution has been introduced as a partial explanation for the permeation enhancing properties of chitosan (Artursson et al., 1994, Dodane et al., 1999, Schipper et al., 1997) whilst others have reported no effect on actin structure (Rosenthal et al., 2012, Smith et al., 2004). Reduced ZO-1 or occludin expression (Dodane et al., 1999, Smith et al., 2004, Smith et al., 2005, Vllasaliu et al., 2010) and their possible relocalization to the cytoskeleton (Smith et al., 2004) has also been proposed to contribute to the permeation enhancing effect of this polymer. Much focus has been on the subcellular localization of actin and ZO-1 but the effects of chitosan on the expression of the barrier forming claudin family has only been occasionally investigated. One study reports that chitosan causes claudin-4 to be internalized into lysosomes, followed by synthesis of claudin-4 after chitosan removal (Yeh et al., 2011). The most recent study, by the same research group, then reported the TJ disruption to be due to electrostatic interaction of chitosan to integrins ultimately leading to claudin-4 internalization (Hsu et al., 2012). Direct evidence of TJ opening after 0.2 mg/ml chitosan treatment has been shown in both Caco-

2 cells and in mice, where the paracellular space stained positive for the trivalent cation lanthanum (Sonaje et al., 2012) which under normal circumstances does not permeate into the paracellular space.

Although most studies report paracellular permeation enhancement after chitosan treatment, one study showed that chitosan affected both para-and transcellular permeation (Rosenthal et al., 2012). Large intracellular vesicles and swollen endoplasmic reticulum have been observed after chitosan treatment indicating induced endocytosis and increased cell metabolism respectively (Dodane et al., 1999). Interestingly, despite the general consensus that chitosan induces TJ opening, the precise mechanism explaining the effect has not been fully elucidated. Several proposed mechanisms are summarized in Table 9. There it can be seen that possible mechanisms for paracellular permeation enhancement are versatile.

Table 9. Possible mechanisms related to permeation enhancing effects of chitosan

Mechanism	Ref
Claudin-4 internalized to lysosomes followed by its synthesis in the recovery phase	**1**
JAM-1 translocation that recovered after treatment	**2**
Activation of the chloride-bicarbonate exchanger resulting in changes in intracellular pH leading to opening of the TJ	**3**
Activation of PKC signal transduction pathways that affect TJ opening	**4**
Electrostatic interaction between chitosan and integrins causing intracellular cascade involving tyrosine kinase phosphorylation leading to TJ disruption	**5**

Ref **1**: (Yeh et al., 2011), **2**: (Sonaje et al., 2012), **3**: (Rosenthal et al., 2012), **4**: (Smith et al., 2005), **5**: (Hsu et al., 2012).

The emergence of chitosan derivatives such as TMC has become more evident owing to their increased water solubility at physiological pH. Since TMC has the potential of being an effective carrier for protein based drugs in oral delivery (Chen et al., 2008) its properties and potential role in airway drug delivery deserve a further exploration.

AIM OF THE THESIS

Systemic delivery of macromolecular drugs through the lungs is a feasible alternative to injections. However, paracellular permeation of macromolecules is limited by the TJs. Permeation enhancers, such as the polysaccharide chitosan, have been proposed to increase the bioavailability of these drugs by transiently opening the TJs. Since chitosan is only soluble below pH 6.5, its potential use in pulmonary drug delivery is limited. By introducing permanent positive charge to the amino group, the polymer becomes soluble in aqueous solutions independent of the pH. However, the synthesis methods previously used are not selective since they also result in undesired *O*-methylation.

The following aims represent each paper/manuscript enclosed within the thesis:

I.   To develop a synthetic strategy that results in selective *N*-quaternization of the chitosan polymer without *O*-methylation (Paper # 1)

II. Regioselectively attach a fluorophore to the reducing end of TMC for molecular weight determination and visualization in a bronchial epithelium (Paper # 2)

III. To demonstrate that the VA10 bronchial epithelial cell line can model the native bronchial barrier, making it suitable to elucidate the permeation enhancing properties of the synthesized chitosan derivatives (Paper # 3)

IV. Determine the structure – activity relationship between the synthesized *N*-quaternary chitosan derivatives and their permeation enhancing effects in the VA10 cell model (Paper # 4)

EXPERIMENTAL METHODS

1. Materials

1.1. General compounds

Chitosan polymer HCl (G020102-1) was used with an average MW of 8.1 kDa, as determined by end-reducing assay (Miller, 1959), and 8.5 kDa, as determined by viscometric methods (Ottoy et al., 1996). The degree of acetylation was 0.03, determined by ^{1}H NMR. Chitosan was obtained by donation from Genis EHF, Iceland. Atenolol, alprenolol HCl, (±)-metoprolol (+)-tartarate, (±)-propranolol HCl, sodium fluorescein (Flu-Na), FD 4, 10, 20 and 40 kDa, Rh123, terbutaline hemisulfate and verapamil HCl were obtained from Sigma-Aldrich (St. Louis, USA). Hanks Balanced Salt solution (HBSS) containing NaCl (146.94 mM), KCl (5.37 mM), Na_2HPO_4 (0.34 mM), KH_2PO_4 (0.44 mM), $CaCl_2$ x 2 H_2O (1.80 mM), $MgSO_4$ (0.81 mM), $NaHCO_3$ (25 mM), D-glucose (5.55 mM) and HEPES (25 mM) was buffered at pH 7.4. All other chemicals (obtained from Sigma-Aldrich®) were reagent grade or higher and used as received, with the exception of dimethylsulfoxide (DMSO), dichloromethane (DCM) and NMP, which were stored over molecular sieves overnight before use. Dialysis membranes (Spectra/Por, MW cutoff 3500 Da) and Float-A-Lyzers (Spectra/Por, MW cutoff 3.5-5 kDa, 5 ml sample volume) were purchased from Spectrum® Laboratories Inc. (Rancho Dominguez, USA).

1.2. Cell culture medium and equipment

The cell culture medium LHC-9 and Dulbecco's minimum essential medium:Ham's F12 1:1 (DMEM/F-12) medium were obtained from Gibco (Burlington, Canada) and supplemented with 50 IU/ml penicillin, 50 μg/ml streptomycin and 40 μg/ml azithromycin (Pfizer). Ultroser-G serum substitute was purchased from Pall Life Sciences (Cergy-Saint-Christophe, France). Fetal bovine serum (FBS) was obtained from Gibco (Life Technologies, NY, USA). Chambered culture slides were purchased from BD Falcon (Bedford, MA, USA). Cell culture plastics were obtained from Becton Dickinson (NJ, USA). Transwell cell culture filters (pore size 0.4 μm, 12 mm diameter, polyester membrane) were purchased from Corning Costar corporation (through Sigma-Aldrich) and were collagen coated with PureCol® solution from Advanced BioMatrix (CA, USA).

2. Synthesis

Equivalent quantities of reagents were calculated on the bases of one glucosamine unit. NMR assignments for hydrogen and carbon atoms on the chitosan backbone are according to Figure 9.
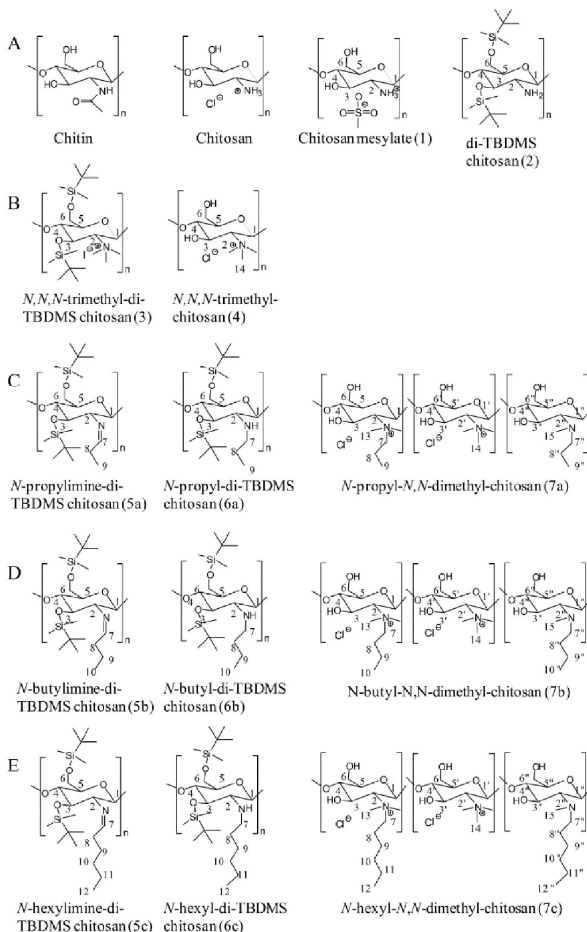
Figure 9. Structure and numbering of all the chitosan derivatives synthesized for the *N*-alkyl-*N*,*N*-dimethyl chitosan final products.

A. chitosan precursors, B. *N*,*N*,*N*-trimethyl chitosan derivatives, C. *N*-propyl chitosan derivatives, D. *N*-butyl chitosan derivatives, E. *N*-hexyl chitosan derivatives.

2.1. di- *tert*-butyldimethylsilyl chitosan (di-TBDMS chitosan)

The di-TBDMS chitosan was synthesized according to a published procedure (Runarsson et al., 2008b, Song et al., 2010). **Chitosan mesylate (1).** FT-IR (KBr): ν 3376 (O-H), 2880 (C–H), 1677 (C=O amide I), 1586 (C=O amide II), 1384 (C-H), 1156-1074 (C-O) cm^{-1}. ^{1}H NMR (400 MHz, D$_2$O): δ 2.10 (CH$_3$, GlcNAc), 2.84 (CH$_3$S), 3.21 (H-2), 3.7–4.1 (H-3, H-4, H-5, H-6), 4.9 ppm (H-1, partially overlapped with the water peak). **3,6-*O*-di-*tert*-butyldimethylsilyl chitosan (di-TBDMS chitosan, 2).** FT-IR (KBr): ν 3469 (N-H), 2957-2859 (C-H), 1705 (C=O amide I), 1573 (C=O amide II), 1474 (C-H), 1390-1362 (C-H), 1109-1050 (C-O), 836-776 (Si-CH$_3$) cm^{-1}. ^{1}H NMR (400 MHz, CDCl$_3$): δ 0.05 ((CH$_3$)$_2$Si), 0.89 ((CH$_3$)$_3$C), 2.71 (H-2), 3.33 (H-5), 3.50 (H-3), 3.68 (H-4), 3.84-3.89 (H-6), 4.30 (H-1), 8.12-8.20 ppm (NH/NH$_2$).

2.2. *N,N,N*-trimethyl chitosan

***N,N,N*-trimethyl-di-TBDMS chitosan (3).** Di-TBDMS chitosan (**2**) (1.42 g, 3.6 mmol di-TBDMS-glucosamine units) was dissolved in dry NMP (20 ml). Cesium carbonate (Cs$_2$CO$_3$, 4.63 g, 14.2 mmol, 4 equiv.) was added and the solution stirred for 3 h, followed by addition of methyl iodide (CH$_3$I, 1.11 ml, 17.8 mmol, 5 equiv.). The reaction was carried out in a closed reaction vial at 50°C. Note: Caution must be taken when handling CH$_3$I; a special chemical vapor-proof mask should be used when appropriate. After 24 and 48 h, additional CH$_3$I (1.11 ml, 17.8 mmol, 5 equiv.) was added to the brown reaction solution, and the reaction was carried out for a total of 96 h. The solution was then dialyzed against deionized water for 4 days and freeze-dried overnight, giving a dark red product. ^{1}H NMR (300 MHz, CDCl$_3$): δ 0.01-0.31((CH$_3$)$_2$Si), 0.86-0.90 ((CH$_3$)$_3$C), 3.64 ppm (N$^+$-(CH$_3$)$_3$. partially overlapped by H-1 to H-6). Yield: 1.856 g (93%).

***N,N,N*-trimethyl chitosan (4).** The trimethylated protected product (**3**) (1.856 g, 3.30 mmol *N,N,N*-trimethyl-di-TBDMS-glucosamine units) was deprotected by treatment with 1M tetrabutylammonium fluoride (TBAF) solution in NMP (10 ml) at 50°C for 72 h. The resulting solution was dialyzed for 4 days against deionized water, then ion-exchanged against 5% aq. NaCl (w/v) overnight followed by dialysis against deionized water for 2 days. The resulting compound was then freeze-dried, giving deprotected, trimethylated chitosan. In cases where NMR analysis showed that the trimethylated chitosan was not fully deprotected (< 0.1% TBDMS), the deprotection process was repeated. The material was then dissolved in 5% aq. NaCl (10 ml) and shaken overnight. The solution was centrifuged and the liquid decanted from grey precipitates, dialyzed for 3 days against deionized water and freeze-dried overnight, resulting in white and fluffy trimethylated chitosan. FT-IR (KBr): ν 3422 (O-H), 2923 (C-H), 1653 (C=O amide I), 1488 (C-H), 1051 (C-O) cm^{-1}. ^{1}H NMR (300 MHz, D$_2$O): δ 2.08 (CH$_3$, GlcNAc), 3.35 (N$^+$-(CH$_3$)$_3$, H-14), 3.75 (H-2), 3.90 (H-6), 3.99 (H-5), 4.36 (H-4), 4.47 (H-3), 5.49 ppm (H-1). ^{13}C NMR (300 MHz, D$_2$O): δ 54.6 (C-14), 61.6 (C-6), 68.7 (C-3), 76.2 (C-5), 77.9 (C-4), 79.4 (C-2), 97.2 ppm (C-1). Yield: 238 mg (29%).

2.3. General procedure for *N*-alkyl-*N,N*-dimethyl chitosan

***N*-alkylimine-di-TBDMS chitosan (5).** Compound **2** (1.50 g, 3.80 mmol di-TBDMS-glucosamine units) was dissolved in DCM (15 ml). Triethylamine (0.575 ml, 4.1 mmol, 1.1 equiv.) was added and the solution stirred for 15 minutes. Then, 5 equivalents of the corresponding aldehyde, (propyl, butyl or hexyl) was added to the solution, along with molecular sieves, and stirred overnight at 45°C in a closed reaction vial. After 24 hours of reaction, another 5 equivalents of aldehyde was added and the reaction carried out for a total of 96 hours at 45°C. The solvent was then partially evaporated under reduced pressure and the resulting material precipitated in acetonitrile (ACN) (150 ml). The white solid was filtered off and washed with ACN (3 x 30 ml), allowed to air-dry and then further dried in a vacuum oven at 40°C overnight, giving an off-white compound. ***N*-propylimine-di-TBDMS chitosan (5a)** FT-IR (KBr): ν 3462 (N-H), 2957-2858 (C-H), 1707 (C=O, amide I), 1675 (N=C), 1473 (C-H), 1390-1362 (C-H), 1257 (C-N), 1116-1052 (C-O), 836-777 (Si-CH$_3$) cm^{-1}. ^{1}H NMR (300 MHz, CDCl$_3$): δ 0.05 ((CH$_3$)$_2$Si), 0.86 ((CH$_3$)$_3$C), 1.06 (H-9), 2.23 (H-8), 2.82 (H-2), 3.13-4.21 (H-3, H-4, H-5, H-6), 4.50 (H-1), 7.50 ppm (H-7). Yield: 1.276 g (76%) starting from 1.200 g of **(2)**. ***N*-butylimine-di-TBDMS chitosan (5b)** FT-IR (KBr): ν 3467 (N-H), 2958-2858 (C-H), 1705 (C=O, amide I), 1673 (N=C), 1473 (C-H), 1389-1362 (C-H), 1256 (C-N). 1113-1056 (C-O), 837-777 (Si-CH$_3$) cm^{-1}. ^{1}H NMR (400 MHz, CDCl$_3$): δ 0.05 ((CH$_3$)$_2$Si), 0.86 ((CH$_3$)$_3$C and H-10) 1.53 (H-9), 2.19 (H-8), 2.81 (H-2), 3.08-4.21 (H-3, H-4, H-5, H-6), 4.52 (H-1), 7.48 ppm (H-7). Yield: 1.433 g (84%) starting from 1.500 g of **(2)**. ***N*-hexylimine-di-TBDMS chitosan (5c)** FT-IR (KBr): ν 3480 (N-H), 2958-2858 (C-H), 1704 (C=O, amide I), 1674 (N=C), 1473 (C-H), 1389-1362 (C-H), 1257 (C-N), 1117-1061 (C-O), 837-777 (Si-CH$_3$) cm^{-1}. ^{1}H NMR (300 MHz, CDCl$_3$): δ 0.05 ((CH$_3$)$_2$Si), 0.86 ((CH$_3$)$_3$C and H-12), 1.32 (H-10, H-11), 1.51 (H-9), 2.19 (H-8), 2.79 (H-2), 3.12-3.90 (H-3, H-4, H-5, H-6), 4.45 (H-1), 7.44 ppm (H-7). Yield: 1.169 g (98%) starting from 1.000 g of **(2)**.

***N*-alkyl-di-TBDMS chitosan (6).** The corresponding imine (2.13 mmol *N*-alkylimine-di-TBDMS-glucosamine units, compounds **5a**, **5b** and **5c**) was dissolved in DCM (20 ml). Sodium triacetoxyborohydrate (STAB-H, 1.81 g, 8.5 mmol, 4 equiv.) was added to the solution, followed by addition of AcOH (488 μL, 8.5 mmol, 4 equiv.). The solution was then stirred for 24 h at room temperature. Finally, the compound was precipitated in ACN (200 ml). The white solid was filtered off and washed with water (2 x 10 ml) and ACN (3 x 30 ml), air-dried and then further dried in a vacuum oven at 40°C overnight, yielding an off-white compound. ***N*-propyl-di-TBDMS chitosan (6a)** FT-IR (KBr): ν 3468 (N-H), 2958-2858 (C-H), 1708 (C=O amide I), 1473 (C-H), 1389-1362 (C-H), 1256 (C-N), 1110-1047 (C-O), 837-777 (Si-CH$_3$) cm^{-1}. ^{1}H NMR (300 MHz, CDCl$_3$): δ 0.07 ((CH$_3$)$_2$Si), 0.9 ((CH$_3$)$_3$C overlapped with H-9), 1.42 (H-8), 2.39 (H-2), 2.58 and 2.72 (H-7), 3.32-3.97 (H-3, H-4, H-5, H-6), 4.21 ppm (H-1). Yield: 827 mg (88%) starting from 935 mg of **5a**. ***N*-butyl-di-TBDMS chitosan (6b)** FT-IR (KBr): ν 3467 (N-H), 2958-2858 (C-H), 1706 (C=O, amide I), 1473 (C-H), 1389-1362 (C-H), 1257 (C-N), 1113-1056 (C-O), 837-777 (Si-CH$_3$) cm^{-1}. ^{1}H NMR (400 MHz, CDCl$_3$): δ 0.07

((CH$_3$)$_2$Si), 0.90 ((CH$_3$)$_3$C overlapped with H-10), 1.33 (H-8, H-9), 2.38 (H-2), 2.59 and 2.77 (H-7), 3.25-3.99 (H-3, H-4, H-5, H-6), 4.21 ppm (H-1). Yield: 1.388 g (98%) starting from 1.405 g of **5b**. *N*-hexyl-di-TBDMS chitosan (6c) FT-IR (KBr): ν 3466 (N-H), 2958-2858 (C-H), 1709 (C=O, amide I), 1473 (C-H), 1390-1362 (C-H), 1257 (C-N), 1115-1053 (C-O), 837-777 (Si-CH$_3$) cm^{-1}. ^{1}H NMR (300 MHz, CDCl$_3$): δ 0.07 ((CH$_3$)$_2$Si), 0.90 ((CH$_3$)$_3$C overlapped with H-12), 1.27 (H-8, H-9, H-10, H-11), 2.38 (H-2), 2.58 and 2.76 (H-7), 3.40-3.98 (H-3, H-4, H-5, H-6), 4.21 ppm (H-1). Yield: 837 mg (97%) starting from 856 mg of **5c**.

N-alkyl-*N,N*-dimethyl chitosan (7). The corresponding *N*-alkyl-di-TBDMS chitosan (1.6 mmol *N*-alkyl-di-TBDMS-glucosamine units; compounds **6a**, **6b**, **6c**) was dissolved in dry DCM (15 ml). Then, Li$_2$CO$_3$ (0.47 g, 6.4 mmol, 4 equiv.) was added to the solution and the mixture stirred for 1 h, followed by addition of dimethyl sulfate (DMS, 1.21 ml, 12.8 mmol, 8 equiv.). Note: Extreme caution must be taken when handling DMS; a special chemical vapor-proof mask should be used when appropriate. The reaction was carried out at 45°C in a closed reaction vial under vigorous stirring. After 24 h reaction time, the addition of DMS (1.21 ml, 12.8 mmol, 8 equiv) was repeated. The reaction was stopped after 96 h, by dialyzing the mixture against saturated NaHCO$_3$ solution for 1 day and then against deionized water for 4 days, followed by freeze-drying overnight. The quaternized protected material was then dissolved in 1M TBAF solution in NMP (10 ml) and stirred at 50°C for 48 h. The yellow solution was then dialyzed against deionized water for 1 day, ion exchanged against 5% aq. NaCl (w/v) solution for 1 day and then against deionized water for 2 days. The resulting material was freeze-dried overnight, yielding a deprotected quaternized material. In cases where NMR analysis indicated that the material was not fully deprotected, the deprotection process was repeated. Finally, the material was dissolved in 5% aq. NaCl (10 ml) and shaken overnight. The solution was centrifuged and the liquid decanted from grey precipitates and dialyzed for 3 days against deionized water, followed by freeze-drying overnight, giving a white and fluffy quaternized material. ***N*-propyl-*N,N*-dimethyl-chitosan (7a).** FT-IR (KBr): ν 3416 (O-H), 2970-2880 (C-H), 1635 (C=O, amide I), 1480 (C-H), 1051 (C-O) cm^{-1}. ^{1}H NMR (300 MHz, D$_2$O): δ 0.88 (H-9''), 0.99 (H-9), 1.50 (H-8''), 1.89 (H-8), 3.27 (H-13), 3.35 (H-14), 3.46 and 3.57 (H-7), 3.79 (H-2), 3.90-3.95 (H-5, H-6), 4.37 (H-4), 4.49 (H-3), 4.89 (H-1''), 5.45 (H-1'), 5.53 ppm (H-1). ^{13}C NMR (300 MHz, D$_2$O): δ 10.5 (C-9), 16.5 (C-8), 51.1 and 51.5 (C-13), 54.6 (C-14), 61.8 (C-6), 67.5 (C-7), 68.5 (C-3), 76.3 (C-5), 78.0 (C-2 and C-4), 96.0 (C-1'), 97.2 ppm (C-1). Yield: 211 mg (46%) starting from 800 mg of **6a**. ***N*-butyl-*N,N*-dimethyl-chitosan (7b).** FT-IR (KBr): ν 3405 (O-H), 2961-2876 (C-H), 1647 (C=O, amide I), 1474 (C-H), 1386 (C-H), 1257 (C-N), 1057 (C-O) cm^{-1}. ^{1}H NMR (400 MHz, D$_2$O): δ 0.97 (H-10, H-10''), 1.41 (H-9, H-9'', H-8''), 1.85 (H-8), 3.17 (H-15), 3.27 (H-13), 3.34 (H-14), 3.49 and 3.61 (H-7), 3.78 (H-2), 3.87 (H-6), 3.94 (H-5), 4.35 (H-4), 4.49 (H-3), 5.11 (H-1''), 5.46 (H-1'), 5.53 ppm (H-1). ^{13}C NMR (400 MHz, D$_2$O): δ 10.5 (C-10''), 13.6 (C-10, C-9''), 19.8 (C-9), 24.7 (C-8, C-8''), 47.3 (C-15), 51.2 and 51.6 (C-13), 54.6 (C-14), 61,8 (C-6), 66.2 (C-7), 68.5 (C-3), 76.3 (C-5), 77.7 (C-2), 77.9 (C-4), 96.0 (C-1'), 97.2 ppm (C-1). Yield:

92 mg (11%) starting from 1.381 g of **6b**. **N-hexyl-N,N-dimethyl-chitosan (7c)**. FT-IR (KBr): ν 3418 (O-H), 2956-2860 (C-H), 1645 (C=O, amide I), 1470 (C-H), 1380 (C-H), 1225 (C-N), 1056 (C-O) cm^{-1}. ^{1}H NMR (300 MHz, D$_2$O): δ 0.90 (H-12), 1.36 (H-9, H-10, H-11), 1.86 (H-8), 3.27 (H-13), 3.34 (H-14), 3.46 and 3.62 (H-7), 3.76 (H-2), 3.89-3.92 (H-6), 3.97 (H-5), 4.32 (H-4), 4.50 (H-3), 5.51 ppm (H-1). ^{13}C NMR (300 MHz, D$_2$O): δ 13.5 (C-12), 21.8 (C-8), 22.0 (C-11), 25.3 (C-9), 30.5 (C-10), 50.8 and 51.1 (C-13), 54.0 (C-14), 61.3 (C-6), 65.8 (C-7), 67.9 (C-3), 76.0 (C-5), 77.0 (C-2), 77.4 (C-4), 96.7 ppm (C-1). Yield: 238 mg (49%) starting from 766 mg of **6c**.

2.4. Dimethyl and trimethyl chitosan

N,N-dimethyl- and *N,N,N* trimethyl chitosan were synthesized according to a published procedure (Verheul et al., 2008).

N,N-dimethyl chitosan (8). ^{1}H NMR (300 MHz, D$_2$O/d-acetic acid): δ 2.06 (CH$_3$, GlcNAc), 3.06 (N-(CH$_3$)$_2$), 3.39 (H-2), 3.75-3.97 (H-5, H-6), 4.10 (H-4), 4.23 (H-3), 5.10 ppm (H-1). ^{13}C NMR (300 MHz, D$_2$O): δ 42.0 (N-(CH$_3$)$_2$), 60.5 (C-6), 67.5 (C-3), 68.3 (C-2), 74.6 (C-5), 75.8 (C-4), 95.2 (C-1) ppm. Yield: 198 mg (82%).

N,N,N trimethyl chitosan (9). Partially trimethylated chitosan was prepared according to a published procedure (Verheul et al., 2008). ^{1}H NMR (300 MHz, D$_2$O): δ 2.10 (CH$_3$, GlcNAc), 2.78 (N-(CH$_3$)$_2$)), 3.35 (N$^+$-(CH$_3$)$_3$), 3.75 (H-2), 3.82-3.97 (H-5, H-6), 4.16-4.25 (H-3, H-4, dimethyl), 4.37 (H-4, trimethyl), 4.47 (H-3, trimethyl), 5.42 (H-1, dimethyl), 5.49 ppm (H-1, trimethyl). ^{13}C NMR (300 MHz, D$_2$O): δ 42.3 (N-(CH$_3$)$_2$), 54.6 (N-(CH$_3$)$_3$), 61.7 (C-6), 68.7 (C-3), 75.1 (C-2, dimethyl), 76.2 (C-5), 77.8 (C-4), 79.3 (C-2, trimethyl), 96.2 (C-1, dimethyl), 97.2 ppm (C-1, trimethyl). Yield: 98.5 mg (63%).

2.5. EDANS-O-NH$_2$

Synthesis of 5-(2-((aminooxyacetyl)amino)ethylamino)naphthalene-1-sulfonic acid (EDANS-O-NH$_2$, **10**) was carried out according to a previously published procedure (Takaoka et al., 2006) but with several modifications. 1,5-EDANS (266 mg, 1 mmol) was added to a solution of *N*-Boc-aminooxyacetic acid (291 mg, 1 mmol), *O*-benzotriazole-*N,N,N',N'*-tetramethyluronium hexafluorophosphate (379 mg, 1 mmol), 1-hydroxy-benzotriazole hydrate (135 mg, 1 mmol) and *N,N'*-diisopropylethylamine (342 μL, 2 mmol) in dimethylformamide. The reaction was stirred at room temperature for 16 h. The product was purified using HPLC on a C18 column with a gradient from 5% to 30% acetonitrile in H$_2$O. The freeze-dried product was then dissolved in trifluoroacetic acid (TFA)/CH$_2$Cl$_2$ (1:1) and stirred for 2 h at room temperature to remove the Boc group. TFA and CH$_2$Cl$_2$ were removed by N$_2$. The resulting solid was then redissolved in water/acetonitrile (1:1) then freeze-dried to provide the title compound (276 mg, 81% for the two steps) as a white solid. ^{1}H NMR (300 MHz, D$_2$O): δ ppm 3.52 (t, J_H = 5.8 Hz, 2H), 3.65 (t, J_H = 5.7 Hz, 2H), 4.13 (s, 2H), 6.95 (d, J_H = 7.8 Hz, 1H), 7.56 (t, J_H = 7.5 Hz,

overlapped, 1H), 7.59 (t, J_H= 7.8 Hz, overlapped, 1H), 8.06 (d, J_H= 8.6 Hz, 1H), 8.14 (dd , J_{H3}= 7.3 Hz, J_{H4}= 0.9 Hz, 1H), 8.20 (d, J_H= 8.7 Hz, 1H).

2.6. End-labeled TMC

TMC-imine-EDANS (11). TMC (36 mg) and 1,5-EDANS (7 mg) were stirred in 3 ml of acetate buffer (100 mM, pH 4.5) in the presence of aniline (100 mM), in a closed reaction vial, protected from light, at 50°C for 72 h. The solution was then dialyzed in the dark against water for 24 h, then against 5% aq. NaCl solution for 24 h and finally against water for an additional 48 h (yield: 33 mg (92%)).

TMC-oxime-EDANS (f-TMC, 12). TMC (36 mg) and EDANS-O-NH$_2$ (7 mg) were dissolved in 3 ml acetate buffer (100 mM, pH 4.5) in the presence of aniline (100 mM) and stirred in a closed reaction vial, protected from light, at 50°C for 72 h. The solution was dialyzed in the dark against water for 24 h, then against 5% aq. NaCl solution for 24 h and finally against water for additional 48 h (yield: 35 mg (98%)). 1H NMR (500 MHz, D2O): δ ppm 2.09 (s, ~0.03H), 3.35 (s, 9H), 3,53 (br m, ~0.06H), 3.65 (br m, ~ 0.06H), 3.76 (s, 1H), 3.88-3.92 (m, 1H), 3.99 (m, 1H), 4.12 (m, ~0.02H), 4.37 (t, 1H), 4.48 (t, 1H), 5.50 (s, 1H), 6.92 (br s, ~0.03H), 7.59 – 7.63 (br s, ~ 0.08H), 8.03-8.07 (m, ~0.03H), 8.16 (m, ~ 0.03H), 8.21 (m, ~ 0.03H).

3. Characterization

3.1. NMR analysis

^{1}H NMR, ^{13}C NMR, ^{1}H-^{1}H COSY and ^{1}H-^{13}C HSQC spectra were recorded with either a Bruker Avance 300 operating at 300.13 MHz and 75.47 MHz at 300K, a Bruker Avance 400 instrument operating at 400.13 and 100.61 MHz at 300K, or a Bruker 500 MHz instrument with an Observe cryoprobe. CDCl$_3$, d$_6$-DMSO and D$_2$O were used as NMR solvents. Acetone was used as reference in D$_2$O NMR spectra for final compounds: proton (δ 2.22 ppm) and carbon (δ 30.9 ppm). Spectra were measured without water suppression. Sample concentrations ranged from 10-25 mg/ml.

3.2. Calculations based on ^{1}H NMR data

Calculations of degree of substitution (DS) for *N*-substituted chitosan derivatives.

Integral values from ^{1}H NMR were used to determine the DS for *N*-substituted chitosan derivatives (Table 10).

Calculations of the average molecular weight of f-TMC (12).

The average molecular weight (MW) was determined from the ^{1}H NMR data by end-group analysis with equations 1-4. First, the ratio of EDANS-O-NH$_2$ protons on the end-group in TMC-oxime-EDANS (D$_{EDANS-O-NH2}$) was determined from ^{1}H NMR spectra using Eq. 1, with the integral from protons H-g (from EDANS-O-NH$_2$) and H-1 (from TMC). Ratio of TMC units in TMC-oxime-EDANS (D$_{TMC}$) was then determined with

Eq. 2. Number of TMC repeating units were calculated according to Eq. 3. Finally, the MW was could be determined from Eq. 4.

3.3. FT-IR analysis

Samples were mixed thoroughly with KBr and then pressed into pellets using a Specac compressor (Specac Inc., Smyrna, USA). FT-IR measurements were performed with an AVATAR 370 FT-IR instrument (Thermo Nicolet Corporation, Madison, USA) with 32 scans and resolution of 4 cm^{-1}.

Table 10. Equations for the calculation of *N*-substituted chitosan derivatives

Chitosan derivative	Structure	Equation	Substitution
***N*-alkylimine-di-*O*-TBDMS-chitosan (5)**. R = -CH2CH3(**a**), -CH₂CH₂CH₃ (**b**) or -CH₂CH₂CH₂CH₃ (**c**)		$A = \left(\dfrac{\int H - 7}{\int (S\dot{i} - (CH_3)_2)_2} \times \dfrac{1}{1} \dfrac{2}{1} \right)$	*N*-alkylation
***N,N,N*-trimethyl chitosan (4)**		$B = \left(\dfrac{\int H - 14}{\int H - 1} \times \dfrac{1}{9} \right)$	*N,N,N*-trimethylation
N*-alkyl-*N,N*-dimethyl chitosan (7) R = -CH2CH₃(**a**), -CH₂CH₂CH₃(**b**) or -CH₂CH₂CH₂CH₃(**c**)		$C = \left(\dfrac{\int (CH_3\;i\;n\;l\;kc\;yh\;la)\;i\;h}{\int (H - 1, 1', 1'')} \times \dfrac{1}{3} \right) - E$	*N*-alkyl-*N,N*-dimethyl
		$D = \left(\dfrac{\int (H - 1,1')}{\int (H - 1, 1', 1'')} \times \dfrac{1}{1} \right) - C$	*N,N,N*-trimethylation
		$E = \left(\dfrac{\int H - 15}{(\int H - 1, 1', 1')_r} \times \dfrac{1}{3} \right)$	*N*-alkyl-*N*-monomethyl

* Substitution determined at pH 3

41

$$D_{EDANS-O-NH_2} = \left(\frac{\int H-g}{\int H-1} \times \frac{\text{Theoretical number of protons } h-s1}{\text{Theoretical number of protons } h-sg} \right) = \left(\frac{\int H-g}{\int H-1} \times \frac{1}{1} \right)$$

Eq.1

$$D_{TMC} = 1 - D_{EDANS-O-NH_2}$$

Eq. 2

$$\text{Number of TMC per amine} = \frac{(D_{TMC})}{(D_{EDANS-O-NH_2})}$$

Eq. 3

$$MW_{TMC-oxime-EDANS} = (\text{Number of TMC per amine} \times MW_{monomer TMC unit})$$

Eq. 4

3.4. Fluorescence spectrometry

Fluorescence intensity was measured using a Spex FluoroMax at 22°C with excitation wavelength of 335 nm. Each spectrum was the average of three accumulations. Equal amount of samples (mg/ml) in water were measured to enable direct comparison of fluorescence intensity. Calibration curve of EDANS fluorescence (0.18-195 ×10^{-6} M) was measured using fluorescence plate reader (Tecan GENios microplate reader, Männedorf, Switzerland) with excitation filter of 360 nm and emission filter of 535 nm. The calibration curve was used to calculate $D_{EDANS-O-NH2}$ and then equations 2-4 were used to calculate the MW of TMC-oxime-EDANS.

3.5. MALDI-TOF MS

Mass spectra of TMC (4) were obtained using Microflex matrix assisted laser desorption/ionization time-of-flight (MALDI-TOF) mass spectrometer (Bruker, Bremen, Germany). Spectra were collected in the positive ion mode with 100 laser shots summed to produce the final spectrum. Measurements were done without baseline correction. Either 2,5-dihydroxybenzoic acid or α-cyano-4-hydroxycinnamic acid was used as the matrix (10 mg/ml). 1 μl of the matrix was mixed on a steel target plate with 1 μl of the TMC (1 mg/ml) and allowed to air-dry at room temperature.

4. In vitro studies

4.1. Culture of the VA10 Bronchial Epithelial Cell Line

The newly established bronchial epithelial cell line, VA10 (Halldorsson et al., 2007), was used between passages 15-21. The cells were maintained in 75 cm^2 flasks in a humidified incubator at 37°C (5% CO$_2$) containing bronchial epithelial growth medium (LHC-9) with supplements. Medium was aspirated and changed every other day with a fresh, prewarmed medium. For chamber slide cultures, the cells were seeded at a density of 7 x 10^5 cells/cm^2 and cultured in LHC-9 until confluent. For uptake studies, the cells were seeded at a density of 2.1 x 10^4 cells/cm^2 on 12 well cell culture plates and cultured in LHC-9 until confluent. For TER and permeability experiments, cells were seeded at

the density of 2×10^5 cells/cm^2 in the upper chamber of collagen coated Transwell filters and cultured with LHC-9 medium for 5-6 days with 0.5 ml medium added to the apical side and 1.5 ml medium to the basolateral side. Subsequently, the cells were cultured in a DMEM/F-12 medium supplemented with 2% Ultroser G with medium changed every other day. For ALI culture, the medium was aspirated after 5 days in LCC from the apical side and filters rinsed with phosphate buffered saline (PBS) to bring the culture into ALI, having 1.5 ml of DMEM/F-12 medium with 2% Ultroser G medium at the basolateral side.

4.2. Visualization of f-TMC in the epithelium

The monolayers, cultured on chamber slides, were treated with either 0.5 mg/ml of f-TMC (12), 0.5 mg/ml of the hypothetical TMC-imine-EDANS (11) or 0.0026 mg/ml of EDANS (similar amount of fluorescent units per ml buffer as in 12) in HBSS buffer for 2 h. Subsequently, the monolayers were rinsed three times with prewarmed HBSS, fixed with 3.7 % formaldehyde in PBS (pH 7.4) for 10 min and fluoromount-G added before visualization. For co-staining with E-cadherin, the monolayer was permeabilized after fixation with 0.1 % Triton X-100/PBS for 7 min and blocked in 10% FBS in PBS for 10 min at room temperature. Subsequently, the monolayer was incubated with primary antibody against E-cadherin (1:125) for 30 min at room temperature followed by incubation with Alexa Fluor secondary antibody (1:1000) for 30 min and fluoromount-G added. All images were obtained with an epi-fluorescent microscope with matching filters (Nicon Eclipse-800) and photographed with Nikon DXM1200F digital camera.

4.3. Uptake studies of f-TMC in VA10 epithelial cells

The VA10 cell monolayers were treated with either 0.0026 mg/ml EDANS in HBSS or 0.5 mg/ml f-TMC (**12**) in HBSS for 2 h. The uptake was terminated by washing the monolayers three times with ice-cold HBSS. Fluorescence of the cell lysate, obtained by applying 300 µl of 2% SDS solution (pH 8) to each well, was measured using fluorescence plate reader (Tecan GENios microplate reader, Männedorf, Switzerland) with excitation filter of 360 nm and emission filter of 535 nm. Protein concentration of the cell lysate was determined using the Bradford assay. Uptake was expressed as the quantity of f-TMC or EDANS (µg) present in 1 mg of protein (Mean ± SD, n= 3-4). The uptake results were compared with unpaired, two tailed Student's *t*-test (GraphPad Prism, GraphPad Software, Inc., CA, USA) with $p < 0.05$ considered as statistical significant.

4.4. Transepithelial electrical resistance (TER) measurements

The TER of VA10 cells was measured with Millicell-ERS volthometer (Millipore, MA, USA) for LCC and ALI culture. Prewarmed PBS was added to the apical side of ALI cultured cells to be able to measure the TER. The corrected TER value was obtained after subtraction of the background from the cell-free culture insert.

4.5. General permeation studies

LCC and ALI cultured VA10 epithelium were used in the Flu-Na permeation studies at different time points to determine the function of the paracellular epithelial barrier. All other permeation studies were done on ALI cultured epithelium with TER above 800 $\Omega*cm^2$. Prior to the permeation studies, the cell layers were washed twice with HBSS (37°C) and then allowed to equilibrate in the incubator for 30 min in HBSS (0.5 ml apical and 1.5 ml basolateral). The TER was measured right before and after the experiment to ensure the epithelial integrity. Flu-Na was dissolved in HBSS buffer to a final concentration of 50 μM. FD with average molecular weight of 4, 10, 20 and 40 kDa (FD4, FD10, FD20, FD40) were dissolved in HBSS to a final concentration of 2.5 mg/ml. The model drugs alprenolol, metoprolol, propranolol and terbutaline were prepared in HBSS at final concentration of 100 μM, with atenolol containing 0.1% DMSO to enable solubilization and at the final concentration of 500 μM.

Before the permeation studies were started, the HBSS buffer was aspirated from the apical surface and replaced by 0.52 ml of prewarmed test solution. Immediately, a sample (20 μl) of this solution was removed to determine the initial concentration (C_0). The cells were incubated at 37°C and agitated on an orbital shaker at 80 rpm. Sampling from the basolateral compartment (100 μl for Flu-Na and FD, 200 μl for model drugs) was done after 20, 40, 60, 80 and 120 min and replaced with equal volume of fresh HBSS buffer. When the experiment was finished, a sample (20 μl) was removed from the apical chamber to determine drug recovery.

Bidirectional transport studies with the P-gp substrate Rh123 were performed with and without the P-gp efflux pump inhibitor verapamil. Flu-Na was used as a negative control. In studies with verapamil, the cell layers were incubated with verapamil (200 μM) for 1 h prior to the transport experiment. To ensure continued inhibition, verapamil was also present during the Rh123 transport experiment. Apical-to-basolateral and basolateral-to-apical transport were initiated by adding 0.52 ml or 1.52 ml respectively of either prewarmed Rh123 (50 μM) or Flu-Na (50 μM) to the donor chamber. Sampling (100 μl) from the receiver chamber was as described above.

4.6. *N*-quaternary chitosan solutions

Prior to use, chitosan derivatives were steri-filtered (0.4 μm) and freeze-dried to give aseptic material. Chitosan derivatives were then dissolved aseptically in HBSS to give the test concentrations of 1 mg/ml, 0.25 mg/ml, 0.063 mg/ml and 0.016 mg/ml.

4.7. MTT viability assay

For the general cell viability assay, cells were seeded on 96 well plates at the density of 1.4×10^4 cells per well and maintained in LHC-9 media for 24 h. Then, the medium was aspirated and cells rinsed with HBSS before incubation with the chitosan derivatives TMC, QuatPropyl, QuatButyl and QuatHexyl at for 2 h at 37°C. After incubation, the test solutions were aspirated and the cells rinsed twice with HBSS. Directly thereafter, 100

μl of HBSS were introduced to each well along with 10 μl of the MTT reagent and incubated for 4 h, to measure instant effects on viability. To measure late effects on cell viability or cell recovery, the cells were incubated for 24 h with LHC-9 after the 2 h treatment with the chitosan derivatives, before the addition of MTT reagent as above. Then, the MTT solution was aspired followed by addition of 80 μl of detergent solution.

For ALI MTT viability assay, confluent VA10 cells cultured on Transwell filters for 30 days under ALI conditions (as described above) were used. The assay was done as previously described (Scherließ, 2011). Briefly, the medium was aspired and cells rinsed twice with HBSS before incubation with the chitosan derivative for 2 h at 37°C. After incubation, the test solutions were aspired and the epithelium rinsed twice with HBSS. Then, 15 μl of MTT solution was introduced to the apical side (0.5 ml) and 45 μl to the basolateral side (1.5 ml) and incubated overnight. The MTT solution was then aspired followed by apical addition of 0.5 ml of detergent solution. Absorbance from the solubilized formazan crystals formed was measured at 570 nm (reference wavelength 650 nm) using microplate reader (SpectraMax, Molecular Probes).

4.8. Measurement of changes in TER after treatment with chitosan derivatives

The TER of VA10 cells was measured with Millicell-ERS volthometer (Millipore, MA, USA) for ALI cultured VA10 cell layers. Prior to the TER studies, the cell layers were washed twice with HBSS (37°C) and then allowed to equilibrate in the incubator with HBSS (0.5 ml apical and 1.5 ml basolateral) for 30 min followed by baseline TER measurement every 20 min for 1 h. At $t = 0$, the HBSS was either replaced with 0.5 ml of the chitosan derivative test solution and 1.5 ml basolateral HBSS or by 0.5 ml apical and 1.5 ml basolateral HBSS as a control. The TER was measured at 0, 20, 40, 60, 80, 100 and 120 min after administration. Thereafter, the test solution was aspired, the epithelium rinsed three times with HBSS and then incubated in culture medium for 24 h to monitor the recovery of the epithelium. The TER value for every epithelial layer at $t = -20$ min was normalized to 100% to minimize any inter-group variation present in the initial TER since $t = 0$ min was measured directly after the addition of the test solutions. Corrected TER value was obtained after subtraction of the background from the cell-free culture insert.

4.9. FD4 transport studies after treatment with chitosan derivatives

Prior to the transport studies, the ALI cultured cell layers were washed twice with HBSS (37°C) and then allowed to equilibrate in the incubator with HBSS for 1 h. Test solutions were either aseptic solution of FD4 dissolved in HBSS buffer to a final concentration of 1.5 mg/ml, as control, or FD4 co-dissolved at 1.5 mg/ml with the chitosan derivative that had the final concentration of 1.0, 0.25, 0.063 or 0.016 mg/ml. Before the FD4 transport studies were started, the HBSS buffer was aspired and replaced by 0.52 ml of prewarmed test solution and 1.5 ml of HBSS at the basolateral side. Immediately, a sample (20 μl) of the test solution was removed to determine the initial concentration (C_0). The cells were incubated at 37°C and agitated on an orbital shaker at 80 rpm. Sampling from the

basolateral compartment (100 µl) was done after 20, 40, 60, 80 and 120 min and replaced with equal volume of fresh HBSS buffer. TER measurements were done at the same time points as the sampling.

5. Immunofluorescence and microscopic imaging

Immunohistochemistry. Cells, cultured at either LCC and ALI until maximum TER was reached, were fixed for 10 min with 3.7% (v/v) formaldehyde (after formaldehyde fixation, acetylated tubulin samples were treated with MeOH for 5 min at -20°C), permeabilized with 0.1% (v/v) Triton X-100 for 7 min and then blocked (5% v/v goat serum, 0.3% v/v Triton X-100 in PBS) for 10 min. The primary antibodies used are listed in Table 11 and were all diluted in a buffer consisting of 0.2% (v/v) Triton X-100, 0.1% (w/v) bovine serum albumin (BSA) and 0.05% (v/v) Tween®20 in PBS with the exception of E-cadherin that was diluted in PBS. Alexa Fluor 488 phalloxin was used for F-actin staining (1:40, Invitrogen, Oregon, USA). Cells were incubated with primary antibodies overnight at 4°C. Then, the cells were incubated with isotype specific Alexa Fluor secondary antibodies (1:1000) and To-Pro-3 for nuclear staining (1:500) all of which were purchase from Invitrogen (Oregon, USA) and were diluted with the same solution as for the primary antibodies, for 30 min.

Table 11. Antibodies

Antibody	Isotype	Clone	Produced in	Dilution	Manufacturer
Acetylated tubulin	IgG_{2b}	6-11B-1	Mouse	1:70	Abcam, UK
β-actin	IgG_1	ACTN05 (C4)	Mouse	1:200*	Abcam, UK
Claudin-4	IgG_1	3E2C1	Mouse	1:125 1:250*	Life Technologies
E-cadherin	IgG_{2a}	36/E-cadherin	Mouse	1:125	BD Bioscience, NJ, USA
P-gp	IgG_1	JSB-1	Mouse	1:30	Abcam, Cambridge, UK

* for western blotting

Protein extraction. After treatment with either HBSS control or TMC (0.25 mg/ml), the Transwell filters were gently washed with icecold PBS that was then completely removed. RIPA lysis buffer (20 µl) was then applied to each well and filters placed on ice for 10 min. The cells were then scraped from the filters and sonicated for 2 min followed by centrifugation at 12000 x g for 20 min at 4°C. The supernatant was collected and the protein concentration determined with the Bradford assay.

Western Blotting. Equal amounts of proteins were separated with 10% SDS Bis-Tris gel followed by transfer onto nitrocellulose membranes. The membranes were then

blocked with 5% BSA in Tris buffered saline containing 0.1% (v/v) Tween$^{®}$20 for 1 h. Primary antibodies (β-actin or Claudin-4) were added to the blocking solution and incubated overnight at 4°C. Then, the membrane was rinsed three times with PBS and subsequently blotted with infrared secondary antibodies (anti-rabbit or anti-mouse at 1:20.000) for 1 h at room temperature and rinsed with PBS before visualization with Odyssey Infrared Image Scanner and the corresponding Image Studio software (LiCOR Biosystems).

Confocal Microscopy. Immunofluorescence images were obtained using Zeiss LSM 5 Pascal confocal laser scanning microscope (CLSM, Carl Zeiss AG, Munich, Germany) with Plan-Neofluar 40x and Plan-Apochromat 63x oil immersion lenses. VA10 epithelia were mounted with Fluoromount-G antifade solution (SouthernBiotech, Birmingham, USA) and coverslips before visualization.

Scanning Electron Microscopy. The VA10 cell layers were grown on Transwell filters until maximum integrity was reached as determined with TER. Then, the epithelia were washed with PBS, fixed in 3.7% formaldehyde for 15 min, post-fixed in 1% OsO_4 for 1 h followed by dehydration through a ethanol gradient of 5, 12.5, 25, 50, 75 and 100% (v/v) in water, each step for 10 min at room temperature. The dehydrated epithelia were then transferred in 100% acetone to a critical point drier (Bio-Rad, England). Dried samples were mounted on aluminum stubs and gold sputter-coated (Edwards Sputter Coater S150B, BOC Edwards, MA, USA). Images were obtained on a Zeiss Supra 25 Field Emission Scanning Electron Microscope (FE-SEM, Carl Zeiss AG, Munich, Germany) at 5kV under high vacuum conditions.

Bright Field Microscopy. Paraffin embedded ALI cultures were stained with hematoxylin and eosin. Imaging was performed using a Leica DMI3000B microscope and Leica DFC310 FX camera.

6. Data analysis and calculations

Sample Analysis. Samples from Flu-Na, FD and Rh123 studies were directly added to black 96 well plates (Eppendorf, Hamburg, Germany). In Flu-Na and FD studies, 10 mM NaOH aqueous solution (100 µl) was added to each sample. Fluorescence was measured with excitation wavelength of 485 nm and emission of 535 nm using fluorospectrometry (Tecan GENios microplate reader, Männedorf, Switzerland). Samples from drug permeation studies were analyzed using a Dionex Ultimate 300 HPLC system, coupled with photodiode array detector using Onyx monolithio C18 column (100 mm × 4.6 mm). The mobile phase consisted of acetonitrile and H_2O/AcOH (99.5/0.5) using conditions described in Table 12.

Table 12. HPLC conditions for model drugs

Drug	UV detector wavelenght (nm)	Acetonitrile (%)	Flow rate (ml/min)	Retention time (min)
Alprenolol	273	31.5	0.8	2.80
Atenolol	274	7	1.0	2.72
Metoprolol	273	22	0.8	2.81
Propranolol	264	30	1.0	2.57
Terbutaline	274	7	1.0	2.49

Calculations and data analysis. cLogD(7.4) and polar surface area (PSA) were calculated using ChemAxon MarvinSketch software. P_{app} coefficients were calculated from the permeation experiment according to equation 5 where dQ/dt is the flux, A is the surface of the cell filter (1.12 cm^2) and C_o is the initial concentration in donor chamber.

$$P_{app} = \frac{dQ}{dt} \times \frac{1}{C_0 A}$$

Eq. 5

P_{app}, TER and f-TMC uptake data were reported as mean ± standard deviation with n representing number of experiments. Unpaired, two tailed Student's t-test was used to compare two means and one-way analysis of variance was used to analyze more than two sets of data (GraphPad Software, Inc., CA, USA) with the difference considered to be statistically significant when $p < 0.05$.

RESULTS AND DISCUSSION

In this chapter I will discuss my data, both published and unpublished, in a retrospective way to give the reader a comprehensive overview of the thesis. Each paper/manuscript can be found in a supplement enclosed with the thesis.

1. Synthesis of *N*-quaternary chitosan derivatives using di-*tert*-butyldimethylsilyl protection strategy (Paper # 1)

Previously used synthetic procedures for *N*-quaternization of chitosan have resulted in compounds with a combination of the desired *N*-quaternization, *N*-dimethylation and undesired *O*-methylation. More homogenously *N*-quaternized chitosan derivatives could be synthesized by protecting the hydroxyl groups with *tert*-butyldimethyl silyl (TBDMS) protection groups. This protection should allow selective modification of the amino group and also help to increase the solubility of the polymer in organic solvents.

1.1. Synthesis of *N,N,N*-trimethyl chitosan

One of the primary objectives of this PhD project was to develop a synthetic strategy to produce a fully trimethylated chitosan, without any *O*-methylation. The highest previously reported degree of trimethylation without *O*-methylation was approximately 80%, achieved by adding CH_3I and NaOH in four portions to chitosan dissolved in a DMF/water mixture (Runarsson et al., 2008a). Although higher degrees of trimethylation have been reported (90.5%), these were accompanied by high degrees of *O*-methylation which has negative effect on aqueous solubility (Polnok et al., 2004). Since these degrees of *N*- vs. *O*-methylation cannot be fully controlled by previously reported procedures the resulting chitosan derivatives will always be mixed heteromeric products, which is a major drawback for structure-activity investigations.

By using the TBDMS protected chitosan, the risk of *O*-methylation was eliminated. Methylating agent of choice was MeI, principally due to its reactivity, solubility in organic solvents and availability. Cesium carbonate was used as base to activate the chitosan as a nucleophile for the methylation process. The choice of solvent was a crucial factor in this synthesis since the reaction did not occur in DCM but went to completion in NMP.
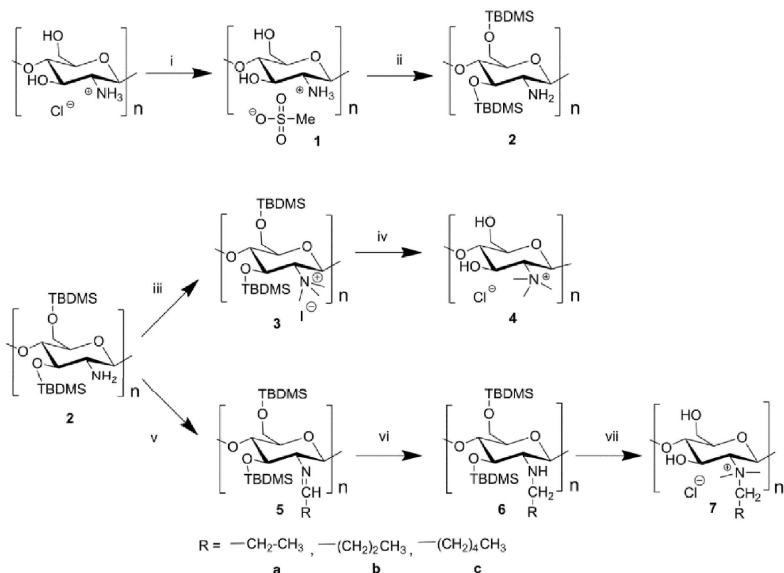
Scheme 1. Synthesis of *N*-quaternary chitosan derivatives

Synthetic route for the preparation of *N,N,N*-trimethyl chitosan (4) and *N*-alkyl-*N,N*-dimethyl chitosan derivatives (7a, 7b, 7c)

This has been observed with other polymers (Jonquieres et al., 2006) and can be attributed to the fact that solvent with high dipole moment and dielectric constant, such as DMF and NMP, provide better reaction conditions for uncharged reactants (Reichardt, 2004). The degree of trimethylation in the current reaction could only be detected after the deprotection due to peak broadening in ^{1}H-NMR spectra of *N,N,N*-trimethyl-di-TBDMS-chitosan (Fig 1.A in Paper # 1).

TBAF in NMP was used to deprotect *N,N,N*-trimethyl-di-TBDMS-chitosan, utilizing the affinity of the fluoride atom to form the strong Si-F bond (Wuts and Greene, 2007). The previously used deprotection strategy, 1% HCl in EtOH (Runarsson et al., 2008b), was avoided in the current work since depolymerization can occur from acid hydrolysis of the *O*-glycosidic bond (Vârum et al., 2001). The deprotection step with TBAF had to be repeated to fully remove the silyl groups.
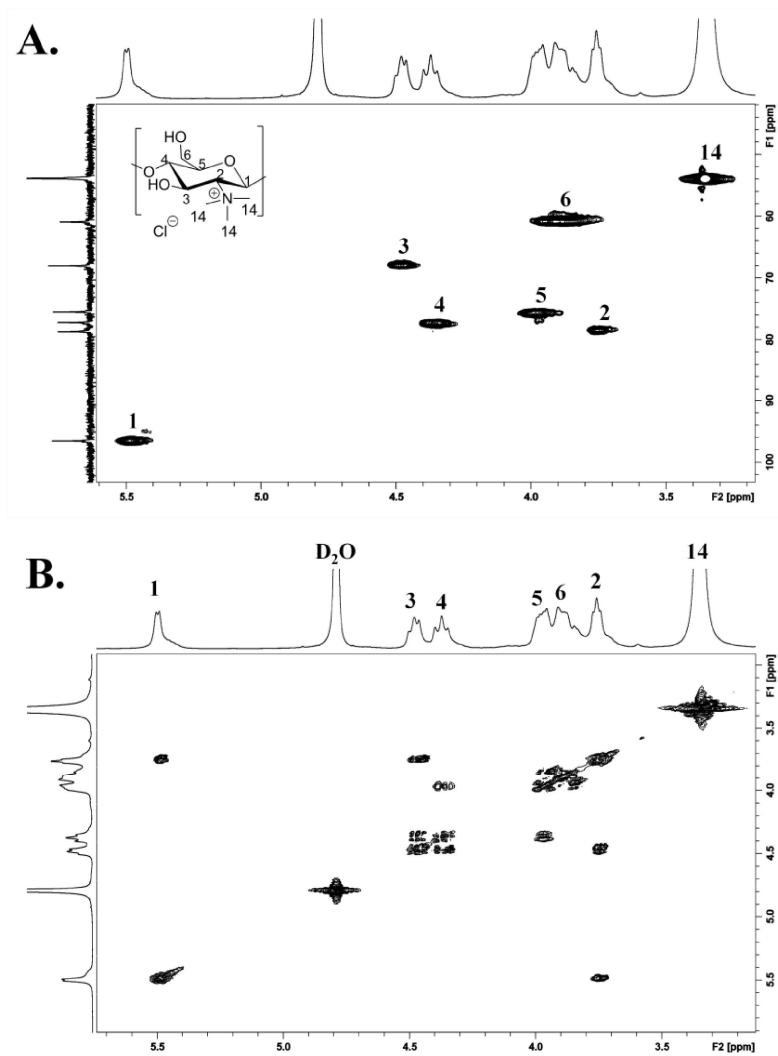
Figure 10. 2D NMR analysis of TMC

NMR analysis of TMC (**4**). A. ^{1}H-^{13}C HSQC. B. ^{1}H-^{1}H COSY spectra.

After desilylation, NMR revealed a TMC homopolymer (Figure 10) with the trimethyl peak observed at 3.35 ppm. The chemical structure of the fully substituted TMC and the assignment of individual peaks was further confirmed by 2D HSQC and COSY NMR analysis (Figure 10.A and 10.B, respectively), revealing a homogenous polymer with clearly resolved peaks for all atoms of the polymer, with no indication of *N,N*-dialkylation, *N*-monoalkylation or *O*-alkylation. The absence of *O*-methylation in this product confirmed that the hydroxyl groups were fully protected in the di-TBDMS chitosan precursor.

1.2. Introduction of *N*-alkylimine to the chitosan backbone

Reductive alkylation is a common procedure for mono-alkylating an amine. This procedure can be done either directly by introducing an aldehyde and reducing agent in one-pot or step-wise, by isolating the imine before reducing the imine to the amine. *N*-alkylation of di-TBDMS chitosan was achieved by stepwise reductive alkylation. The risk of possible dialkylation was eliminated (AbdelMagid et al., 1996) by using this approach. For example, significant *N,N*-dialkylation was reported as a side-product in the *N*-monoalkylation of *O*-acetyl protected glucosamine (Liberek et al., 2005), where imine formation and reduction were performed simultaneously. Conventionally, the primary amine is used in excess to avoid dialkylation (AbdelMagid et al., 1996). However, this approach cannot be used with polyamines such as chitosan, if a high degree of substitution is desired. Furthermore, the risk of aldehyde reduction, which can take place when reducing agents such as borohydrides are used, (Gribble and Ferguson, 1975) is also circumvented, since the imine was isolated before reduction. The reaction between the di-TBDMS chitosan and different alkyl aldehydes resulted in *N*-alkylimine-di-TBDMS chitosan (Scheme 1.v), as evidenced by the appearance of an imine proton at 7.4 ppm by ^{1}H NMR analysis (Figure 11.A.b.) and confirmed by COSY NMR (Appendix B, Paper # 1). IR spectra also showed a characteristic stretch for the imine C=N group at 1673 cm^{-1} (Figure 11.B.b). Calculations from the ^{1}H NMR peaks indicated a partial *N*-substitution of 74-80%. Although various reaction conditions were investigated, including extended heating, prolonged reaction times and varying amounts of aldehyde, this did not significantly affect the degree of substitution (data not shown), which remained in the previously stated range. Molecular sieves were used to drive the reaction to completion by water removal. The full substitution was, however, probably

not obtained because of the instability of the *N*-alkyl imine. This is the disadvantage of the step-wise method as the imine can convert back to a primary amine and the corresponding aldehyde (Layer, 1963). It is also possible that steric hindrance, caused by the bulky di-TBDMS protection groups prevented full substitution.

1.3. Reduction of the *N*-alkylimine chitosan

In order to obtain a stable carbon-amine bond, the imine bond has to be reduced to an amine bond and the typical procedure is done with sodium borohydrate. However, only partial reduction was established (29%) of the *N*-alkylimine chitosan derivatives (Table 2, paper #1). Catalytic hydrogenation with H_2/Pd also resulted in a partial conversion of 52%. Therefore, sodium triacetoxyborohydrate (STAB-H) was used. STAB-H gives better yields and faster reactions than other reducing agents, including $NaBH_4$ or catalytic hydrogenation (AbdelMagid et al., 1996). Acetic acid in DCM was used in combination with STAB-H, since acids can facilitate complete conversion from imine to amine (AbdelMagid et al., 1996). Under these reaction conditions, the *N*-alkylimine-di-TBDMS chitosan derivatives were completely converted into the *N*-alkyl-di-TBDMS chitosan form (Scheme 1. vi.). The successful reduction was confirmed with ^{1}H NMR spectra that revealed the disappearance of the N=C-H proton, (Figure 11.A.c), while COSY spectra showed a distinct correlation for reduced *N*-alkylated chitosan (Appendix C, paper # 1). Interestingly, prochiral H-7 protons in the *N*-alkyl chain were observed as two peaks at 2.6 and 2.7 ppm. Similar observations were made for the N-CH$_2$ peaks of *N*-alkyl-D-glucosamine, where the two protons were also found to have slightly different chemical shifts (Liberek et al., 2005). Reduction was also confirmed by IR, where the imine stretch at 1673 cm^{-1} was absent (Figure 11.B.c.).

1.4. Quaternization of *N*-alkyl chitosan

The first choice for quaternization reagent for *N*-alkylated chitosan derivatives was MeI as it had commonly been used for trimethylating chitosan. Yet, only low degree of quaternization could be achieved with this reagent (Table 3, Paper # 1). Since cesium base has been reported to suppress overalkylation (Salvatore et al., 2002), lithium carbonate was tested as alternative base, but this also resulted in low DQ. An alternative methylating strategy was therefore needed. DMS is a more reactive methylating agent than CH$_3$I (Friedl, 1990). DMS is a highly reactive methylating agent and is, along with MeI, considered to be very hazardous (Poirier et al., 1975, Selva and Perosa, 2008).
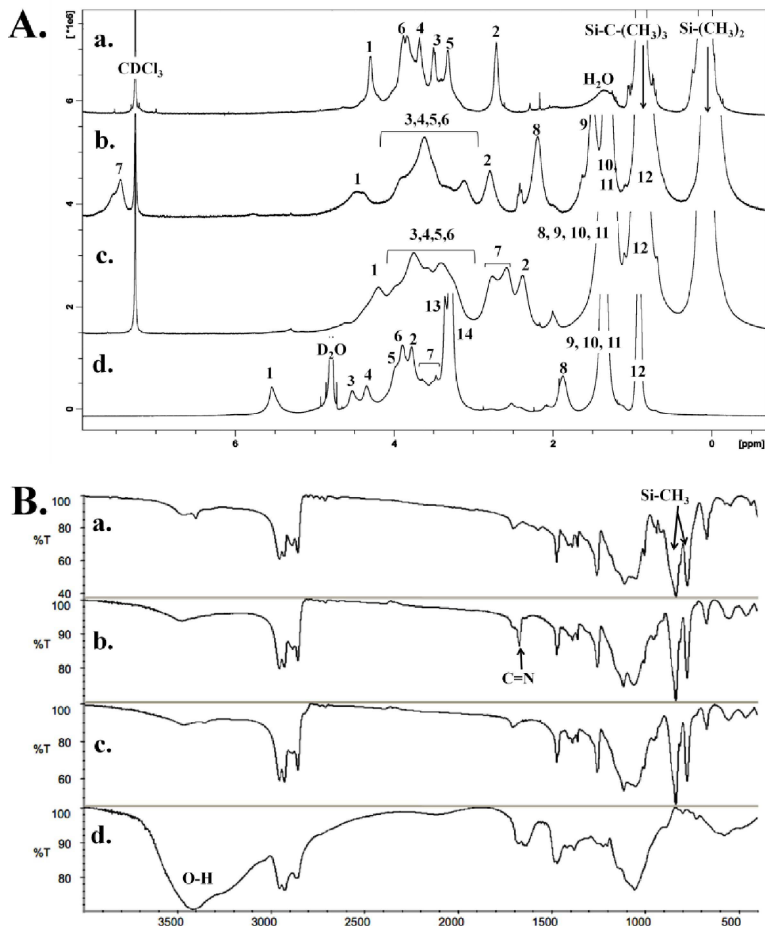
Figure 11. **¹H-NMR** **spectra** **and** **FT-IR** **spectra** **of** *N*-**quaternized chitosan derivatives**

¹H NMR (A) and FT-IR spectra (B) of the main chitosan compounds in the synthesis of *N*-hexyl-*N*,*N*-dimethyl chitosan. a. di-TBDMS chitosan (2). b. *N*-hexylimine-di-TBDMS chitosan (5c). c. *N*-hexyl-di-TBDMS chitosan (6c). d. *N*-hexyl-*N*,*N*-dimethyl chitosan (7c).

Dimethyl carbonate could have been considered as safe- and eco-friendly alternative (Memoli et al., 2001) providing a more cost effective approach but was not investigated in the current work. Different solvent conditions were also investigated. When NMP was used as solvent, the reaction was < 5% but when DCM was used (Scheme 1. vii.), the reaction was successful, with a degree of *N,N*-dimethylation of 65% for *N*-propyl-, 72% for *N*-butyl- and 68% for *N*-hexyl chitosan derivatives.

Broad peaks were observed for the *N,N*-dimethyl-*N*-alkyl-di-TBDMS chitosan derivatives that were poorly resolved in ^{1}H NMR, and were therefore not characterized before deprotection. Deprotection by TBAF was confirmed by the disappearance of the silyl peaks in the ^{1}H NMR spectra (Figure 11.A.d), the disappearance of the Si-CH$_3$ band at 837-777 cm^{-1} and the appearance of a large band at 3418 cm^{-1} in FT-IR spectra, corresponding to the O-H bond in the IR spectra (Figure 11.B.d.). A peak corresponding to the dimethyl peak at 3.27 ppm for *N*-propyl-, *N*-butyl-, and *N*-hexyl-*N,N*-dimethyl chitosan appeared (Figure 11.A.d.), which did not shift when NMR samples were acidified with DCl. Consequently, characterization of quaternized chitosan derivatives can be challenging. In the previous synthesis of *N*-ethyl-*N,N*-dimethyl chitosan, where the *N*-monoethyl material was produced in one step, followed by dimethylation with CH$_3$I (Bayat et al., 2006), the possibility of *N,N*-diethylation or *O*-methylation was not discussed and detailed NMR characterization of the derivative was not reported. Steric hindrance appears to be involved in the reactivity of di-TBDMS chitosan. The *N,N,N*-trialkylation of di-TBDMS chitosan by MeI proceeded to completion, giving 100% trimethylated material. The *N,N*-dimethylation of *N*-propyl-, *N*-butyl- and *N*-hexyl-di-TBDMS chitosan with the more reactive DMS methylation reagent resulted in 65, 72 and 68% *N*-quaternization of these chitosan derivatives, respectively. A complete absence of *N,N*-dimethylation was observed in the case of *N*-dodecyl-di-TBDMS chitosan (data not shown).

The degree of *N*-monomethylation of *N*-alkyl chitosan derivatives was 15-18%. When the solvent was acidified, the *N*-alkyl peaks of the *N*-monomethylated residue shifted downfield towards the values of their *N*-alkyl-*N,N*-dimethyl counterparts. As the starting materials were not fully *N*-alkylated, 13-17% *N,N,N*-trimethylation was detected at 3.34-3.35 ppm. The substitution pattern of each *N*-quaternary derivative is shown in Figure 12, excluding the 3% *N*-acetylation found in all the derivatives. The structure was

further investigated by detailed 2D COSY and HSQC NMR, which confirmed the positions of the different protons on the chitosan backbone, as well as protons on the alkyl chain (Figure 13.A and B).
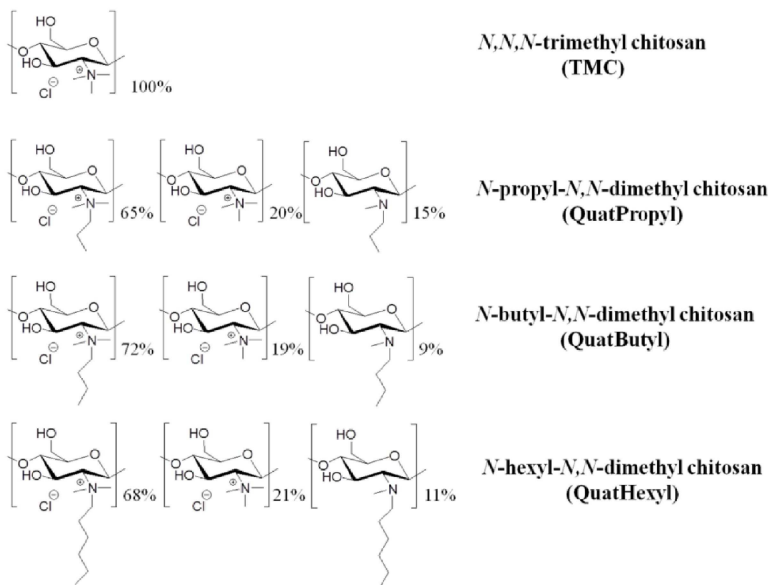
Figure 12. **Structures of the *N*-quaternary chitosan derivatives synthesized.**
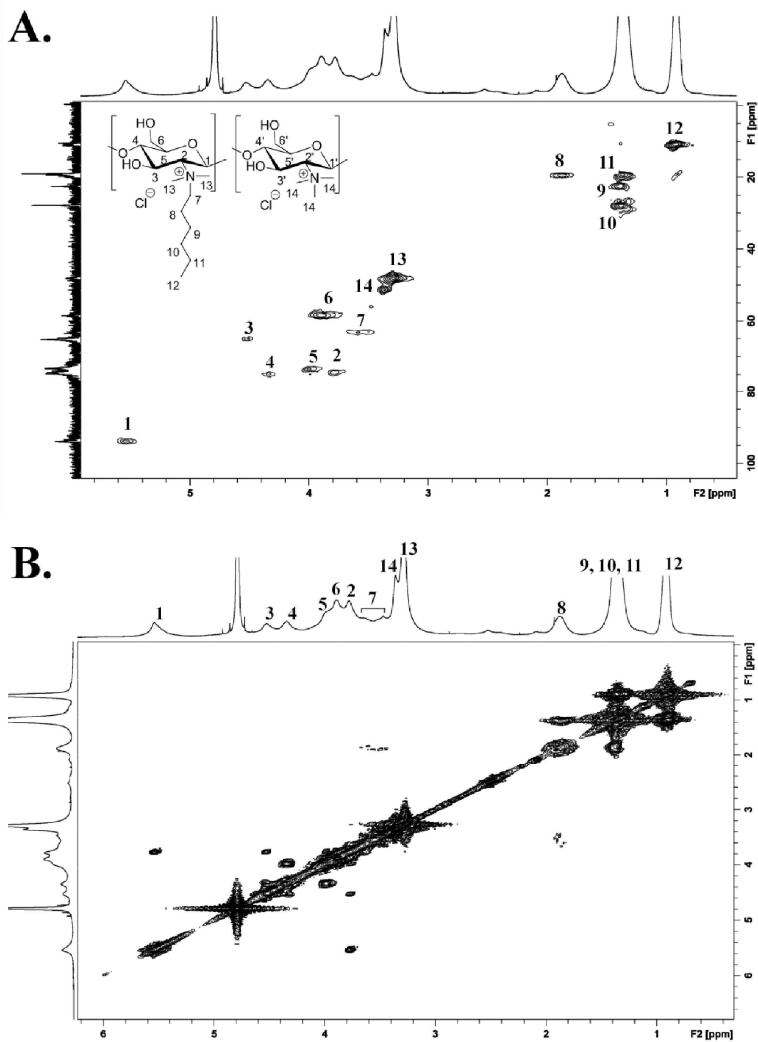
Figure 13. 2D NMR analysis of *N*-hexyl-*N*,*N*-dimethyl chitosan.
A. ^{1}H-^{13}C HSQC. B. ^{1}H-^{1}H COSY spectra.

57

2. Fluorophore oxime end-conjugation to TMC (Paper # 2)

The focus of this part of the PhD work was to utilize the reactivity of the aminooxy group towards an aldehyde group to allow effective conjugation of an aminooxy functionalized fluorophore to the reducing end of fully trimethylated chitosan (Figure 14). By establishing this conjugation, a proof of concept for the oxime functionalization of chitosan derivatives was established.
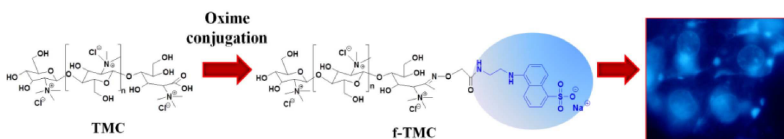
Figure 14. The oxime fluorescent conjugation to TMC.

2.1 Conjugation of an aminooxy functionalized fluorophore to TMC

End-functionalizing of TMC with a fluorescent group, to from f-TMC, can be used for characterization of the conjugated product. The fluorescent EDANS moiety can be detected with fluorospectrometry and with an epi-fluorescent microscope. Furthermore, the EDANS fluorophore appears at the aromatic region separate from the carbohydrate proton in ^{1}H NMR, thereby also enabling good detection. Peak-broadening of the fluorophore in the ^{1}H NMR spectra is a general sign of a covalent linkage to the chitosan polymer. The reducing end of TMC (**4**) was conjugated with an aminooxy functionalized EDANS (**10**, EDANS-O-NH$_2$, Scheme 2.A) fluorophore forming TMC-oxime-EDANS (**12**, f-TMC, Scheme 2.B, Figure 15). Direct confirmation of the oxime conjugation should be the downfield shift of the H-1 oxime proton in TMC linked to the aminooxy group in the ^{1}H-NMR. Inconveniently, the estimated location of this oxime proton was at the same place as the aromatic EDANS protons or approximately 7.6 ppm (Jiménez-Castells et al., 2008, Novoa-Carballal and Muller, 2012, Thygesen et al., 2009) as can be seen in Figure 15 Despite signal intensity was near the detection limit, ^{1}H-^{1}H COSY NMR spectra showed the H-1' at 7.63 ppm that correlated with H-2' at 4.12 ppm (Appendix 1.B, paper # 2). In addition, correlation between the H-1' signal and the C-1' signal at 152 ppm was observed in ^{1}H-^{13}C HSQC NMR spectrum (Appendix 1.D, paper # 2), further supporting the oxime conjugation.
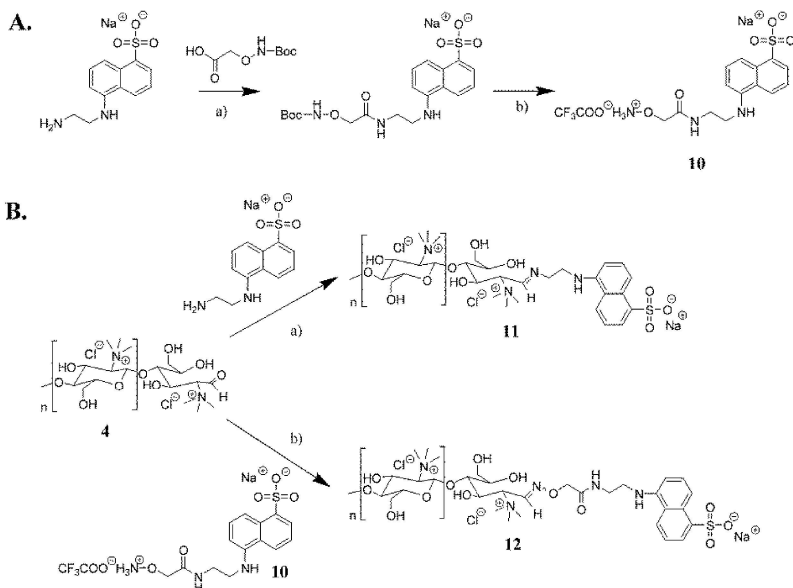
Scheme 2. Synthesis scheme for fluorescently end-labeled TMC.

Synthesis of EDANS-O-NH$_2$ (**10**), TMC-imine-EDANS (**11**) and TMC-oxime-EDANS (f-TMC, **12**).

Although the amino ethylene protons in the fluorophore (H-k and H-l) were located in the same region as the TMC protons, making their existence barely detectable, the ^{1}H-^{1}H COSY revealed correlating peaks confirming their existence at 3.65 and 3.53 ppm (Appendix 1.A, paper # 2). The fact that the reducing end of TMC could be conjugated further supports the efficiency of the di-*tert*-butyldimethylsilyl protection strategy as it shows that reducing end hydroxyl groups of chitosan in the previous trimethylation step were also protected (paper # 1).
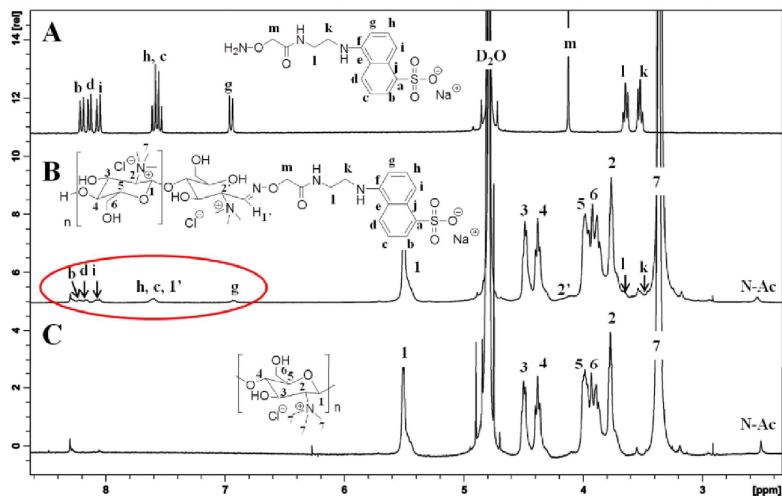
Figure 15. ^{1}H NMR spectra comparison of f-TMC and precursors.

A. EDANS-O-NH$_2$. B. f-TMC (TMC-oxime-EDANS) with EDANS conjugation marked with circle. C. TMC.

A reaction between TMC and the amino group of EDANS, to form TMC-imine-EDANS (**11**), was carried out to confirm that the aminooxy group was more reactive than the amino group under the given reaction conditions. The isolated polymer did not show any signs of conjugation to the fluorophore in the proton NMR spectra and fluorescent studies of the isolated material, consistent with the unmodified TMC. This is likely due to relative instability of the imine bond (Layer, 1963) compared to the oxime bond that has been reported to be relatively stable towards hydrolysis in aqueous solutions (Kalia and Raines, 2008). Due to the alpha effect, the amino group on the aminooxy group is less basic but more nucleophilic than the normal amino group. This enhanced nucleophilicity makes the oxime formation more thermodynamically favorable in water than imine formation.

The reactions were buffered in an acetate buffer at 4.5, according to previously reported optimized conditions (Thygesen et al., 2010). Mildly acidic conditions enhance selectivity since the attenuated basicity of the amine in the EDANS-O-NH$_2$, leaves this amino group unprotonated while other amino groups, such as those for EDANS remain

protonated. Consequently, the aminooxy group presents a more suitable approach for covalent linkage at the reducing end of TMC, compared to an amino group, under current reaction conditions. GlcNAc, the basic unit of chitin, has lower reactivity towards the aminooxy group compared to glucose (Lohse et al., 2006, Thygesen et al., 2010) showing that the substitution on the C-2 carbon affects the reactivity. Therefore, the reducing end of TMC can be expected to have relatively low reactivity due to the electron withdrawing effects of the *N,N,N*-trimethyl group. As a consequence, the reaction was carried out with heating to 50°C for 72 h to enable full conjugation.

The f-TMC showed fluorescent properties when excited at the excitation maxima for EDANS, 335 nm. The fluorescence intensity was low compared to the fluorophore itself at the same concentration, which is to be expected for fluorescently end-labeled TMC (Fig. 3.A and B, paper # 2). Both ^{1}H-NMR and fluorescent data indicated that the oxime conjugation was successful, with 1:1 molar ratio between EDANS-O-NH$_2$ to TMC, enabling the calculation of the average molecular weight.

2.2. Molecular weight determination

The end-group analysis of EDANS (i.e. ratio between EDANS and trimethyl glucosamine units) in f-TMC (**12**), calculated from ^{1}H NMR data (Fig. 15.B and Eq. 1), was 0.03. These data, assuming that all reducing ends were labeled, were used to calculate the average MW of f-TMC polymer of 7.75 kDa (Eq. 2-4). MALDI-TOF molecular weight measurements were also collected for the TMC polymer. Either 2,5-dihydroxybenzoic acid or α-cyano-4-hydroxycinnamic acid was used as a matrix and MALDI-TOF measurements gave peak MW of 4.2 kDa and 5.2 kDa respectively (Fig. 2, paper # 2). The linear ($r^2 \geq 0.99$) fluorescence calibration curve of EDANS was also used to calculate the average MW of f-TMC (from Eq. 2-4) and was found to be 7.74 kDa. Calculations from the NMR and fluorospectroscopy data give very similar results whereas MALDI-TOF gives a very crude average MW determination. Accordingly, it can be estimated that the molecular weight of f-TMC is around 7.7 kDa, which is somewhat less than MW of starting chitosan (~8.3 kDa). However, this is not unexpected and can be due to some degradation in the number of reaction steps needed to obtain the final compound (Holappa et al., 2004, Snyman et al., 2002).

2.3. Localization of f-TMC *in vitro*

The fluorescent properties of f-TMC were further explored in the VA10 bronchial epithelial cell line in order to establish the localization of the polymer. The cells were cultures on chambered slides, a convenient method due to short incubation period. However, the monolayer thus formed does not differentiate into the typical epithelium observed when VA10 cells are cultured on Transwell filters in ALI.
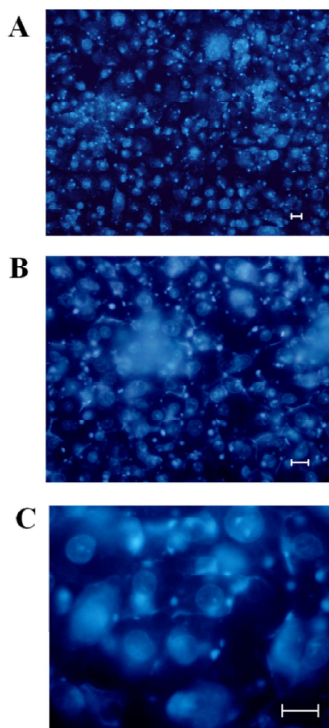
Figure 16. Fluorescent microscopy images of VA10 cells in monolayer after incubation with f-TMC.

A. Incubation for 20 min at 37°C. B. Incubation for 2 h at 37°C (40x) and C. (100x); bar = 10 μm.

The visualization was carried out using an epi-fluorescent microscope since confocal scanning microscopy was not equipped with the excitation and emission wavelengths required to visualize fluorophore. The fluorescently labeled TMC was expected to be only found at the cell membrane as has been reported with solubilized chitosan (Huang et al., 2004, Jia et al., 2009, Schipper et al., 1997). Chitosan has been shown not to infiltrate into the paracellular space but mainly to adhere to the microvilli in the Caco-2 cell line. Additionally, that same study showed that FITC-labeled chitosan, after oral administration in mice, was not absorbed but was eliminated through the colon (Sonaje et al., 2012). This was, however, not the case for f-TMC since it was found at the cell membrane as well as intracellularly after only 20 min of incubation (Figure 16.A). A fundamental difference in the localization between chitosan and TMC could exist due to the different physical properties of their amino group. One possibility is that chitosan precipitates when localized at the cell membrane leading to no internalization. Internalization of solubilized polyethylene glycol (PEG)-TMC copolymer has been described, with localization

mainly in the perinuclear region of the cell when complexed with insulin (Mao et al., 2005). In addition, gene delivery studies have shown that TMC-DNA polyplexes are more efficiently internalized than chitosan-DNA polyplexes (Germershaus et al., 2008, Thanou et al., 2002). No fluorescence was observed after incubation for 2 h with the hypothetical TMC-imine-EDANS (**11**) or with the EDANS fluorophore itself (data not shown) which further supports the reactivity and selectivity of the aminooxy group in the synthesis of f-TMC. Due to low amount available, EDANS-O-NH$_2$ was not tested for localization, however, the aminooxy group should not have specific affinity beyond the fluorophore.

Co-staining of f-TMC and the adherence junction protein E-cadherin (E-cad) showed intracellular localization of f-TMC and co-localization with E-Cad at the membrane surface (Figure 17.C). A slightly different expression between the control and f-TMC treated cells was observed, consistent with possible dissociation of E-cad proteins. The cellular uptake study provided further confirmation of the internalization of f-TMC in the epithelial monolayer with significantly higher uptake ($p < 0.0001$) of f-TMC (32.01 ± 3.60 µg/mg protein) than EDANS control (0.073 ± 0.038 µg/mg protein). Since the fluorescence microscopy shows that f-TMC is largely found intracellularly but also partially membrane bound, the amount detected in the uptake study contains both membrane bound and intracellularly localized f-TMC. Furthermore, these results show that the EDANS moiety of f-TMC does not contribute to the adhesion or internalization of the f-TMC polymer. It has been considered an advantage that chitosan only adheres to the mucosal membrane and is not internalized. The internalization of f-TMC could raise some concerns in regards to cytotoxicity. Although not included in paper # 2, viability was determined with MTT in a 96 well plate format. Those results showed that both TMC and f-TMC reduced the viability to 45.9 ± 7.4 and 44.3 ± 15.9 % of HBSS control respectively. Consequently, the internalization of f-TMC could have been the result of loss of cell membrane integrity.
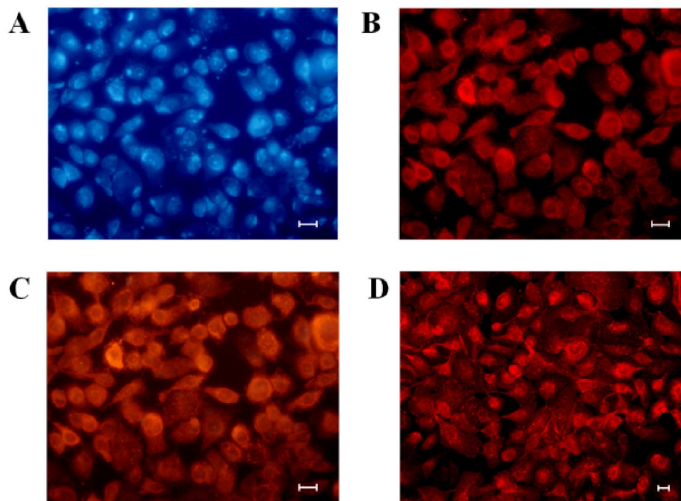
Figure 17. Co-staining of f-TMC with E-cadherin.

Fluorescent microscopy images of VA10 cells incubated with f-TMC in monolayer. A. After incubation with 0.5 mg/ml f-TMC (366 nm) for 2 h at 37°C. B. Immuno-fluorescence staining for E-cadherin (526 nm) of the same section as shown in A. C. Co-localization of f-TMC and E-cadherin. D. Immunofluorescence staining for E-cadherin (526 nm) in non-treated cells; bar = 10 µm.

In this study, we report the first synthesis of a fluorescently labeled TMC obtained by highly regioselective oxime formation at the reducing end. Advantages of this novel approach include conjugation that should induce minimal structural changes to the chitosan backbone and fluorescent labeling that enables accurate molecular weight determination that does not rely on the use of molecular weight standards such as dextrans that could give inaccurate molecular weight determination. In addition, this conjugation provided means to show the localization of the polymer *in vitro*, revealing localization both at the cell membrane as well as intracellularly. Selective oxime conjugation to the reducing end of TMC introduces new opportunities in chitosan chemistry. In addition to allowing selective conjugation of other fluorophores, that offers numerous potential applications for gene- and drug delivery studies; this method also introduces the possibility of conjugating chitosan polymers to other functionally active moieties.

3. Characterization of the VA10 cell line as a drug permeation model (Paper # 3)

In vitro models of the airway epithelial barrier are important for investigating possible inhaled drug candidates. The VA10 human bronchial epithelial cell line has emerged as a viable candidate for studying epithelial barrier properties as well as progenitor properties, since this cell line has basal cell characteristics (Halldorsson et al., 2007). This is of particular importance because the repeated cycle of injury, repair and regeneration is of great importance in the pathogenesis of common lung diseases such as asthma, chronic bronchitis and bronchial carcinoma. Therefore the VA10 cell line should be particularly suitable to study the effects of drugs on these common diseases. However, data describing its basic pharmacologic profile, such as permeability properties, are lacking which is imperative for its acceptance as an *in vitro* airway drug permeation model. For this upper airway epithelial cell line to be considered as an *in vitro* permeation model, its properties should reflect the epithelium *in vivo* as closely as possible; discriminating between compounds depending on their lipophilicity, size and transport mechanism and represent the *in vivo* phenotype. In particular, this work was paramount for assessing the effects of the synthesized chitosan derivatives on the bronchial epithelium. The purpose of this work was, therefore, to validate the VA10 cell line, as a possible drug permeation model.

3.1 Morphology of the VA10 cell line

It has been established that the VA10 cell line shows cobblestone morphology in culture and staining with some of the cilia markers indicate a ciliated differentiation (Halldorsson et al., 2010). Culture conditions, such as ALI or LCC, time, and culture medium used, clearly affect the nature of the cultured epithelium. In the current study, we did not investigate thoroughly the impact of different culture time and medium, possibly leading to shorter incubation time but decided to focus on the difference between LCC and ALI. There is a general consensus that ALI culture induces more differentiated epithelium than LCC (Mathias et al., 1995, Yamaya et al., 1992) and that ALI cultured epithelium has similar gene expression profile as epithelial cells *in vivo* (Dvorak et al., 2011) possibly due to the change in access to oxygen (Adler et al., 1990). Still, there are some studies indicating that LCC yields more suitable epithelia (Ehrhardt

et al., 2002b). Therefore, VA10 cells were cultured under both LCC and ALI in order to determine the differentiation potential of the cell line under the current culture conditions. One of the primary purposes was to investigate the surface morphology of the VA10 cells under these two culture conditions. SEM revealed that LCC resulted in undifferentiated epithelium whilst ALI cultures showed more differentiated epithelia with pronounced ciliated-like protrusions (Figure 18.a and b). This is in line with previous reports that ALI cultures yield a more differentiated phenotype than LCC (Mathias et al., 1995, Yamaya et al., 1992). ALI cultured VA10 cells have been shown to stain positive for the cilia markers cystic fibrosis transmembrane conductance regulator (CFTR) and ezrin (Halldorsson et al., 2010).
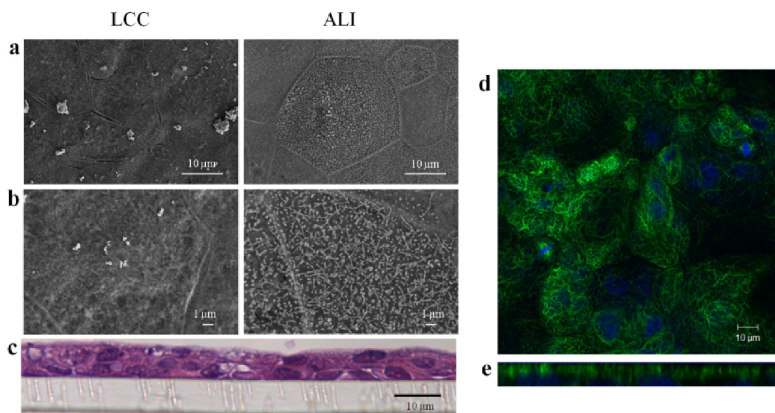
Figure 18. VA10 epithelium produces ciliated-like structures in ALI culture.

VA10 epithelia were cultured on Transwell filters and visualized when maximum integrity was reached. SEM images (a, b) of VA10 epithelium cultured in LCC or ALI culture and light microscopy image of semi-thin sections of the epithelium in ALI culture (c). Ciliated differentiation was observed within the ALI cultured epithelium forming 2-3 cell layers while epithelia grown in LCC generated an undifferentiated phenotype. Immunofluorescent staining of acetylated tubulin (green), a marker for ciliated epithelium, and nuclear staining (blue) in ALI cultured VA10 epithelium was visualized in confocal microscopy in either regular plane (d) or vertical xz cross sections of VA10 cell layer (e) showing the apical distribution of acetylated tubulin.

To further determine that the VA10 epithelium differentiated towards ciliated cells, the ALI epithelium was stained with the cilia marker acetylated tubulin (Figure 18.d and e). The staining showed a predominant apical tubulin location, showing differentiation towards ciliated epithelial cells. Additionally, under ALI conditions, a part of the VA10 cell culture has been observed to have beating cilia amounting to 6-7 Hz (This observation has not been published). Ciliary beating frequency (CBF) in *ex vivo* cell cultures of ~6 Hz has been reported (Clary-Meinesz et al., 1998, Clary-Meinesz et al., 1997) although researchers have also reported CBF of 11-14 Hz (Rutland et al., 1982). Therefore, the differentiation towards ciliated cells in VA10 was evident. Since basal and ciliated cells occupy a large proportion of the bronchial epithelial lining (Boers et al., 1998), the VA10 cell line can be considered to capture the *in vivo*-like phenotype of the respiratory epithelium. The naturally occurring condition in the bronchial region is the pseudostratified epithelium. However, primary bronchial epithelial cells cultured into an epithelium usually form a 1-3 layered epithelium (Pohl et al., 2009). VA10 cells formed a cell layer, 2-3 cells in thickness in ALI culture, showing cuboidal morphology and contact inhibition growth thereby approaching the physiological pseudostratified airway epithelium. The VA10 cell thickness differs from the cell lines Calu-3 and 16HBE14o- since Calu-3 cells form either a monolayer in culture (Fiegel et al., 2003, Florea et al., 2003, Shen et al., 1994) or a couple of cell layers (Grainger et al., 2006, Stentebjerg-Andersen et al., 2011) and 16HBE14o- generate 10-16 layers (Ehrhardt et al., 2002b, Pohl et al., 2009).

3.2 Epithelial barrier properties

One of the major hallmarks of bronchial epithelia is its ability form a confluent epithelium with tight junctions expressed, thereby forming a selective barrier for paracellular transport of hydrophilic solutes. The VA10 cell line generates a polarized cell layer, expressing the TJ proteins occludin, JAM-A, Claudin-1, Claudin-4 and ZO-1 (Asgrimsson et al., 2006, Halldorsson et al., 2007). Therefore, VA10 has been used to model TJ related events under both normal and pathophysiological conditions (Halldorsson et al., 2010). In the current study, VA10 cells cultured at LCC or ALI expressed the TJ protein occludin that was co-localized with F-actin, forming a highly organized structure (Figure 2, paper # 3). Expression of these TJ markers indicates a

structural barrier that can be functionally monitored with transepithelial electrical resistance (TER) (Kim, 2002).

The most common techniques to assess barrier properties are the measurement of TER and the permeability of hydrophilic paracellular marker such as Flu-Na. These properties were determined for both LCC and ALI culture to follow the gradual development of barrier properties in the VA10 cell model. TER reached a peak value for LCC ~ 2600 $\Omega \times cm^2$ between days 18 and 27 compared to a TER of ~ 1300 $\Omega \times cm^2$ was reached between days 27 and 48 in ALI culture (Figure 19).
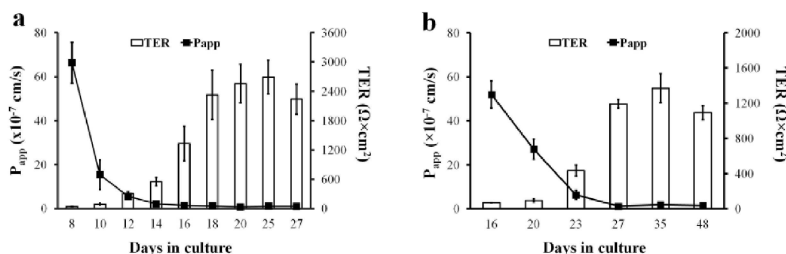
Figure 19. Epithelial integrity of VA10 cell layers increases over time.

Transepithelial electrical resistance (TER) and apparent permeability (Papp) of Flu-Na for VA10 epithelia, grown on Transwell filters, as a function of time. (a) LCC conditions, (b) ALI culture conditions. All values are mean ± SD, n = 3-5.

Consequently, this difference in TER values was dependent on culture conditions, in agreement with data from the Calu-3 and 16HBE14o- cell lines (Ehrhardt et al., 2002a, Ehrhardt et al., 2002b, Fiegel et al., 2003, Grainger et al., 2006) and outlined in Table 13. The difference in peak TER did not translate into significant difference in P_{app} values for Flu-Na since P_{app} reached a plateau for TER exceeding 1000 $\Omega \times cm^2$. This has been observed for Calu-3 cells where the TER values over 450 $\Omega \times cm^2$ provided similar P_{app} values for Flu-Na (Ehrhardt et al., 2002a). TER obtained with ALI cultured VA10 exhibit similar values as ALI cultured primary NHBE cells or 766 - 1300 $\Omega^* cm^2$ (Jakiela et al., 2008, Lin et al., 2007b) and the Calu-3 cell line or 1126 $\Omega^* cm^2$, with P_{app} for Flu-Na of 1.47 $*10^{-7}$ cm/s (Mathias et al., 2002). Although both LCC and ALI conditions provided functional tight junctions, further permeability characteristics were studied in the ALI model due to its abovementioned relevance. Various cell culture conditions are

considered to affect the outcome of the permeation studies such as cell seeding density, pore diameter and coating of inserts, culture time, serum supplement, ALI vs. LCC and cell passage (Forbes et al., 2003, Geys et al., 2007). Although most studies report that culturing epithelial cells under ALI conditions results in more differentiation than LCC and medium TER (Table 13), culturing the 16HBE14o- cell line under ALI conditions resulted in a very low TER value of 127 ± 20 $\Omega*cm^2$ and multiple cell layers that do not show a functional barrier to solutes (Ehrhardt et al., 2002b). In order to ensure that the phenotypic characteristics of the cell line remain consistent it is highly advisable to use the cell within defined number of passages. As Table 13 shows there is a great variability in cell culture conditions between labs making direct comparison of permeability values difficult.

Table 13. Comparison of culture conditions, TER and P_{app} for Na-Flu for 16HBE14o[-] , Calu-3 and the VA10 cell lines

Respiratory cell layer	Passage number	Seeding density ($\times 10^5$ cells/cm^2)	Serum suppl.	TER[a] ($\Omega \times cm^2$)	P_{app} Na-Flu ($\times 10^{-7}$)	ALI / LCC	Ref
16HBE14o[-]	47-78	1	FCS	671 ± 133	8.5 ± 0.3	LCC	**1**
				127 ± 20	49 ± 5.4	ALI	**1**
	47-87	1	FCS	NR	8.5 ± 0.3	LCC	**2**
Calu-3	-	1	FBS	~900	~1[b]	ALI	**3**
				~500	~1[b]	LCC	**3**
	38-56	1	FBS	~700	2.20 ± 0.2	LCC	**4**
				~700	2.20 ± 0.4	ALI	**4**
	38-50	5	FCS	1086 ± 113	1.48 ± 0.2	LCC	**5**
				306 ± 53	3.36 ± 0.5	ALI	**5**
	20-40	5	FBS	1126 ± 222	1.47 ± 0.1	ALI	**6**
	33-40	5	FCS	474 ± 45	2.33 ± 0.4	ALI	**7**
VA10	15-21	2	UG	2481 ± 208	1.06 ± 0.2	LCC	
	15-21	2	UG	1217 ± 47	1.51 ± 0.3	ALI	

FCS: Fetal calf serum; FBS: Fetal bovine serum; UG: Ultroser-G; [*]When then epithelium had reached equilibrium, [b] it was not clear whether the reported P_{app} value of 1.05 ± 0.22 was for ALI or LCC but the figure showed an average value of ~ 1 for both ALI and LCC and was therefore used. Ref. **1**:(Ehrhardt et al., 2002b), **2**: (Ehrhardt et al., 2003), **3**: (Ehrhardt et al., 2002a), **4**: (Fiegel et al., 2003), **5**: (Grainger et al., 2006), **6**: (Mathias et al., 2002), **7**: (Haghi et al., 2010).

To further investigate the barrier properties of VA10 epithelium, apical-to-basolateral paracellular permeability of Flu-Na and different molecular weight FDs was investigated in ALI culture (Table 14, Figure 20). Rapid decrease was observed in the P_{app} between

Flu-Na and FD10, but a modest decrease in P_{app} values was observed between FD10 and FD40. This inverse relationship observed between paracellular permeability of FD and their molecular weight is consistent with previously reported studies with Calu-3 (Grainger et al., 2006, Mathias et al., 2002) although individual values were higher in the current study. This relationship shows that the VA10 model distinguishes between compounds depending on their size.
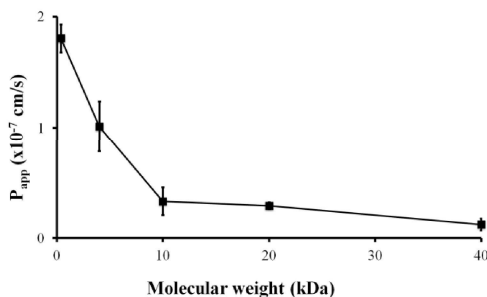
Figure 20. Paracellular permeability in the VA10 epithelium is size dependent.

Permeability (P_{app}) of Flu-Na and FITC labeled dextrans (FD4, FD10, FD20, FD40) as a function of molecular weight for ALI cultured VA10 epithelium. All values are mean ± SD, n = 3-4.

3.3 Permeation of drugs with different physiochemical properties

Lipophilicity and degree of hydrogen bonding have been reported to be the major physiochemical properties affecting the *in vivo* pulmonary absorption in rats (Tronde et al., 2003b). Therefore, *in vitro* cultured bronchial epithelia need to distinguish between compounds depending on these physiochemical properties. Apical-to-basolateral permeability of drugs with different physiochemical properties across ALI cultured VA10 epithelium was determined with four β-adrenoreceptor antagonists (alprenolol, atenolol, metoprolol and propranolol) and one β-adrenoreceptor agonist (terbutaline) chosen as model drugs. For highly lipophilic drugs, one could have ensured appropriate sink conditions with transfer experiment i.e. after each sampling the filter is moved to a new well containing the acceptor solvent. Sink conditions were assumed to be maintained under current experimental conditions since the P_{app} did not exceed 10^{-4} cm/s. Permeability increased with increased lipophilicity, ranging from $5.21 \pm 0.69 \times 10^{-7}$ cm/s for the hydrophilic atenolol, to $92.87 \pm 6.41 \times 10^{-7}$ cm/s for the lipophilic alprenolol

(Table 14) confirming that passive permeation in VA10 is dependent on lipophilicity, in line with results from the Calu-3 cell line (Foster et al., 2000, Mathias et al., 2002).

Table 14. Apical-to-basolateral P_{app} values for compounds tested in ALI cultured VA10 epithelium

Compounds	MW (Da)	cLogD[a]	PSA[b]	P_{app} ($\times 10^{-7}$ cm/s)[c]
Alprenolol	286	0.67	41	92.87 ± 6.41
Atenolol	266	-1.73	85	5.21 ± 0.69
FD-4	4000	-	-	1.01 ± 0.23
FD-10	10000	-	-	0.33 ± 0.13
FD-20	20000	-	-	0.29 ± 0.03
FD-40	40000	-	-	0.12 ± 0.05
Flu-Na	376	-0.77	76	1.51 ± 0.33
Metoprolol	685	-0.20	51	69.95 ± 7.92
Propranolol	296	0.54	41	62.90 ± 7.33
Rhodamine-123	381	0.78	-	3.99 ± 0.57
Terbutaline	274	-0.87	73	10.80 ± 3.24

[a] cLogD: logarithm of the calculated octanol/water partitioning coefficient at pH 7.4
[b] PSA: molecular polar surface area (Å^2)
[c] Mean ± SD, n = 3-5

A linear relationship (r^2 = 0.89) was observed between the extent of lipophilicity (cLogD) of the drug at pH 7.4 and its log (P_{app}) value (Figure 21.a). cLogD values were chosen to correlate with P_{app} values of the drugs, since cLogD has a stronger correlation to permeability values of model drugs, taking drug charge into account, than cLogP (Tronde et al., 2003a). Passive permeability through biological membranes is also influenced by the degree of hydrogen bonding (Conradi et al., 2008). To that end, molecular polar surface area (PSA), which is suitable to describe the hydrogen bonding capacity of a drug (Clark, 1999), showed a strong negative correlation (r^2 = 0.96) with the permeability data from the VA10 cell line with decreasing permeability as the PSA increased (Figure 21.b). This demonstrates that permeability of drugs through the VA10 epithelium depends on their lipophilic nature and degree of hydrogen bonding
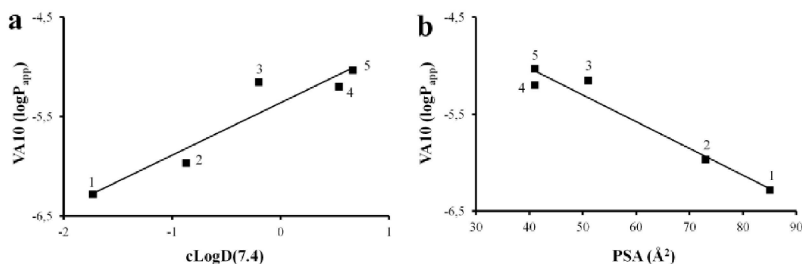
Figure 21. Drug permeability in the VA10 epithelium is dependent on physiochemical properties of the drugs.

Relationship between apparent permeability (P_{app}) of drugs across VA10 cells, cultured under ALI conditions, with their (a) calculated LogD (cLogD) at pH 7.4 ($r^2 = 0.89$) and (b) with the polar surface area (PSA, $r^2 = 96$). All values are mean ± SD, n = 4. Drug labels: 1-atenolol, 2-terbutaline, 3-metoprolol, 4-propranolol, 5-alprenolol.

Correlation of the current permeability data with previously published P_{app} data from the bronchial epithelial cell lines 16HBE14o- (Manford et al., 2005) and Calu-3 (Mathias et al., 2002) was done in order determine if the permeability characteristics of the VA10 cell model were similar to these established cell lines. Positive log-linear relationship was observed with both the 16HBE14o- and Calu-3 cell lines (Figure 22.a and b), $r^2 = 0.999$ and $r^2 = 0.96$ respectively, suggesting similar permeability characteristics.
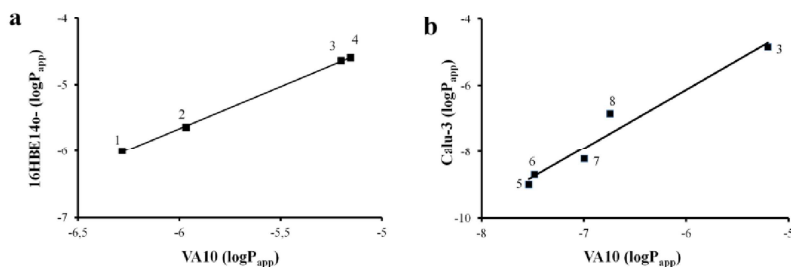
Figure 22. VA10 permeability values correlate with other *in vitro* cell models.

Correlation of the apical-to-basolateral P_{app} in VA10 with bronchial epithelial cell lines 16HBE14o- (Manford et al., 2005) ($r^2 = 0.999$) (a) and Calu-3 ($r^2 = 0.96$) (Mathias et al., 2002) (b). Each data point represents mean values for each drug. Drug labels: 1-atenolol, 2-terbutaline, 3-propranolol, 4-metoprolol, 5-FD20, 6-FD10, 7-FD4, 8-Flu-Na.

72

Direct comparison of the VA10 cell line to *in vivo* lung absorption remains to be performed. Although this current data set was limited in size, the values obtained provided good correlation with data from the 16HBE14o- (Manford et al., 2005) and Calu-3 (Mathias et al., 2002) cell lines, suggesting that VA10 has similar permeability characteristics.

3.4. Expression of the drug efflux P-glycoprotein

P-gp is a member of the ATP binding cassette transporter superfamiliy of membrane proteins and is responsible for the efflux of many drugs leading to lower than expected therapeutic concentrations (Balimane et al., 2006). P-gp has been reported to be expressed in normal human bronchial epithelial cells (Lehmann et al., 2001) and in the native human bronchus (Lechapt-Zalcman et al., 1997). Although the majority of articles using *in vitro* respiratory cells report P-gp efflux, there are articles reporting both non-existing P-gp activity and net absorptive values (Table 15). Consequently, the impact of P-gp on pulmonary drug transport *in vivo* has not been clarified. In order to determine whether the VA10 cell line expressed P-gp, when grown under ALI conditions, both transport studies and immunofluorescent studies were done. Rh123 was used as a P-gp substrate. Although Rh123 has been reported to be a substrate of both P-gp and multidrug resistance related protein-1 (MRP1) in mouse tumor cell lines (Twentyman et al., 1994), other results show that Rh123 is mainly a P-gp substrate in Calu-3 cells (Hamilton et al., 2001a). Therefore, the transport of Rh123 was determined to be mainly due to the P-gp. Predominant apical expression (Figure 23) was observed, consistent with the expression in Calu-3, 16HBE14o- and normal human bronchus (Ehrhardt et al., 2003, Hamilton et al., 2001b, Lechapt-Zalcman et al., 1997).

Table 15. Comparison of P-gp function for different P-gp substrates in different airway cell models

Respiratory cell layer	Passage number	Days in culture	P-gp substrate	Inhibitor	Direction of polarized transport	$sER^{control}/$ $sER^{P\text{-}gp\ inhibition}$	Other methods of P-gp detection	P-gp location	Ref
16HBE14o⁻	47-87	7	Rh123	Verapamil	B-A	2.95/1.03	CLSM	Apical	1
CFBE41o-	35-62	14	Rh123	Verapamil	B-A	1.65/0.94	CLSM	Apical	2
Calu-3	22-30	15	Moxifloxacin	Verapamil	B-A	2.0/1.0	Western blot	NR	3
	33	14 or 21	Digoxin	GF120918A	No polarized transport	Non existent	NR	NR	4
	53	14	Digoxin	GF120918A	B-A	2.08/~2	NR	NR	4
	53	21	Digoxin	GF120918A	B-A	2.08/~1.2	NR	NR	4
	20-62	18	Flunisolide	Verapamil	A-B	0.15/1.13	Western blot, CLSM	Basal	5
	19-40	13-15	Etoposide	Cyclosporin A	B-A	3.05/1.4	CLSM	Apical	6
NHBE	2-3	7	Rh123	Verapamil	B-A	2.95/1.65	RT-PCR	NR	7
	2-3	14	Digoxin	GF120918A	No polarized transport	Non existent	NR	NR	4
	2-3	21	Digoxin	GF120918A	A-B	0.4/1.71	NR	NR	4
hAEpC[a]	NR	8	Rh123	Verapamil	B-A	3.09/~1.1	Western blot, RT-PCR, CLSM	Apical	8
VA10	15-21	35	Rh123	Verapamil	B-A	1.44/1.07	CLSM	Apical	

sER: Secretory efflux ratio ($P_{app}^{B\text{-}A}/P_{app}^{A\text{-}B}$); CLSM: confocal laser scanning microscopy; RT-PCR: reverse transcription polymerase chain reaction; hAEpC: Human alveolar epithelial cells. Ref. **1**: (Ehrhardt et al., 2003). **2**: (Ehrhardt et al., 2006). **3**: (Brillault et al., 2009). **4**: (Madlova et al., 2009). **5**: (Florea et al., 2001), **6**: (Hamilton et al., 2001b), **7**: (Lin et al., 2007b), **8**: (Endter et al., 2007).
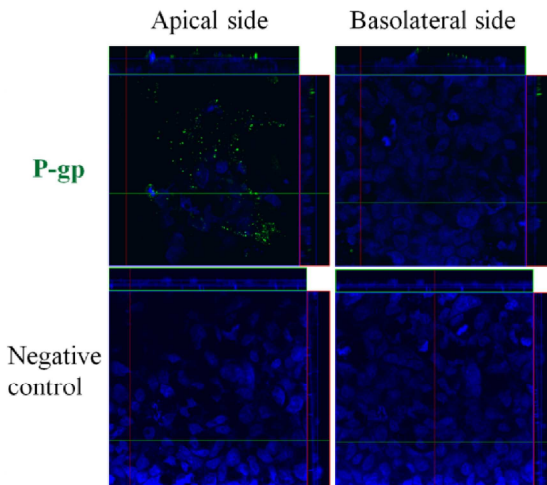
Figure 23. Localization of P-gp in VA10 epithelium.

VA10 cells were cultured under ALI conditions for 34 days. Immunofluorescent localization of P-gp (green), and nucleus (blue) in either regular plane or vertical xz cross sections, showing the apical localization of the P-gp protein.

To establish the activity of the P-gp, apical-to-basolateral (A-B) permeability for the P-gp substrate Rh123 was compared to the basolateral-to-apical (B-A) permeability (Table 16). The efflux ratio of 1.44 (B-A/A-B) suggested a trend towards asymmetric transport of Rh123; however, the difference was not significant (p > 0.05). When VA10 epithelia were simultaneously treated with Rh123 and the P-gp inhibitor verapamil (200 μM), the B-A transport of Rh123 decreased to 69 % (p < 0.05) producing efflux ratio of 1.07, thereby confirming the P-gp mediated efflux of Rh123. To show that this efflux potential was specific to Rh123, the A-B and B-A P_{app} for the reference compound Flu-Na was carried out with no significant change (p > 0.05) when treated with verapamil.

As can be seen in Table 15, the efflux ratio of 1.44 reflects relatively low functional activity compared to 16HBE14o-, Calu-3 and the NHBE cells (Brillault et al., 2009, Ehrhardt et al., 2003, Lin et al., 2007b) but has similar ratio to the cell line CFBE41o- or 1.65 (Ehrhardt et al., 2006). There are also findings reporting no efflux (Madlova et al., 2009) or net secretion (Florea et al., 2001) of P-gp substrates in

respiratory cells. This could be attributed to the difference in culture conditions since higher passage number and time in culture have been reported to promote the expression of P-gp (Lin et al., 2007b, Madlova et al., 2009). In our work, we used VA10 cells of early passage but the cell layers used had been cultured for ~34 days. Therefore, P-gp function could have been more evident using VA10 cells at later passages.

Table 16. P_{app} values for permeation markers in the presence or absence of the P-gp inhibitor verapamil in ALI cultured VA10 epithelium

Compounds	± Verapamil	P_{app} ($\times 10^{-7}$ cm/s)[a]	
		A-B	**B-A**
Rhodamine 123	-	3.99 ± 0.57	5.74 ± 1.16
Rhodamine 123	+	3.73 ± 0.73	3.97 ± 0.45[b]
Fluorescein-Na	-	1.42 ± 0.21	1.67 ± 0.05
Fluorescein-Na	+	1.43 ± 0.06	1.54 ± 0.12

[a] All values are mean ± SD, n = 3-5. Cell layers cultured for 49 days
[b] Significantly different (p < 0.05) from B-A without verapamil

Compared to the Calu-3 and 16HBE14o- cell lines, the major limitation of our model is its relatively long culture time needed to obtain good barrier properties. This can possibly be due to the progenitor nature of VA10 cells, taking longer time to develop functional barrier integrity. Despite the long culture time before full integrity is reached in ALI culture, this integrity can be maintained for as long as 2-3 weeks in culture. Furthermore, VA10 is an important addition to the previously existing cell lines, introducing a basal to ciliated phenotype that does not form multiple cell layers and is not of cancerous origin. This progenitor cell line would be useful to study passive drug permeation, both para- and transcellularly as well as specific intracellular events. In particular, this cell line provides opportunities to investigate the effects of drugs and other compounds on the cellular development and differentiation potential, such as the involvement of transcription factors and receptors in induced tumor progression, and the effects of possible paracellular permeation enhancers.

4. Permeation enhancing effects of *N*-quaternary chitosan derivatives (Paper # 4)

By using VA10 cell line that mimics the bronchial epithelium, the determination of permeation enhancement properties of *N*-quaternary chitosan derivatives in addition to their possible cellular mechanisms, such as TJ alterations, was enabled. Paper #1 showed the detailed structural analysis of four *N*-alkyl-*N*,*N*-dimethyl chitosan derivatives (TMC, QuatPropyl, QuatButyl and QuatHexyl), elucidating the composition of each polymer. Longer *N*-alkyl chains of these *N*-quaternary chitosan derivatives possess an increased degree of amphiphilicity that could have marked influence on the paracellular permeation of inert markers compared to shorter *N*-quaternary derivatives. Therefore, the aim of this study was to investigate the relationship between the different *N*-alkylation of those chitosan derivatives and their paracellular permeation enhancement in bronchial epithelia *in vitro*.

4.1. *N*-Quaternary chitosan derivatives cause dose dependent decrease in TER

TER is the principal technique to investigate TJ integrity. VA10 bronchial epithelium was treated with the *N*-quaternary chitosan derivatives in different concentrations resulting in a clear dose-dependent decrease in TER (Figure 24). The decrease was different between derivatives. TMC and QuatPropyl caused a slow and gradual decrease in TER (Figure 24.A and B) while QuatButyl chitosan and QuatHexyl chitosan caused a more rapid decrease (Figure 24.C and D). Table 17 gives the decrease in TER after 2 h treatment with all the *N*-quaternary chitosan derivatives at different concentrations and the subsequent TER after 24h recovery. Fully quaternized TMC caused a moderate decrease in TER. A significant decrease ($p < 0.05$) in TER as early as 20 min after beginning of treatment was observed for 1 mg/ml and after 60 min of treatment, 0.25 mg/ml also caused a significant decrease in TER (Figure 24.A). These differences were maintained throughout the experiment resulting in 55 % decrease in TER for 1 mg/ml and 46 % decrease for 0.25 mg/ml.
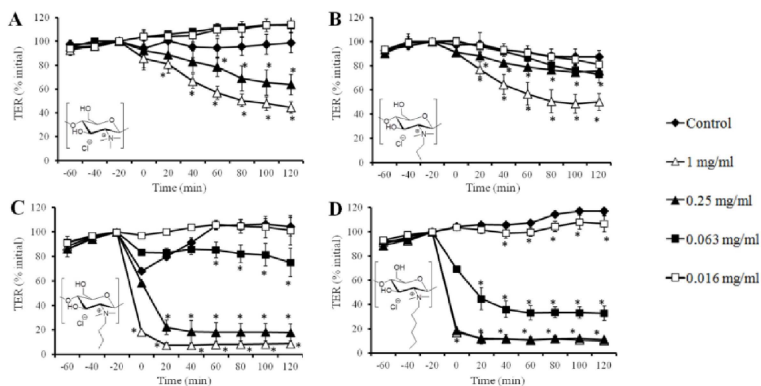
Figure 24. Effect of *N*-quaternized chitosan derivatives on TER in ALI cultured VA10 cell layers.

TMC, B. QuatPropyl, C. QuatButyl and D. QuatHexyl. Each point represents the mean ± SD of 3-5 experiments, *significantly different from control (p< 0.05).

Slightly stronger effects were seen for QuatPropyl, causing a significant decrease in TER after 20 min both with 1 mg/ml and 0.25 mg/ml with 0.063 mg/ml reaching significantly lower TER than control at 120 min (Figure 24.B). At the end of the experiment, TER had decreased by 50%, 24% and 26% for 1, 0.25 and 0.063 mg/ml respectively (Table 17). QuatButyl caused a dramatic decrease in TER right after the addition of the polymer (0 min) to the epithelium with a significant decrease observed for 1 mg/ml and 0.25 mg/ml (Figure 24.C). After 60 min, 0.063 mg/ml QuatButyl also caused a significant decrease in TER. The treatment resulted in a 91 %, 82% and 19% reduction in TER for 1, 0.25 and 0.063 mg/ml respectively. Treatment with QuatHexyl resulted in the most prominent effect on TER (Figure 24.D). Derivatives at the concentrations of 1, 0.25 and 0.063 mg/ml produced a rapid and significant decrease in TER that remained throughout the experiment resulting in 90%, 89% and 67% decrease respectively in TER after 120 min (Table 17).

Table 17. TER values (% initial value) after treatment with *N*-quaternary chitosan derivatives and subsequent recovery

Concentration (mg/ml)	TMC[a]		QuatPropyl[a]		QuatButyl[a]		QuatHexyl[a]	
	TER 2h treatment	TER 24h recovery	TER 2h treatment	TER 24h recovery	TER 2h treatment	TER 24h recovery	TER 2h treatment	TER 24h recovery
0.016	114.1 ± 6.3	101.2 ± 3.7	81.2 ± 7.1	62.2 ± 5.0	101.3 ± 11.6	42.1 ± 7.2	106.6 ± 6.7^b	82.9 ± 7.5
0.063	113.9 ± 4.2	112.5 ± 10.2	74.2 ± 5.5^b	51.8 ± 3.7	80.5 ± 10.8^b	45.9 ± 3.8	32.9 ± 5.3^b	70.2 ± 7.7
0.25	63.7 ± 8.6^b	80.0 ± 12.2	76.1 ± 1.6^b	52.9 ± 2.4	17.9 ± 6.6^b	52.5 ± 5.8	11.2 ± 1.3^b	14.4 ± 2.3
1	44.6 ± 4.8^b	63.7 ± 13.6	50.2 ± 7.3^b	45.4 ± 2.1	8.7 ± 0.5^b	67.2 ± 4.4	10.0 ± 2.2^b	8.6 ± 2.3

[a] Each value represents the mean $\pm$ SD of 3-4 experiments

[b] Significantly different from control, $p < 0.05$

Table 18. P_{app} for FD4 and permeation enhancement ratio for *N*-quaternized chitosan derivatives

Concentration (mg/ml)	TMC		QuatPropyl		QuatButyl		QuatHexyl	
	P_{app} ($\times 10^{-7}$ cm/s)[a]	ER[b]	P_{app} ($\times 10^{-7}$ cm/s)[a]	ER[b]	P_{app} ($\times 10^{-7}$ cm/s)[a]	ER[b]	P_{app} ($\times 10^{-7}$ cm/s)[a]	ER[b]
0.016	4.01 ± 0.32	1.4	5.00 ± 2.07^c	1.8	3.50 ± 0.31	1.2	5.24 ± 0.67^c	1.8
0.063	4.07 ± 0.54	1.4	7.01 ± 1.49^c	2.5	6.90 ± 1.30^c	2.4	7.41 ± 1.35^c	2.6
0.25	5.43 ± 1.11^c	1.9	6.61 ± 1.78^c	2.3	12.35 ± 2.83^c	4.3	14.18 ± 2.85^c	5.0
1	10.03 ± 1.14^c	3.5	13.03 ± 3.47^c	4.6	18.11 ± 1.73^c	6.4	15.26 ± 2.47^c	5.4

[a] Each value represents the mean $\pm$ SD with 3-4 experiments

[b] Permeation enhancement ratio (ER) is calculated by: P_{app} sample/P_{app} control

[c] Significantly different from control ($p < 0.05$)

Ideally, the effects on the paracellular space should only be transient; therefore it is important to determine the epithelial recovery after treatment with these derivatives. As can be seen in Table 17, the VA10 epithelium nearly fully recovered after 0.25 mg/ml TMC, suggesting that this dose enhances permeation reversibly. No recovery in TER was observed after treatment with QuatPropyl and partial recovery after QuatButyl. Interestingly, recovery was most prominent after treatment with 1 mg/ml QuatButyl, followed by 0.25 mg/ml and then 0.063 mg/ml (Table 17). Higher concentrations of QuatButyl could have caused the strongest effects on the paracellular space leading to possible upregulation of TJ proteins that results in higher relative recovery compared to the lower concentrations used. Treatment with QuatHexyl resulted in recovery only after the 0.063 mg/ml dose.

4.2. Influence on paracellular permeability

In agreement with the reduction in TER, general increase in the paracellular permeability of FD4 was observed. The paracellular permeation of FD4 is routinely used as a method to show the functional restriction of paracellular transport and, consequently, the effects of paracellular permeation enhancers. There was a clear dose dependent relationship between the P_{app} of FD4 and the *N*-quaternary chitosan derivatives (Figure 25).
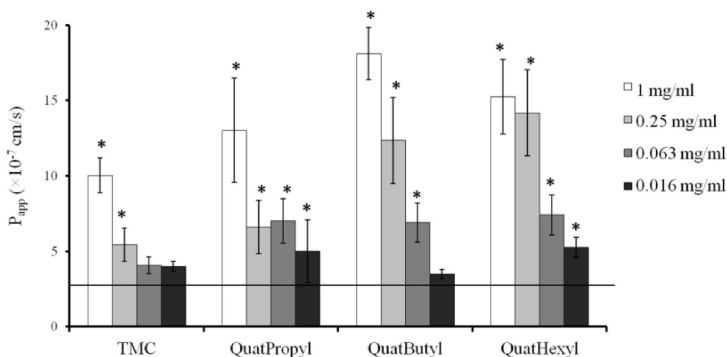
Figure 25. Comparison of FD4 P_{app} values between chitosan derivatives

Effect of quaternized chitosan TMC, QuatPropyl chitosan, QuatButyl chitosan and QuatHexyl chitosan on P_{app} of FD4. The line represents the FD4 control. Each bar represents a mean ± SD of 3-5 experiments, *significantly different from control (p < 0.05).

TMC and QuatPropyl produced a moderate permeation enhancement ratio (ER) of 3.5 and 4.6 respectively for the highest concentration (Table 18). QuatButyl produced the largest increase in permeability at 1 mg/ml with the permeation enhancement ratio of 6.4, followed closely with QuatHexyl of 5.4.

4.3. Effect of the quaternary chitosan derivatives on cell viability

Reduced viability can cause increased permeability and decreased TER and should consequently be studied. Viability was determined with an MTT assay in 96 well plates for all quaternary chitosan derivatives. A clear dose dependent effect on viability was observed, with the lowest overall viability observed for QuatHexyl chitosan (Figure 26.A). TMC and QuatPropyl decreased viability in concentrations from 0.063 mg/ml, QuatButyl from 0.001 mg/ml while QuatHexyl affected viability in all concentrations used. The viability of the VA10 cells was also determined 24 h after treatment with the N-quaternary chitosan derivatives (Figure 26.B).

In line with the TER data that showed recovery 24 after treatment, a moderate effect on viability after TMC and QuatPropyl chitosan treatment was observed, showing epithelial recovery after treatment with these two derivatives. Treatment with 0.063 mg/ml QuatButyl resulted in around 60% reduced viability while treatment with 0.016 mg/ml QuatHexyl resulted in 50% reduced viability. Cationic detergents have been reported to affect viability in all concentrations tested (Whitehead et al., 2008), similar to QuatHexyl in the current study. It is therefore possible that QuatHexyl simply disrupts the structure of the lipid bilayer, with consequent increase in permeation.

The viability of the VA10 cells after treatment with HBSS buffer at pH 6.0 was compared to the viability after treatment in HBSS buffer at pH 7.4. The viability at pH 6 was 68 ± 8 % of the control value, suggesting that acidic pH significantly reduces viability of bronchial epithelia *in vitro*, thereby practically excluding the use of chitosan in the airways. Such adverse effects have also been reported with Calu-3 and 16HBE14o- bronchial epithelial cell lines (Kudsiova and Lawrence, 2008, Scherließ, 2011), showing that testing chitosan at pH 6.0 is not relevant.
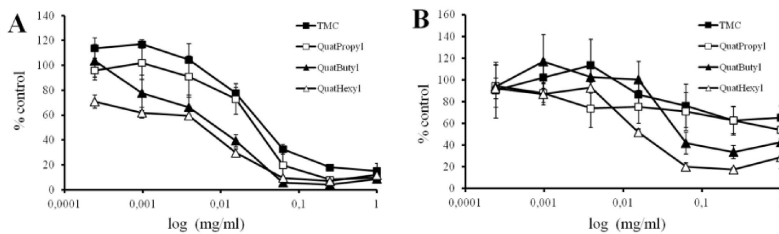
Figure 26. Effect of quaternized chitosan derivatives on viability in VA10 cells as determined by MTT in 96 well plate assay.

A. Viability of VA10 cells after 2 h incubation with *N*-quaternary chitosan derivatives. **B.** Viability of VA10 cells after 24 h recovery from *N*-quaternary chitosan treatment. Each point represents the mean ± SD of 4 experiments.

As previously mentioned, the trypan blue cytotoxicity staining has been the predominant method in determining cytotoxicity of TMC, showing that viability was not affected after TMC treatment (Kotze et al., 1997b, Kotze et al., 1999b, Kotze et al., 1999c, Thanou et al., 2000b). However, disparities are in the MTT viability assays for TMC. While one study shows that TMC (DQ 43%) reduced viability at 0.1 mg/ml in the Caco-2 cell line (Verheul et al., 2009) another study demonstrated that treatment with TMC (DQ 20 and 60%) did not result in reduced viability in Calu-3 cells after treatment with 15 mg/ml TMC (Florea et al., 2006). Interestingly, that study reported that acidic buffer (pH 5.5) did not decrease the viability of Calu-3 cells, in contrast to our observation and previous studies in Calu-3 and 16HBE14o- (Kudsiova and Lawrence, 2008, Scherließ, 2011) bronchial epithelial cells.

As determined with the 96 well MTT viability assay, there was transient reduction in viability after treatment with TMC at 1 mg/ml and 0.25 mg/ml. However, there were no visible alterations in the morphology of ALI cultured epithelium after the permeation studies using TMC (data not shown). The viability was therefore investigated using MTT in ALI grown VA10 epithelium after treatment with TMC, with no significant change in the viability observed (Figure 27). This has also been reported for 16HBE14o- bronchial epithelial cells cultured at ALI, where no effect on the viability, as determined by MTT, was reported after treatment with chitosan nanoparticles (Lim et al., 2001). Conversely, Calu-3 cells treated with chitosan solutions have reported to be more sensitive when cultured on Transwell filters than in the 96 well system (Scherließ,
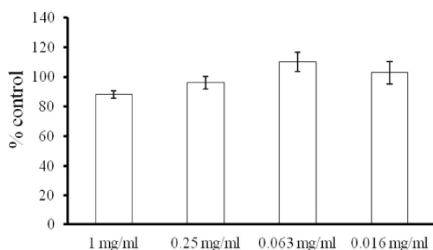
Figure 27. Effect of TMC on viability as determined with the MTT assay in ALI cultured VA10 cell layers.

Each bar represents the mean ± SD of 4 experiments.

2011). There is, however, marked difference between these two cell lines. The Calu-3 cell line is derived from adenocarcinoma (Fogh et al., 1977) and produces mucus that the polymer must traverse before reaching the cells. Immortalized VA10 cells were, on the other hand, isolated from a normal human lung (Halldorsson et al., 2007). VA10 is a progenitor cell line, differentiating towards ciliated cells when cultured under ALI but does not produce mucus under current culture conditions. Consequently, testing the viability in a 96 well assay where the cells are in a more basal phenotype could explain their sensitivity to the quaternary chitosan derivatives compared to the ALI culture.

4.4. Effects of chitosan derivatives on TJ protein expression

TJs form a barrier between cells, thereby regulating the paracellular permeability across the cell layer (Shin et al., 2006). Confocal microscopy of the TJ protein claudin-4 and the TJ associated protein F-actin expression after treatment with fully quaternized TMC and QuatHexyl were done. TMC did not induce any apparent effect on F-actin structure, while QuatHexyl caused a clear disbandment (Figure 28.A). Pronounced alterations of claudin-4 expression in confocal microscopy were also observed after QuatHexyl treatment while TMC did not significantly alter the claudin-4 expression as seen in confocal microscopy at different time points, which was confirmed with western blotting (Figure 28.A and B).
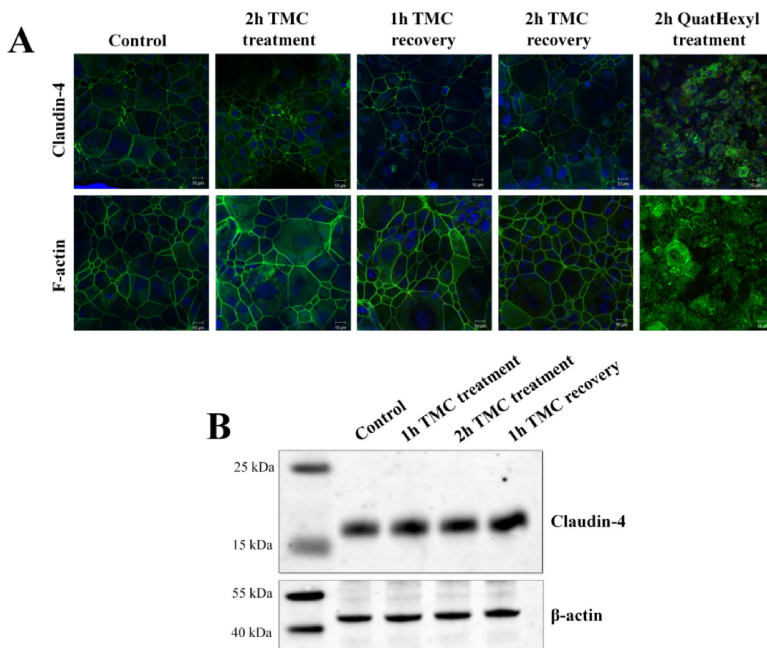
Figure 28. Expression of the TJ protein claudin-4 and the TJ associated protein F-actin in ALI cultured VA10 cell layers after treatment with TMC and QuatHexyl.

A. Confocal fluorescent expression of claudin-4 and F-actin after treatment with 0.25 mg/ml TMC and 0.25 mg/ml QuatHexyl. B. Western blot of claudin-4 after treatment with 0.25 mg/ml TMC.

4.5. Structure-activity relationship

There are several factors that could influence the permeation enhancing properties of *N*-quaternary chitosan derivatives such as the DQ, *N*-alkylation and DA. The quaternary chitosan derivatives used in the current study have high DQ; TMC of~ 100%, QuatPropyl ~85%, QuatButyl ~91% and QuatHexyl ~89%. With TMC at pH ~7.4, the DQ is a major participant in the permeation enhancement (Jonker et al., 2002) with higher DQ producing higher ER (Kotze et al., 1999b, Thanou et al., 2000b). In contrast to earlier TMCs, the TMC used in the current study was fully trimethylated and therefore has more charge density. Earlier studies of TMC with 20% DQ produced an ER of 5 for FD-4 at 15 mg/ml (Kotze et al., 1999c) compared to ER of 3.5 at 1 mg/ml in the current

study. Accordingly, the high charge density for all the *N*-quaternized chitosan derivatives used in the current study could explain why relatively low concentrations are sufficient to increase ER.

Although TMC had the highest DQ, it was not as potent in increasing the permeation as the other *N*-quaternary chitosan derivatives. Here, the degree of *N*-alkylation comes into play. By increasing the length of the *N*-alkyl chain, the polymer becomes more amphiphilic thereby resembling quaternary ammonium surfactants such as cetyltrimethylammonium bromide, a known permeation enhancer in transdermal drug delivery (Ashton et al., 1992, Nokhodchi et al., 2003). There is an interesting association between the *N*-alkyl chain length and the degree of permeation and viability. Increased amphiphilicity of QuatButyl and QuatHexyl clearly aided in their permeation enhancing properties since they were as follows; QuatHexyl ≈ QuatButyl > QuatPropyl > TMC at pH 7.4. The effect of the longer *N*-alkylated chitosan derivatives might be different from that of TMC, since concomitant decrease in viability was observed with increase in the *N*-alkyl chain length. This could be attributed to less steric hindrance of the cation in the longer alkyl chains and more flexibility than in the shorter chains, producing stronger effects.

DA and *O*-methylation have been reported to influence the permeation enhancing properties of TMC (Polnok et al., 2004, Verheul et al., 2008, Verheul et al., 2009). In the current study, all the *N*-quaternary chitosan derivatives originate from the same batch of chitosan, almost fully deacetylated (around 3%) without *O*-methylation (paper # 1). The different effects of these derivatives on permeation and viability should therefore be regarded to be due to *N*-alkylation. The fully *N*-quaternized TMC could be considered as the chitosan derivative possessing an optimal balance between increasing permeation without producing prolonged adverse effects to the bronchial epithelium. Consequently, the fully quaternized TMC should be considered as a promising candidate for the development of future pulmonary dosage forms.

4.6. Possible mechanism of action

The definite mechanism behind the permeation enhancing effects of chitosan and its derivatives remains to be elucidated. Yet, possible mechanisms behind this effect can be theorized. Chitosan could have direct effects on TJs. The TJ protrude into the paracellular space, are highly hydrated and contain fixed negative sites (Madara, 1987). Consequently, changes in the ionic concentration in these pores, as with the cationic chitosan derivative TMC, could lead to delicately modulated displacement of the TJ structures leading to their transient "opening" to larger solutes such as FDs without significantly altering the TJ architecture. Larger quantities of TMC could, consequently, cause increased dissociation of the TJ and other adhesion proteins such as integrins, leading to cell death due to loss in adhesion, also called anoikis (Frisch and Francis, 1994).

Secondary or alternatively to this action could be the specific or unspecific binding of chitosans to integrins. Recently, a study has showed that chitosan interacts with the integrin αvβ3 in the Caco-2 cell line, proposed to result in claudin-4 relocalization and subsequent permeation enhancement (Hsu et al., 2012). Integrins are transmembrane glycoproteins that serve as adhesion and signaling receptors and help regulating wound repair, cellular polarization and modulation of local inflammation in epithelial cells (Sheppard, 2003). Additionally, integrins have been utilized as targets for viruses and bacteria, resulting in their uptake and subsequent pathogenesis (Sheppard, 2003) and have consequently been proposed to serve as epithelial pattern recognition receptors (Ulanova et al., 2009). Chitin, the precursor of chitosan, is found ubiquitously in fungi, insects and parasites (Lee, 2009) and is recognized by pattern recognition receptors in the murine lungs (Da Silva et al., 2009). Although no study has shown that bronchial integrins recognize chitin or chitosan, various integrins are expressed on airway epithelial cells. They are involved in the epithelial adhesion to the extracellular matrix, with the integrins α2β1 and α3β1 been hypothesized to serve in the cell-cell adhesion (Carter et al., 1990, Symington et al., 1993). Interestingly, the integrin α2β1 has been linked to the direct binding of the human echovirus (Bergelson et al., 1992) causing the internalization of the virus-integrin complex to the perinuclear region (Rintanen et al., 2012). This process is mediated by the protein kinase C alpha (PKCα) (Ng et al., 1999), the same protein kinase linked to the mediated permeation

enhancement of chitosan (Smith et al., 2005). Therefore the question arises whether TMC is internalized through this mechanism. As shown in paper #2, end-labeled f-TMC is internalized into the VA10 cells, an action that was not anticipated due to previous literature reporting no internalization of chitosan. If integrin recognizes chitosan and its derivatives selectively, fluorescently labeling the polymer backbone could result in its inefficient binding and internalization compared to the fluorescently end-labeled TMC.

The gradual decrease in TER accompanied with no apparent effect on TJ relocalization after treatment with TMC compared to the rapid decrease in TER and complete dissociation of the TJ protein investigated for QuatHexyl also indicates a different mode of action. Increased *N*-alkyl chain length in quaternary chitosan could exert its effect both in the paracellular space as with TMC but also on the cell membrane itself, thereby causing severe decrease in viability.

Summary and conclusions

Administration of macromolecular drugs with the aid of permeation enhancers is an ever-growing research field within the pharmaceutical sector. The structure of the permeation enhancer needs to be well defined if the relationship between structure and the direct effect on the epithelial membrane is to be elucidated. The model, in which the permeation enhancement is determined, needs to resemble the native epithelium in terms of morphology and permeation characteristics. The effort presented in this thesis has been aimed at carrying out a detailed synthesis of chitosan derivatives and to characterize their permeation enhancing effect in the VA10 bronchial epithelial model.

The main results of this work are as follows:

- The use of di-TBDMS chitosan precursor enabled selective *N*-modifications of the chitosan polymers under homogenous conditions, in common organic solvents, at moderate temperatures and under different reaction conditions.

- Fully *N,N,N*-trimethylated chitosan and 85-91% quaternized *N*-alkyl-*N,N*-dimethyl chitosan derivatives without *O*-methylation could be synthesized using di-TBDMS chitosan as a precursor.

- Selective labeling with EDANS-O-NH$_2$ fluorophore to the reducing end of TMC formed a TMC-oxime-fluorophore, showing the proof-of-concept for chitosan oxime linkage.

- The selectivity of the oxime-linkage strategy enabled the visualization of the TMC-oxime-conjugate in the VA10 cell line, revealing both intra-and extracellular localization.

- The human bronchial epithelial cell line VA10 generated cell layers with barrier function, permeability characteristics and ciliated morphology that closely resembles the native airway epithelium. Therefore, the VA10 cell line is a useful model to study airway drug delivery *in vitro*.

- Longer *N*-alkyl chain on *N*-quaternary chitosans produced the most prominent effect on TER, paracellular permeability of FD4 and reduced viability in the VA10 cell line.

- The fully quaternized TMC should be considered as a promising candidate for the development of future pulmonary dosage forms.

Future perspectives

Synthesis and *in vitro* applications of quaternary chitosan derivatives were the focus of this PhD thesis. The di-TBDMS chitosan has proven to be a useful precursor for selective *N*-modifications. Detailed characterization of the resulting *N*-quaternized chitosan derivatives, as was performed as part of the work for the current thesis, would be crucial for their acceptance as possible pharmaceutical excipients. In addition to reducing the reaction time for the synthesis of these *N*-quaternary chitosan derivatives, more streamlined synthetic approach could also be beneficial. This could be performed by applying a direct reductive alkylation, allowing the reaction to proceed to form *N,N*-dimethyl-di-TBDMS chitosan. Subsequently, the chitosan derivatives could be quaternized with either alkyl halides or alkyl triflates.

By utilizing hydroxylamine reactivity, I was able to conjugate a fluorophore to the reducing end of TMC through the oxime linkage. This enabled the study of the *in vitro* localization and the MW of the conjugated product. To elucidate the specificity of the f-TMC internalization i.e. if it is restricted to the VA10 cell line and if only f-TMC and not chitosan is internalized, further studies would benefit from comparing the studies in paper #2 to another relevant cell line using both f-TMC and f-chitosan. Choices of fluorophores in my study were dictated by the fact that the EDANS-O-NH$_2$ had previously been synthesized as an aminooxy conjugated fluorophore and was therefore used. However, for further localization studies with TMC, I would recommend derivatives of FITC or tetramethylrhodamine-isothiocyanate (TRITC) as fluorophores since they are detectable with our confocal microscope and would aid in visualizing TMC or other chitosan derivatives in greater detail.

I have shown that all the *N*-quaternary chitosan derivatives increased the paracellular permeation that was dependent on the amphilicity of the derivative. However, elucidating specific cellular events, such as possible TJ relocalization, taking place during treatment with these derivatives could benefit from more direct approach. Protein separation of the plasma membrane fractions from other membranous organs and cytosol would have given a better picture of possible cellular trafficking of TJ proteins or other adherent proteins. However, time constrains limited these attempts and these

studies could not be completed as a part of the current PhD project. Alternatively, stable transfection of VA10 cell line with a plasmid containing a specific TJ with a fluorescent tag could be introduced to monitor real time TJ related events.

The quaternary chitosan derivatives showed a dose dependent relationship with the permeation enhancing effects that was dependent on the *N*-alkylation. Longer *N*-alkyl chain of the quaternary chitosan derivatives were effective at lower concentrations, than the shorter *N*-alkyl quaternized chitosan derivatives, but produced adverse effects linked to their increased amphiphilic nature. Polyethylene glycol modification of these N-quaternized chitosan derivatives could prove to be beneficial in improving their biocompatibility. Perhaps QuatButyl and QuatHexyl could be efficient in transdermal drug delivery at lower dosage and/or in treatment of skin infections since the quaternary moiety of chitosan has been shown to act against Gram + bacteria with potential beneficial antibacterial effects from the long alkyl chain.

Using cell lines requires certain compromises. While they have many attractive qualities they do not represent the entire cell population as it is *in vivo*. The VA10 cell line can be considered to be more anatomically correct than cancerous cell lines such as Caco-2 and Calu-3 providing us with opportunities to investigate the effects of drugs and other compounds on the cellular development and differentiation potential, such as the involvement of transcription factors and receptors in induced tumor progression, and the effects of possible paracellular permeation enhancers. Furthermore, by culturing VA10 cells under ALI conditions, we get closer to mimicking the *in vivo* airway barrier that enables us to take the next step in drug permeation studies using aerosols.

REFERENCES

AbdelMagid AF, Carson KG, Harris BD, Maryanoff CA, and Shah RD. Reductive amination of aldehydes and ketones with sodium triacetoxyborohydride. Studies on direct and indirect reductive amination procedures. J Org Chem. 1996; 61(11):3849-3862.

Adjei A, Doyle R, Pratt M, Finley R, and Johnson E. Bioavailability of Leuprolide Following Intratracheal Administration to Beagle Dogs. Int J Pharm. 1990; 61(1-2):135-144.

Adler KB, Holdenstauffer WJ, and Repine JE. Oxygen Metabolites Stimulate Release of High-Molecular-Weight Glycoconjugates by Cell and Organ-Cultures of Rodent Respiratory Epithelium Via an Arachidonic Acid-Dependent Mechanism. Journal of Clinical Investigation. 1990; 85(1):75-85.

Ahsan F, Arnold JJ, Yang TZ, Meezan E, Schwiebert EM, and Pillion DJ. Effects of the permeability enhancers, tetradecylmaltoside and dimethyl-beta-cyclodextrin, on insulin movement across human bronchial epithelial cells (16HBE14o(-)). Eur J Pharm Sci. 2003; 20(1):27-34.

American Type Culture Collection Catalog: HTB-55. LGC Group. 2012 [cited 5th of july]. Available from: http://www.atcc.org/ATCCAdvancedCatalogSearch/ProductDetails/tabid/452/Default.aspx?ATCCNum=HTB-55&Template=cellBiology.

Amidi M, Romeijn SG, Borchard G, Junginger HE, Hennink WE, and Jiskoot W. Preparation and characterization of protein-loaded N-trimethyl chitosan nanoparticles as nasal delivery system. J Controlled Release. 2006; 111(1-2):107-116.

Anthonsen MW, and Smidsrod O. Hydrogen-Ion Titration of Chitosans with Varying Degrees of N-Acetylation by Monitoring Induced H-1-Nmr Chemical-Shifts. Carbohydr Polym. 1995; 26(4):303-305.

Artursson P, Lindmark T, Davis SS, and Illum L. Effect of Chitosan on the Permeability of Monolayers of Intestinal Epithelial-Cells (Caco-2). Pharm Res. 1994; 11(9):1358-1361.

Asgrimsson V, Gudjonsson T, Gudmundsson GH, and Baldursson O. Novel effects of azithromycin on tight junction proteins in human airway epithelia. Antimicrob Agents Ch. 2006; 50(5):1805-1812.

Ashton P, Walters KA, Brain KR, and Hadgraft J. Surfactant effects in percutaneous absorption I. Effects on the transdermal flux of methyl nicotinate. Int J Pharm. 1992; 87(1–3):261-264.

Avadi MR, Erfan M, Sadeghi AMM, Moezi L, Dehpour AR, Younessi P, Tehrani MR, and Shafiee A. N,N-diethyl N-methyl chitosan as an enhancing agent for colon drug delivery. Journal of Bioactive and Compatible Polymers. 2004; 19(5):421-433.

Avadi MR, Zohuriaan-Mehr MJ, Younessi P, Amini M, Tehrani MR, and Shafiee A. Optimized synthesis and characterization of N-triethyl chitosan. Journal of Bioactive and Compatible Polymers. 2003; 18(6):469-479.

Baldrick P. The safety of chitosan as a pharmaceutical excipient. Regul Toxicol Pharmacol. 2010; 56(3):290-299.

Balimane PV, Han YH, and Chong SH. Current industrial practices of assessing permeability and P-glycoprotein interaction. Aaps J. 2006; 8(1):E1-E13.

Bayat A, Sadeghi AMM, Avadi MR, Amini A, Rafiee-Tehrani M, Shafiee A, Majlesi R, and Junginger HE. Synthesis of N,N-dimethyl N-ethyl chitosan as a carrier for oral delivery of peptide drugs. Journal of Bioactive and Compatible Polymers. 2006; 21(5):433-444.

Bergelson J, Shepley M, Chan B, Hemler M, and Finberg R. Identification of the integrin VLA-2 as a receptor for echovirus 1. Science. 1992; 255(5052):1718-1720.

Binette A, and Gagnon J. Regioselective Silylation of N-Phthaloylchitosan with TBDMS and TBDPS Groups. Biomacromolecules. 2007; 8(6):1812-1815.

Bitonti AJ, Dumont JA, Low SC, Peters RT, Kropp KE, Palombella VJ, Stattel JM, Lu Y, Tan CA, Song JJ, Garcia AM, Simister NE, Spiekermann GM, Lencer WI, and Blumberg RS. Pulmonary delivery of an erythropoietin Fc fusion protein in non-human primates through an immunoglobulin transport pathway. Proceedings of the National Academy of Sciences of the United States of America. 2004; 101(26):9763-9768.

Blank F, Rothen-Rutishauser BM, Schurch S, and Gehr P. An optimized in vitro model of the respiratory tract wall to study particle cell interactions. J Aerosol Med. 2006; 19(3):392-405.

Boers JE, Ambergen AW, and Thunnissen FBJM. Number and proliferation of basal and parabasal cells in normal human airway epithelium. Am J Resp Crit Care. 1998; 157(6):2000-2006.

Borchard G, Luessen HL, deBoer AG, Verhoef JC, Lehr CM, and Junginger HE. The potential of mucoadhesive polymers in enhancing intestinal peptide drug absorption .3. Effects of chitosan-glutamate and carbomer on epithelial tight junctions in vitro. J Controlled Release. 1996; 39(2-3):131-138.

Boucher RC, Stutts MJ, and Gatzy JT. Regional differences in bioelectric properties and ion flow in excised canine airways. Journal of Applied Physiology. 1981; 51(3):706-714.

Brillault J, De Castro WV, Harnois T, Kitzis A, Olivier JC, and Couet W. P-Glycoprotein-Mediated Transport of Moxifloxacin in a Calu-3 Lung Epithelial Cell Model. Antimicrob Agents Ch. 2009; 53(4):1457-1462.

Carter WG, Wayner EA, Bouchard TS, and Kaur P. The role of integrins alpha 2 beta 1 and alpha 3 beta 1 in cell-cell and cell-substrate adhesion of human epidermal cells. The Journal of Cell Biology. 1990; 110(4):1387-1404.

Guidance for industry: Waiver of *in vivo* bioavailability and bioequivalance studies for immediate-release solid oral dosage forms based on a biopharmaceutics classification system. 2000, CDER/FDA. Available from:
http://www.fda.gov/downloads/Drugs/GuidanceComplianceRegulatoryInformation/Guidances/ucm070246.pdf.

Cereijido M, Contreras RG, Flores-Benítez D, Flores-Maldonado C, Larre I, Ruiz A, and Shoshani L. New Diseases Derived or Associated with the Tight Junction. Archives of Medical Research. 2007; 38(5):465-478.

Chen F, Zhang Z-R, Yuan F, Qin X, Wang M, and Huang Y. In vitro and in vivo study of N-trimethyl chitosan nanoparticles for oral protein delivery. Int J Pharm. 2008; 349(1–2):226-233.

Clark DE. Rapid calculation of polar molecular surface area and its application to the prediction of transport phenomena. 1. Prediction of intestinal absorption. J Pharm Sci. 1999; 88(8):807-814.

Clary-Meinesz C, Mouroux J, Cosson J, Huitorel P, and Blaive B. Influence of external pH on ciliary beat frequency in human bronchi and bronchioles. European Respiratory Journal. 1998; 11(2):330-333.

Clary-Meinesz C, Mouroux Jrm, Huitorel P, Cosson J, Schoevaert D, and Blaive B. Ciliary Beat Frequency in Human Bronchi and Bronchioles. CHEST Journal. 1997; 111(3):692-697.

Conradi RA, Burton PS, and Borchardt RT. Physico-chemical and biological factors that influence a drug's cellular permeability by passive diffusion. In: Pliška V, Testa B, van de Waterbeemd H, editors. Lipophilicity in Drug Action and Toxicology. Weinheim: Wiley-VCH Verlag GmbH; 2008. p. 233-252.

Cozens AL, Yezzi MJ, Kunzelmann K, Ohrui T, Chin L, Eng K, Finkbeiner WE, Widdicombe JH, and Gruenert DC. CFTR expression and chloride secretion in polarized immortal human bronchial epithelial cells. American Journal of Respiratory Cell and Molecular Biology. 1994; 10(1):38-47.

Crystal RG, Randell SH, Engelhardt JF, Voynow J, and Sunday ME. Airway Epithelial Cells. Proceedings of the American Thoracic Society. 2008; 5(7):772-777.

Da Silva CA, Chalouni C, Williams A, Hartl D, Lee CG, and Elias JA. Chitin Is a Size-Dependent Regulator of Macrophage TNF and IL-10 Production. The Journal of Immunology. 2009; 182(6):3573-3582.

de Britto D, and Assis OBG. A novel method for obtaining a quaternary salt of chitosan. Carbohydr Polym. 2007; 69(2):305-310.

Deli MA. Potential use of tight junction modulators to reversibly open membranous barriers and improve drug delivery. Bba-Biomembranes. 2009; 1788(4):892-910.

Dershwitz M, Walsh JL, Morishige RJ, Conners PM, Rubsamen RM, Shafer SL, and Rosow CE. Pharmacokinetics and pharmacodynamics of inhaled versus intravenous morphine in healthy volunteers. Anesthesiology. 2000; 93(3):619-628.

Dodane V, Amin Khan M, and Merwin JR. Effect of chitosan on epithelial permeability and structure. Int J Pharm. 1999; 182(1):21-32.

Domard A, Rinaudo M, and Terrassin C. New Method for the Quaternization of Chitosan. International Journal of Biological Macromolecules. 1986; 8(2):105-107.

Dorkoosh FA, Broekhuizen CAN, Borchard G, Rafiee-Tehrani M, Verhoef JC, and Junginger HE. Transport of octreotide and evaluation of mechanism of opening the paracellular tight junctions using superporous hydrogel polymers in Caco-2 cell monolayers. J Pharm Sci. 2004; 93(3):743-752.

Dorscheid D, Conforti A, Hamann K, Rabe K, and White S. Characterization of cell surface lectin-binding patterns of human airway epithelium. The Histochemical Journal. 1999; 31(3):145-151.

Dünnhaupt S, Barthelmes J, Iqbal J, Perera G, Thurner CC, Friedl H, and Bernkop-Schnürch A. In vivo evaluation of an oral drug delivery system for peptides based on S-protected thiolated chitosan. J Controlled Release. 2012; 160(3):477-485.

Dvorak A, Tilley AE, Shaykhiev R, Wang R, and Crystal RG. Do airway epithelium air–liquid cultures represent the *in vivo* airway epithelium transcriptome? American Journal of Respiratory Cell and Molecular Biology. 2011; 44(4):465-473.

Ehrhardt C, Collnot E-M, Baldes C, Becker U, Laue M, Kim K-J, and Lehr C-M. Towards an in vitro model of cystic fibrosis small airway epithelium: characterisation of the human bronchial epithelial cell line CFBE41o. Cell Tissue Res. 2006; 323(3):405-415.

Ehrhardt C, Fiegel J, Fuchs S, Abu-Dahab R, Schaefer UF, Hanes J, and Lehr CM. Drug absorption by the respiratory mucosa: Cell culture models and particulate drug carriers. Journal of Aerosol Medicine. 2002a; 15(2):131-139.

Ehrhardt C, Forbes B, and Kim K-J. In Vitro Models of the Tracheo-Bronchial Epithelium Drug Absorption Studies. In: Ehrhardt C, Kim K-J, editors. Drug Absorption Studies: *In Situ, In Vitro* and *In Silico* Models: Springer US; 2008. p. 235-257.

Ehrhardt C, Kneuer C, Fiegel J, Hanes J, Schaefer U, Kim K-J, and Lehr C-M. Influence of apical fluid volume on the development of functional intercellular junctions in the human epithelial cell line 16HBE14o- implications for the use of this cell line as an *in vitro* model for bronchial drug absorption studies. Cell Tissue Res. 2002b; 308(3):391-400.

Ehrhardt C, Kneuer C, Laue M, Schaefer UF, Kim KJ, and Lehr CM. 16HBE14o- human bronchial epithelial cell layers express P-glycoprotein, lung resistance-related protein, and caveolin-1. Pharm Res. 2003; 20(4):545-551.

Endter S, Becker U, Daum N, Huwer H, Lehr CM, Gumbleton M, and Ehrhardt C. P-glycoprotein (MDR1) functional activity in human alveolar epithelial cell monolayers. Cell Tissue Res. 2007; 328(1):77-84.

Fei X, and Gu Y. Progress in modifications and applications of fluorescent dye probe. Progress in Natural Science. 2009; 19(1):1-7.

Fiegel J, Ehrhardt C, Schaefer UF, Lehr C-M, and Hanes J. Large porous particle impingement on lung epithelial cell monolayers—Toward improved particle characterization in the lung. Pharm Res. 2003; 20(5):788-796.

Finkbeiner WE, Carrier SD, and Teresi CE. Reverse transcription-polymerase chain reaction (RT-PCR) phenotypic analysis of cell cultures of human tracheal epithelium, tracheobronchial glands, and lung carcinomas. American Journal of Respiratory Cell and Molecular Biology. 1993; 9(5):547-556.

Florea BI, Cassara ML, Junginger HE, and Borchard G. Drug transport and metabolism characteristics of the human airway epithelial cell line Calu-3. J Controlled Release. 2003; 87(1–3):131-138.

Florea BI, Thanou M, Junginger HE, and Borchard G. Enhancement of bronchial octreotide absorption by chitosan and N-trimethyl chitosan shows linear in vitro/in vivo correlation. J Control Release. 2006; 110(2):353-361.

Florea BI, van der Sandt ICJ, Schrier SM, Kooiman K, Deryckere K, de Boer AG, Junginger HE, and Borchard G. Evidence of P-glycoprotein mediated apical to basolateral transport of flunisolide in human broncho-tracheal epithelial cells (Calu-3). Brit J Pharmacol. 2001; 134(7):1555-1563.

Fogh J, Fogh JM, and Orfeo T. 127 Cultured human tumor-cell lines producing tumors in nude mice. J Natl Cancer I. 1977; 59(1):221-226.

Forbes B. Human airway epithelial cell lines for in vitro drug transport and metabolism studies. Pharmaceutical Science & Technology Today. 2000; 3(1):18-27.

Forbes B, and Ehrhardt C. Human respiratory epithelial cell culture for drug delivery applications. Eur J Pharm Biopharm. 2005; 60(2):193-205.

Forbes B, Shah A, Martin GP, and Lansley AB. The human bronchial epithelial cell line 16HBE14o-as a model system of the airways for studying drug transport. Int J Pharm. 2003; 257(1-2):161-167.

Foster KA, Avery ML, Yazdanian M, and Audus KL. Characterization of the Calu-3 cell line as a tool to screen pulmonary drug delivery. Int J Pharm. 2000; 208(1–2):1-11.

Franzdottir S, Axelsson I, Arason A, Baldursson O, Gudjonsson T, and Magnusson M. Airway branching morphogenesis in three dimensional culture. Resp Res. 2010; 11(1):162.

Friedl FE, editor. Rate of Quaternization as a function of the Alkylating Agent. World Conference on Oleochemicals into the 21st Centaury; 1990; Kuala Lumpur, Malaysia: American Oil Chemists' Society.

Frisch S, and Francis H. Disruption of epithelial cell-matrix interactions induces apoptosis. The Journal of Cell Biology. 1994; 124(4):619-626.

Germershaus O, Mao S, Sitterberg J, Bakowsky U, and Kissel T. Gene delivery using chitosan, trimethyl chitosan or polyethylenglycol-graft-trimethyl chitosan block copolymers: Establishment of structure–activity relationships in vitro. J Controlled Release. 2008; 125(2):145-154.

Geys J, Nemery B, and Hoet PHM. Optimisation of culture conditions to develop an in vitro pulmonary permeability model. Toxicol in Vitro. 2007; 21(7):1215-1219.

Giard DJ, Aaronson SA, Todaro GJ, Arnstein P, Kersey JH, Dosik H, and Parks WP. In Vitro Cultivation of Human Tumors: Establishment of Cell Lines Derived From a Series of Solid Tumors. J Natl Cancer I. 1973; 51(5):1417-1423.

Gonda I. Systemic delivery of drugs to humans via inhalation. J Aerosol Med. 2006; 19(1):47-53.

Grainger C, Greenwell L, Lockley D, Martin G, and Forbes B. Culture of Calu-3 cells at the air interface provides a representative model of the airway epithelial barrier. Pharm Res. 2006; 23(7):1482-1490.

Gribble GW, and Ferguson DC. Reactions of Sodium-Borohydride in Acidic Media - Selective Reduction of Aldehydes with Sodium Triacetoxyborohydride. Journal of the Chemical Society-Chemical Communications. 1975; (13):535-536.

Guo Z, Xing R, Liu S, Zhong Z, Ji X, Wang L, and Li P. Antifungal properties of Schiff bases of chitosan, N-substituted chitosan and quaternized chitosan. Carbohydrate Research. 2007; 342(10):1329-1332.

Haghi M, Young PM, Traini D, Jaiswal R, Gong J, and Bebawy M. Time- and passage-dependent characteristics of a Calu-3 respiratory epithelial cell model. Drug Dev Ind Pharm. 2010; 36(10):1207-1214.

Halldorsson S, Asgrimsson V, Axelsson I, Gudmundsson GH, Steinarsdottir M, Baldursson O, and Gudjonsson T. Differentiation potential of a basal epithelial cell line established from human bronchial explant. In Vitro Cell Dev-An. 2007; 43(8-9):283-289.

Halldorsson S, Gudjonsson T, Gottfredsson M, Singh PK, Gudmundsson GH, and Baldursson O. Azithromycin maintains airway epithelial integrity during pseudomonas aeruginosa infection. Am J Respir Cell Mol Biol. 2010; 42(1):62-68.

Hamilton KO, Backstrom G, Yazdanian MA, and Audus KL. P-glycoprotein efflux pump expression and activity in Calu-3 cells. J Pharm Sci. 2001a; 90(5):647-658.

Hamilton KO, Topp E, Makagiansar I, Siahaan T, Yazdanian M, and Audus KL. Multidrug Resistance-Associated Protein-1 Functional Activity in Calu-3 Cells. Journal of Pharmacology and Experimental Therapeutics. 2001b; 298(3):1199-1205.

Hamman JH, Stander M, and Kotze AF. Effect of the degree of quaternisation of N-trimethyl chitosan chloride on absorption enhancement: in vivo evaluation in rat nasal epithelia. Int J Pharm. 2002; 232(1-2):235-242.

Hersey SJ, and Jackson RT. Effect of Bile-Salts on Nasal Permeability Invitro. J Pharm Sci. 1987; 76(12):876-879.

Hinchcliffe M, Jabbal-Gill I, and Smith A. Effect of chitosan on the intranasal absorption of salmon calcitonin in sheep. J Pharm Pharmacol. 2005; 57(6):681-687.

Holappa J, Nevalainen T, Safin R, Soininen P, Asplund T, Luttikhedde T, Masson M, and Jarvinen T. Novel water-soluble quaternary piperazine derivatives of chitosan: Synthesis and characterization. Macromol Biosci. 2006; 6(2):139-144.

Holappa J, Nevalainen T, Savolainen J, Soininen P, Elomaa M, Safin R, Suvanto S, Pakkanen T, Masson M, Loftsson T, and Jarvinen T. Synthesis and characterization of chitosan N-betainates having various degrees of substitution. Macromolecules. 2004; 37(8):2784-2789.

Holappa J, Nevalainen T, Soininen P, Elomaa M, Safin R, Másson M, and Järvinen T. N-Chloroacyl-6-O-triphenylmethylchitosans: Useful Intermediates for Synthetic Modifications of Chitosan. Biomacromolecules. 2005; 6(2):858-863.

Hsu L-W, Lee P-L, Chen C-T, Mi F-L, Juang J-H, Hwang S-M, Ho Y-C, and Sung H-W. Elucidating the signaling mechanism of an epithelial tight-junction opening induced by chitosan. Biomaterials. 2012; 33(26):6254-6263.

Huang M, Khor E, and Lim L-Y. Uptake and Cytotoxicity of Chitosan Molecules and Nanoparticles: Effects of Molecular Weight and Degree of Deacetylation. Pharm Res. 2004; 21(2):344-353.

Huang M, Ma Z, Khor E, and Lim L-Y. Uptake of FITC-Chitosan Nanoparticles by A549 Cells. Pharm Res. 2002; 19(10):1488-1494.

Hussain A, Arnold JJ, Khan MA, and Ahsan F. Absorption enhancers in pulmonary protein delivery. J Controlled Release. 2004; 94(1):15-24.

Illum L, Farraj NF, and Davis SS. Chitosan as a Novel Nasal Delivery System for Peptide Drugs. Pharm Res. 1994; 11(8):1186-1189.

Illum L, Jabbal-Gill I, Hinchcliffe M, Fisher AN, and Davis SS. Chitosan as a novel nasal delivery system for vaccines. Adv Drug Delivery Rev. 2001; 51(1–3):81-96.

Jakiela B, Brockman-Schneider R, Amineva S, Lee W-M, and Gern JE. Basal Cells of Differentiated Bronchial Epithelium Are More Susceptible to Rhinovirus Infection. American Journal of Respiratory Cell and Molecular Biology. 2008; 38(5):517-523.

Jayaraman S, Song Y, and Verkman AS. Airway surface liquid pH in well-differentiated airway epithelial cell cultures and mouse trachea. American Journal of Physiology - Cell Physiology. 2001; 281(5):C1504-C1511.

Jia X, Chen X, Xu Y, Han X, and Xu Z. Tracing transport of chitosan nanoparticles and molecules in Caco-2 cells by fluorescent labeling. Carbohydr Polym. 2009; 78(2):323-329.

Jia Z, shen D, and Xu W. Synthesis and antibacterial activities of quaternary ammonium salt of chitosan. Carbohydrate Research. 2001; 333(1):1-6.

Jiang T, Kumbar SG, Nair LS, and Laurencin CT. Biologically active chitosan systems for tissue engineering and regenerative medicine. Curr Top Med Chem. 2008; 8(4):354-364.

Jiménez-Castells C, de la Torre B, Andreu D, and Gutiérrez-Gallego R. Neo-glycopeptides: the importance of sugar core conformation in oxime-linked glycoprobes for interaction studies. Glycoconjugate Journal. 2008; 25(9):879-887.

Johansson F, Hjertberg E, Eirefelt S, Tronde A, and Hultkvist Bengtsson U. Mechanisms for absorption enhancement of inhaled insulin by sodium taurocholate. Eur J Pharm Sci. 2002; 17(1–2):63-71.

Jonker C, Hamman JH, and Kotze AF. Intestinal paracellular permeation enhancement with quaternised chitosan: in situ and in vitro evaluation. Int J Pharm. 2002; 238(1-2):205-213.

Jonquieres A, Awkal M, Clement R, and Lochon P. Synthesis and characterization of film-forming poly(urethaneimide) cationomers containing quaternary ammonium groups. Polymer. 2006; 47(16):5724-5735.

Kalia J, and Raines RT. Hydrolytic Stability of Hydrazones and Oximes. Angewandte Chemie International Edition. 2008; 47(39):7523-7526.

Ke Y, Reddel RR, Gerwin BI, Miyashita M, McMenamin M, Lechner JF, and Harris CC. Human bronchial epithelial cells with integrated SV40 virus T antigen genes retain the ability to undergo squamous differentiation. Differentiation. 1988; 38(1):60-66.

Kim CH, Choi JW, Chun HJ, and Choi KS. Synthesis of chitosan derivatives with quaternary ammonium salt and their antibacterial activity. Polym Bull. 1997; 38(4):387-393.

Kim K-J. Bioelectrical characterization of cultured epithelial cell (mono)layers and excised tissues. In: Lehr CM, editor. Cell Culture Models of Biological Barriers: CRC Press; 2002. p. 41-51.

Knight DA, and Holgate ST. The airway epithelium: Structural and functional properties in health and disease. Respirology. 2003; 8(4):432-446.

Kong M, Chen XG, Xing K, and Park HJ. Antimicrobial properties of chitosan and mode of action: A state of the art review. International Journal of Food Microbiology. 2010; 144(1):51-63.

Korjamo T, Holappa J, Taimisto S, Savolainen J, Jarvinen T, and Monkkonen J. Effect of N-betainate and N-piperazine derivatives of chitosan on the paracellular transport of mannitol in Caco-2 cells. Eur J Pharm Sci. 2008; 35(3):226-234.

Kotze AF, de Leeuw BJ, Luessen HL, de Boer AG, Verhoef JC, and Junginger HE. Chitosans for enhanced delivery of therapeutic peptides across intestinal epithelia: in vitro evaluation in Caco-2 cell monolayers. Int J Pharm. 1997a; 159(2):243-253.

Kotze AF, Luessen HL, de Boer AG, Verhoef JC, and Junginger HE. Chitosan for enhanced intestinal permeability: Prospects for derivatives soluble in neutral and basic environments. Eur J Pharm Sci. 1999a; 7(2):145-151.

Kotze AF, Luessen HL, de Leeuw BJ, de Boer BG, Verhoef JC, and Junginger HE. Comparison of the effect of different chitosan salts and N-trimethyl chitosan chloride on the permeability of intestinal epithelial cells (Caco-2). J Controlled Release. 1998; 51(1):35-46.

Kotze AF, Luessen HL, deLeeuw BJ, deBoer BG, Verhoef JC, and Junginger HE. N-trimethyl chitosan chloride as a potential absorption enhancer across mucosal surfaces: In vitro evaluation in intestinal epithelial cells (Caco-2). Pharm Res. 1997b; 14(9):1197-1202.

Kotze AF, Thanou MM, Luebetaen HL, de Boer AG, Verhoef JC, and Junginger HE. Enhancement of paracellular drug transport with highly quaternized N-trimethyl chitosan chloride in neutral environments: in vitro evaluation in intestinal epithelial cells (Caco-2). J Pharm Sci. 1999b; 88(2):253-257.

Kotze AF, Thanou MM, Luessen HL, de Boer BG, Verhoef JC, and Junginger HE. Effect of the degree of quaternization of N-trimethyl chitosan chloride on the permeability of intestinal epithelial cells (Caco-2). Eur J Pharm Biopharm. 1999c; 47(3):269-274.

Kowapradit J, Opanasopit P, Ngawhirunpat T, Rojanarata T, and Sajomsang W. Structure-activity relationships of methylated N-aryl chitosan derivatives for enhancing paracellular permeability across Caco-2 cells. Carbohydr Polym. 2011; 83(2):430-437.

Kudsiova L, and Lawrence MJ. A comparison of the effect of chitosan and chitosan-coated vesicles on monolayer integrity and permeability across Caco-2 and 16HBE14o-cells. J Pharm Sci. 2008; 97(9):3998-4010.

Kurita K. Chitin and chitosan: Functional biopolymers from marine crustaceans. Mar Biotechnol. 2006; 8(3):203-226.

Kurita K, Hirakawa M, Kikuchi S, Yamanaka H, and Yang J. Trimethylsilylation of chitosan and some properties of the product. Carbohydr Polym. 2004; 56(3):333-337.

Kurita K, Ikeda H, Yoshida Y, Shimojoh M, and Harata M. Chemoselective Protection of the Amino Groups of Chitosan by Controlled Phthaloylation: Facile Preparation of a Precursor Useful for Chemical Modifications. Biomacromolecules. 2001; 3(1):1-4.

Layer RW. The Chemistry of Imines. Chemical Reviews. 1963; 63(5):489-510.

Lechapt-Zalcman E, Hurbain I, Lacave R, Commo F, Urban T, Antoine M, Milleron B, and Bernaudin JF. MDR1-Pgp 170 expression in human bronchus. European Respiratory Journal. 1997; 10(8):1837-1843.

Ledung P, Milas M, Rinaudo M, and Desbrieres J. Water-Soluble Derivatives Obtained by Controlled Chemical Modifications of Chitosan. Carbohydr Polym. 1994; 24(3):209-214.

Lee CG. Chitin, Chitinases and Chitinase-like Proteins in Allergic Inflammation and Tissue Remodeling. Yonsei Med J. 2009; 50(1):22-30.

Lehmann T, Kohler C, Weidauer E, Taege C, and Foth H. Expression of MRP1 and related transporters in human lung cells in culture. Toxicology. 2001; 167(1):59-72.

Lehr CM, Bouwstra JA, Schacht EH, and Junginger HE. Invitro Evaluation of Mucoadhesive Properties of Chitosan and Some Other Natural Polymers. Int J Pharm. 1992; 78(1):43-48.

Lenzer J. Inhaled insulin is approved in Europe and United States. Brit Med J. 2006; 332(7537):321-321.

Liberek B, Melcer A, Osuch A, Wakiec R, Milewski S, and Wisniewski A. N-Alkyl derivatives of 2-amino-2-deoxy-d-glucose. Carbohydrate Research. 2005; 340(11):1876-1884.

Lim ST, Forbes B, Martin GP, and Brown MB. In vivo and in vitro characterization of novel microparticulates based on hyaluronan and chitosan hydroglutamate. Aaps Pharmscitech. 2001; 2(4):1-12.

Lin H, Gebhardt M, Bian S, Kwon KA, Shim C-K, Chung S-J, and Kim D-D. Enhancing effect of surfactants on fexofenadine·HCl transport across the human nasal epithelial cell monolayer. Int J Pharm. 2007a; 330(1–2):23-31.

Lin H, Li H, Cho H-J, Bian S, Roh H-J, Lee M-K, Kim JS, Chung S-J, Shim C-K, and Kim D-D. Air-liquid interface (ALI) culture of human bronchial epithelial cell monolayers as an in vitro model for airway drug transport studies. J Pharm Sci. 2007b; 96(2):341-350.

Lindmark T, Kimura Y, and Artursson P. Absorption enhancement through intracellular regulation of tight junction permeability by medium chain fatty acids in Caco-2 cells. Journal of Pharmacology and Experimental Therapeutics. 1998; 284(1):362-369.

Lindmark T, Söderholm JD, Olaison G, Alván G, Ocklind G, and Artursson P. Mechanism of Absorption Enhancement in Humans After Rectal Administration of Ampicillin in Suppositories Containing Sodium Caprate. Pharm Res. 1997; 14(7):930-935.

Lohse A, Martins R, Jørgensen MR, and Hindsgaul O. Solid-Phase Oligosaccharide Tagging (SPOT): Validation on Glycolipid-Derived Structures. Angewandte Chemie International Edition. 2006; 45(25):4167-4172.

Luessen HL, deLeeuw BJ, Langemeyer MWE, deBoer AG, Verhoef JC, and Junginger HE. Mucoadhesive polymers in peroral peptide drug delivery .6. Carbomer and chitosan improve the intestinal absorption of the peptide drug buserelin in vivo. Pharm Res. 1996; 13(11):1668-1672.

Luessen HL, Rentel CO, Kotze AF, Lehr CM, deBoer AG, Verhoef JC, and Junginger HE. Mucoadhesive polymers in peroral peptide drug delivery .4. Polycarbophil and chitosan are potent enhancers of peptide transport across intestinal mucosae in vitro. J Controlled Release. 1997; 45(1):15-23.

Machida M, Hayashi M, and Awazu S. The effects of absorption enhancers on the pulmonary absorption of recombinant human granulocyte colony-stimulating factor (rhG-CSF) in rats. Biol Pharm Bull. 2000; 23(1):84-86.

Madara JL. Intestinal absorptive cell tight junctions are linked to cytoskeleton. American Journal of Physiology - Cell Physiology. 1987; 253(1):C171-C175.

Madlova M, Bosquillon C, Asker D, Dolezal P, and Forbes B. In-vitro respiratory drug absorption models possess nominal functional P-glycoprotein activity. J Pharm Pharmacol. 2009; 61(3):293-301.

Magnusson MK, Baldursson O, and Gudjonsson T. Lung Epithelial Stem Cells Stem Cells & Regenerative Medicine. In: Appasani K, Appasani RK, editors.: Humana Press; 2011. p. 227-241.

Maher S, Leonard TW, Jacobsen J, and Brayden DJ. Safety and efficacy of sodium caprate in promoting oral drug absorption: from in vitro to the clinic. Adv Drug Delivery Rev. 2009; 61(15):1427-1449.

Malmo J, Sørgård H, Vårum KM, and Strand SP. siRNA delivery with chitosan nanoparticles: Molecular properties favoring efficient gene silencing. J Controlled Release. 2012; 158(2):261-268.

Manford F, Tronde A, Jeppsson A-B, Patel N, Johansson F, and Forbes B. Drug permeability in 16HBE14o- airway cell layers correlates with absorption from the isolated perfused rat lung. Eur J Pharm Sci. 2005; 26(5):414-420.

Mao S, Germershaus O, Fischer D, Linn T, Schnepf R, and Kissel T. Uptake and Transport of PEG-Graft-Trimethyl-Chitosan Copolymer–Insulin Nanocomplexes by Epithelial Cells. Pharm Res. 2005; 22(12):2058-2068.

Mathews S, Gupta PK, Bhonde R, and Totey S. Chitosan enhances mineralization during osteoblast differentiation of human bone marrow-derived mesenchymal stem cells, by upregulating the associated genes. Cell Proliferation. 2011; 44(6):537-549.

Mathias NR, Kim K-J, Robison TW, and Lee VHL. Development and characterization of rabbit tracheal epithelial cell monolayer models for drug transport studies. Pharm Res. 1995; 12(10):1499-1505.

Mathias NR, Timoszyk J, Stetsko PI, Megill JR, Smith RL, and Wall DA. Permeability characteristics of Calu-3 human bronchial epithelial cells: *In vitro-in vivo* correlation to predict lung absorption in rats. J Drug Target. 2002; 10(1):31-40.

Mathieu C, and Gale E. Inhaled insulin: gone with the wind? Diabetologia. 2008; 51(1):1-5.

Matter K, and Balda MS. Signalling to and from tight junctions. Nature Reviews Molecular Cell Biology. 2003; 4(3):225-236.

Mei D, Mao SR, Sun W, Wang YJ, and Kissel T. Effect of chitosan structure properties and molecular weight on the intranasal absorption of tetramethylpyrazine phosphate in rats. Eur J Pharm Biopharm. 2008; 70(3):874-881.

Memoli S, Selva M, and Tundo P. Dimethylcarbonate for eco-friendly methylation reactions. Chemosphere. 2001; 43(1):115-121.

Mercer RR, Russell ML, Roggli VL, and Crapo JD. Cell number and distribution in human and rat airways. American Journal of Respiratory Cell and Molecular Biology. 1994; 10(6):613-624.

Merkel OM, Zheng M, Debus H, and Kissel T. Pulmonary Gene Delivery Using Polymeric Nonviral Vectors. Bioconjugate Chem. 2012; 23(1):3-20.

Miller GL. Use of Dinitrosalicylic Acid Reagent for Determination of Reducing Sugar. Analytical Chemistry. 1959; 31(3):426-428.

Monnaert V, Tilloy S, Bricout H, Fenart L, Cecchelli R, and Monflier E. Behavior of α-, β-, and γ-Cyclodextrins and Their Derivatives on an in Vitro Model of Blood-Brain Barrier. Journal of Pharmacology and Experimental Therapeutics. 2004; 310(2):745-751.

Muzzarelli RAA. Human enzymatic activities related to the therapeutic administration of chitin derivatives. Cellular and Molecular Life Sciences. 1997; 53(2):131-140.

Muzzarelli RAA, Greco F, Busilacchi A, Sollazzo V, and Gigante A. Chitosan, hyaluronan and chondroitin sulfate in tissue engineering for cartilage regeneration: A review. Carbohydr Polym. 2012; 89(3):723-739.

Muzzarelli RAA, and Tanfani F. The N-Permethylation of Chitosan and the Preparation of N-Trimethyl Chitosan Iodide. Carbohydr Polym. 1985; 5(4):297-307.

Nam T, Park S, Lee S-Y, Park K, Choi K, Song IC, Han MH, Leary JJ, Yuk SA, Kwon IC, Kim K, and Jeong SY. Tumor Targeting Chitosan Nanoparticles for Dual-Modality Optical/MR Cancer Imaging. Bioconjugate Chem. 2010; 21(4):578-582.

Nardone R. Eradication of cross-contaminated cell lines: A call for action. Cell Biology and Toxicology. 2007; 23(6):367-372.

Ng T, Shima D, Squire A, Bastiaens PIH, Gschmeissner S, Humphries MJ, and Parker PJ. PKC[alpha] regulates [beta]1 integrin-dependent cell motility through association and control of integrin traffic. EMBO J. 1999; 18(14):3909-3923.

Nicod LP. Pulmonary defence mechanisms. Respiration. 1999; 66(1):2-11.

Nishimura S, Kohgo O, Kurita K, and Kuzuhara H. Chemospecific manipulations of a rigid polysaccharide: syntheses of novel chitosan derivatives with excellent solubility in common

organic solvents by regioselective chemical modifications. Macromolecules. 1991; 24(17):4745-4748.

Nokhodchi A, Shokri J, Dashbolaghi A, Hassan-Zadch D, Ghafourian T, and Barzcgar-Jalali M. The enhancement effect of surfactants on the penetration of lorazepam through rat skin. Int J Pharm. 2003; 250(2):359-369.

Note for guidance on the investigation of bioavailability and bioequivalence. December 2000, EMEA. Available from: http://www.emea.europa.eu/docs/en_GB/document_library/Scientific_guideline/2009/09/WC500003519.pdf.

Novoa-Carballal R, and Muller AHE. Synthesis of polysaccharide-b-PEG block copolymers by oxime click. Chem Commun. 2012; 48(31):3781-3783.

Ohtake K, Maeno T, Ueda H, Natsume H, and Morimoto Y. Poly-L-arginine predominantly increases the paracellular permeability of hydrophilic macromolecules across rabbit nasal epithelium in vitro. Pharm Res. 2003a; 20(2):153-160.

Ohtake K, Maeno T, Ueda H, Ogihara M, Natsume H, and Morimoto Y. Poly-l-arginine enhances paracellular permeability via serine/threonine phosphorylation of ZO-1 and tyrosine dephosphorylation of occludin in rabbit nasal epithelium. Pharm Res. 2003b; 20(11):1838-1845.

Onishi H, and Machida Y. Biodegradation and distribution of water-soluble chitosan in mice. Biomaterials. 1999; 20(2):175-182.

Opanasopit P, Aumklad P, Kowapradit J, Ngawhiranpat T, Apirakaramwong A, and Rojanarata T. Effect of salt forms and molecular weight of chitosans on in vitro permeability enhancement in intestinal epithelial cells (Caco-2). Pharm Dev Technol. 2007; 12(5):447-455.

Otton A. Cell culture forensics of Calu-3: A human lung epithelial cell line. Ethnic Dis. 2009; 19(2):S78-S79.

Ottoy MH, Varum KM, and Smidsrod O. Compositional heterogeneity of heterogeneously deacetylated chitosans. Carbohydr Polym. 1996; 29(1):17-24.

Patton JS. Mechanisms of macromolecule absorption by the lungs. Adv Drug Delivery Rev. 1996; 19(1):3-36.

Patton JS. Unlocking the opportunity of tight glycaemic control. Diabetes, Obesity and Metabolism. 2005; 7:S5-S8.

Patton JS, Bukar JG, and Eldon MA. Clinical Pharmacokinetics and Pharmacodynamics of Inhaled Insulin. Clinical Pharmacokinetics. 2004; 43(12):781-801.

Patton JS, and Byron PR. Inhaling medicines: delivering drugs to the body through the lungs. Nat Rev Drug Discov. 2007; 6(1):67-74.

Patton JS, and Platz RM. (D) Routes of delivery: Case studies: (2) Pulmonary delivery of peptides and proteins for systemic action. Adv Drug Delivery Rev. 1992; 8(2–3):179-196.

Perry DG, Wisniowski P, Daugherty GL, Downing J, and Martin WJ. Nonimmune Phagocytosis of Liposomes by Rat Alveolar Macrophages Is Enhanced by Vitronectin and Is Vitronectin-receptor Mediated. American Journal of Respiratory Cell and Molecular Biology. 1997; 17(4):462-470.

Pillion DJ, Atchison JA, Wang RX, and Meezan E. Alkylglycosides enhance systemic absorption of insulin applied topically to the rat eye. Journal of Pharmacology and Experimental Therapeutics. 1994; 271(3):1274-1280.

Pohl C, Hermanns MI, Uboldi C, Bock M, Fuchs S, Dei-Anang J, Mayer E, Kehe K, Kummer W, and Kirkpatrick CJ. Barrier functions and paracellular integrity in human cell culture models of the proximal respiratory unit. Eur J Pharm Biopharm. 2009; 72(2):339-349.

Poirier LA, Stoner GD, and Shimkin MB. Bioassay of Alkyl-Halides and Nucleotide Base Analogs by Pulmonary Tumor Response in Strain-a Mice. Cancer Res. 1975; 35(6):1411-1415.

Polnok A, Borchard G, Verhoef JC, Sarisuta N, and Junginger HE. Influence of methylation process on the degree of quaternization of N-trimethyl chitosan chloride. Eur J Pharm Biopharm. 2004; 57(1):77-83.

Qaqish R, and Amiji M. Synthesis of a fluorescent chitosan derivative and its application for the study of chitosan–mucin interactions. Carbohydr Polym. 1999; 38(2):99-107.

Rabinowitz JD, Wensley M, Lloyd P, Myers D, Shen W, Lu A, Hodges C, Hale R, Mufson D, and Zaffaroni A. Fast Onset Medications through Thermally Generated Aerosols. Journal of Pharmacology and Experimental Therapeutics. 2004; 309(2):769-775.

Ranaldi G, Marigliano I, Vespignani I, Perozzi G, and Sambuy Y. The effect of chitosan and other polycations on tight junction permeability in the human intestinal Caco-2 cell line. J Nutr Biochem. 2002; 13(3):157-167.

Reddel RR, Ke Y, Gerwin BI, McMenamin MG, Lechner JF, Su RT, Brash DE, Park J-B, Rhim JS, and Harris CC. Transformation of Human Bronchial Epithelial Cells by Infection with SV40 or Adenovirus-12 SV40 Hybrid Virus, or Transfection via Strontium Phosphate Coprecipitation with a Plasmid Containing SV40 Early Region Genes. Cancer Res. 1988; 48(7):1904-1909.

Reichardt C. Solvent Effects on the Rates of Homogeneous Chemical Reactions. Weinheim: Wiley-VCH Verlag GmbH & Co. KGaA; 2004.

Rintanen N, Karjalainen M, Alanko J, Paavolainen L, Mäki A, Nissinen L, Lehkonen M, Kallio K, Cheng RH, Upla P, Ivaska J, and Marjomäki V. Calpains promote α2β1 integrin turnover in nonrecycling integrin pathway. Molecular Biology of the Cell. 2012; 23(3):448-463.

Rock JR, Onaitis MW, Rawlins EL, Lu Y, Clark CP, Xue Y, Randell SH, and Hogan BLM. Basal cells as stem cells of the mouse trachea and human airway epithelium. Proceedings of the National Academy of Sciences. 2009; 106(31):12771-12775.

Rojas A, Gonzalez I, and Figueroa H. Cell line cross-contamination in biomedical research: a call to prevent unawareness. Acta Pharmacologica Sinica. 2008; 29(7):877-880.

Rosenthal R, Günzel D, Finger C, Krug SM, Richter JF, Schulzke J-D, Fromm M, and Amasheh S. The effect of chitosan on transcellular and paracellular mechanisms in the intestinal epithelial barrier. Biomaterials. 2012; 33(9):2791-2800.

Runarsson OV, Holappa J, Jonsdottir S, Steinsson H, and Masson M. N-selective 'one pot' synthesis of highly N-substituted trimethyl chitosan (TMC). Carbohydr Polym. 2008a; 74(3):740-744.

Runarsson OV, Holappa J, Nevalainen T, Hjalmarsdottir M, Jarvinen T, Loftsson T, Einarsson JM, Jonsdottir S, Valdimarsdottir M, and Masson M. Antibacterial activity of methylated chitosan and chitooligomer derivatives: Synthesis and structure activity relationships. European Polymer Journal. 2007; 43(6):2660-2671.

Runarsson OV, Malainer C, Holappa J, Sigurdsson ST, and Masson M. tert-Butyldimethylsilyl O-protected chitosan and chitooligosaccharides: useful precursors for N-modifications in common organic solvents. Carbohydrate Research. 2008b; 343(15):2576-2582.

Rutland J, Griffin WM, and Cole PJ. Human ciliary beat frequency in epithelium from intrathoracic and extrathoracic airways. The American review of respiratory disease. 1982; 125(1):100-105.

Sadeghi AMM, Dorkoosh FA, Avadi MR, Weinhold M, Bayat A, Delie F, Gurny R, Larijani B, Rafiee-Tehrani M, and Junginger HE. Permeation enhancer effect of chitosan and chitosan derivatives: Comparison of formulations as soluble polymers and nanoparticulate systems on insulin absorption in Caco-2 cells. Eur J Pharm Biopharm. 2008; 70(1):270-278.

Sahni JK, Chopra S, Ahmad FJ, and Khar RK. Potential prospects of chitosan derivative trimethyl chitosan chloride (TMC) as a polymeric absorption enhancer: synthesis, characterization and applications. J Pharm Pharmacol. 2008; 60(9):1111-1119.

Sajomsang W, Tantayanon S, Tangpasuthadol V, and Daly WH. Synthesis of methylated chitosan containing aromatic moieties: Chemoselectivity and effect on molecular weight. Carbohydr Polym. 2008; 72(4):740-750.

Sajomsang W, Tantayanon S, Tangpasuthadol V, and Daly WH. Quaternization of N-aryl chitosan derivatives: synthesis, characterization, and antibacterial activity. Carbohydrate Research. 2009; 344(18):2502-2511.

Sakagami M. In vivo, in vitro and ex vivo models to assess pulmonary absorption and disposition of inhaled therapeutics for systemic delivery. Adv Drug Delivery Rev. 2006; 58(9-10):1030-1060.

Salvatore RN, Nagle AS, and Jung KW. Cesium Effect: High Chemoselectivity in Direct N-Alkylation of Amines. The Journal of Organic Chemistry. 2002; 67(3):674-683.

Sandri G, Bonferoni MC, Rossi S, Ferrari F, Boselli C, and Caramella C. Insulin-Loaded Nanoparticles Based on N-Trimethyl Chitosan: In Vitro (Caco-2 Model) and Ex Vivo (Excised Rat Jejunum, Duodenum, and Ileum) Evaluation of Penetration Enhancement Properties. Aaps Pharmscitech. 2010; 11(1):362-371.

Scherließ R. The MTT assay as tool to evaluate and compare excipient toxicity in vitro on respiratory epithelial cells. Int J Pharm. 2011; 411(1–2):98-105.

Scheuch G, Brand P, Meyer T, Herpich C, Mullinger B, Brom J, Weidinger G, Kohlhaufl M, Haussinger K, Spannagl M, Schramm W, and Siekmeier R. Anticoagulative effects of the inhaled low molecular weight heparin certoparin in healthy subjects. J Physiol Pharmacol. 2007; 58:603-614.

Schiller RN, Barrager E, Schauss AG, and Nichols EJ. A Randomized, Double-Blind, Placebo-Controlled Study Examining the Effects of a Rapidly Soluble Chitoasan Dietary Supplement on Weight Loss and Body Composition in Overweight and Mildly Obese Individuals. The Journal of the American Neutraceutical Association. 2001; 4(1):42-49.

Schipper NGM, Olsson S, Hoogstraate JA, deBoer AG, Vårum KM, and Artursson P. Chitosans as Absorption Enhancers for Poorly Absorbable Drugs 2: Mechanism of Absorption Enhancement. Pharm Res. 1997; 14(7):923-929.

Schipper NGM, Vårum KM, and Artursson P. Chitosans as Absorption Enhancers for Poorly Absorbable Drugs. 1: Influence of Molecular Weight and Degree of Acetylation on Drug Transport Across Human Intestinal Epithelial (Caco-2) Cells. Pharm Res. 1996; 13(11):1686-1692.

Schipper NGM, Varum KM, Stenberg P, Ocklind G, Lennernas H, and Artursson P. Chitosans as absorption enhancers of poorly absorbable drugs 3: Influence of mucus on absorption enhancement. Eur J Pharm Sci. 1999; 8(4):335-343.

Schneeberger EE, and Lynch RD. The tight junction: a multifunctional complex. American Journal of Physiology-Cell Physiology. 2004; 286(6):C1213-C1228.

Schreier H, Mcnicol KJ, Bennett DB, Teitelbaum Z, and Derendorf H. Pharmacokinetics of Detirelix Following Intratracheal Instillation and Aerosol Inhalation in the Unanesthetized Awake Sheep. Pharm Res. 1994; 11(7):1056-1059.

Selva M, and Perosa A. Green chemistry metrics: a comparative evaluation of dimethyl carbonate, methyl iodide, dimethyl sulfate and methanol as methylating agents. Green Chemistry. 2008; 10(4):457-464.

Shao ZZ, Li YP, and Mitra AK. Cyclodextrins as Mucosal Absorption Promoters of Insulin .3. Pulmonary Route of Delivery. Eur J Pharm Biopharm. 1994; 40(5):283-288.

Shen BQ, Finkbeiner WE, Wine JJ, Mrsny RJ, and Widdicombe JH. Calu-3: a human airway epithelial cell line that shows cAMP-dependent Cl- secretion. American Journal of Physiology - Lung Cellular and Molecular Physiology. 1994; 266(5):L493-L501.

Sheppard D. Functions of pulmonary epithelial integrins: From development to disease. Physiol Rev. 2003; 83(3):673-686.

Shin K, Fogg VC, and Margolis B. Tight junctions and cell polarity. Annu Rev Cell Dev Bi. 2006; 22:207-235.

Sieval AB, Thanou M, Kotze AF, Verhoef JE, Brussee J, and Junginger HE. Preparation and NMR characterization of highly substituted N-trimethyl chitosan chloride. Carbohydr Polym. 1998; 36(2-3):157-165.

Smith J, Wood E, and Dornish M. Effect of Chitosan on Epithelial Cell Tight Junctions. Pharmaceut Res. 2004; 21(1):43-49.

Smith JM, Dornish M, and Wood EJ. Involvement of protein kinase C in chitosan glutamate-mediated tight junction disruption. Biomaterials. 2005; 26(16):3269-3276.

Snyman D, Hamman JH, and Kotze AF. Evaluation of the mucoadhesive properties of N-trimethyl chitosan chloride. Drug Dev Ind Pharm. 2003; 29(1):61-69.

Snyman D, Hamman JH, Kotze JS, Rollings JE, and Kotze AF. The relationship between the absolute molecular weight and the degree of quaternisation of N-trimethyl chitosan chloride. Carbohydr Polym. 2002; 50(2):145-150.

Sonaje K, Chuang EY, Lin KJ, Yen TC, Su FY, Tseng MT, and Sung HW. Opening of Epithelial Tight Junctions and Enhancement of Paracellular Permeation by Chitosan: Microscopic, Ultrastructural, and Computed-Tomographic Observations. Mol Pharmaceut. 2012; 9(5):1271-1279.

Sonaje K, Lin KJ, Tseng MT, Wey SP, Su FY, Chuang EY, Hsu CW, Chen CT, and Sung HW. Effects of chitosan-nanoparticle-mediated tight junction opening on the oral absorption of endotoxins. Biomaterials. 2011; 32(33):8712-8721.

Song WL, Gaware VS, Runarsson OV, Masson M, and Mano JF. Functionalized superhydrophobic biomimetic chitosan-based films. Carbohydr Polym. 2010; 81(1):140-144.

Sporty JL, Horalkova L, and Ehrhardt C. *In vitro* cell culture models for the assessment of pulmonary drug disposition. Expert Opin Drug Met. 2008; 4(4):333-345.

Stentebjerg-Andersen A, Notlevsen IV, Brodin B, and Nielsen CU. Calu-3 cells grown under AIC and LCC conditions: Implications for dipeptide uptake and transepithelial transport of substances. Eur J Pharm Biopharm. 2011; 78(1):19-26.

Stone KC, Mercer RR, Gehr P, Stockstill B, and Crapo JD. Allometric Relationships of Cell Numbers and Size in the Mammalian Lung. American Journal of Respiratory Cell and Molecular Biology. 1992; 6(2):235-243.

Strand SP, Tømmeraas K, Vårum KM, and Østgaard K. Electrophoretic Light Scattering Studies of Chitosans with Different Degrees of N-acetylation. Biomacromolecules. 2001; 2(4):1310-1314.

Symington BE, Takada Y, and Carter WG. Interaction of integrins alpha 3 beta 1 and alpha 2 beta 1: potential role in keratinocyte intercellular adhesion. The Journal of Cell Biology. 1993; 120(2):523-535.

Takaoka Y, Tsutsumi H, Kasagi N, Nakata E, and Hamachi I. One-Pot and Sequential Organic Chemistry on an Enzyme Surface to Tether a Fluorescent Probe at the Proximity of the Active Site with Restoring Enzyme Activity. Journal of the American Chemical Society. 2006; 128(10):3273-3280.

Tang VW, and Goodenough DA. Paracellular ion channel at the tight junction. Biophysical Journal. 2003; 84(3):1660-1673.

Thanou M, Florea BI, Geldof M, Junginger HE, and Borchard G. Quaternized chitosan oligomers as novel gene delivery vectors in epithelial cell lines. Biomaterials. 2002; 23(1):153-159.

Thanou M, Florea BI, Langemeyer MWE, Verhoef JC, and Junginger HE. N-trimethylated chitosan chloride (TMC) improves the intestinal permeation of the peptide drug buserelin in vitro (Caco-2 cells) and in vivo (rats). Pharm Res. 2000a; 17(1):27-31.

Thanou M, Nihot MT, Jansen M, Verhoef JC, and Junginger HE. Mono-N-carboxymethyl chitosan (MCC), a polyampholytic chitosan derivative, enhances the intestinal absorption of low molecular weight heparin across intestinal epithelia in vitro and in vivo. J Pharm Sci. 2001a; 90(1):38-46.

Thanou M, Verhoef JC, Verheijden JHM, and Junginger HE. Intestinal absorption of octreotide using trimethyl chitosan chloride: Studies in pigs. Pharm Res. 2001b; 18(6):823-828.

Thanou MM, Kotze AF, Scharringhausen T, Luessen HL, de Boer AG, Verhoef JC, and Junginger HE. Effect of degree of quaternization of N-trimethyl chitosan chloride for enhanced transport of hydrophilic compounds across intestinal Caco-2 cell monolayers. J Controlled Release. 2000b; 64(1-3):15-25.

Thipphawong J. Inhaled cytokines and cytokine antagonists. Adv Drug Delivery Rev. 2006; 58(9–10):1089-1105.

Thygesen MB, Munch H, Sauer J, Clo E, Jorgensen MR, Hindsgaul O, and Jensen KJ. Nucleophilic Catalysis of Carbohydrate Oxime Formation by Anilines. J Org Chem. 2010; 75(5):1752-1755.

Thygesen MB, Sauer J, and Jensen KJ. Chemoselective Capture of Glycans for Analysis on Gold Nanoparticles: Carbohydrate Oxime Tautomers Provide Functional Recognition by Proteins. Chemistry – A European Journal. 2009; 15(7):1649-1660.

Tight Junction Biology. Nastech Pharmaceutical Company; 2007; Available from: http://nastech.com/nastech/junctions_biology.

Tomita M, Hayashi M, and Awazu S. Absorption-enhancing mechanism of EDTA, caprate, and decanoylcarnitine in Caco-2 cells. J Pharm Sci. 1996; 85(6):608-611.

Tomita M, Sawada T, Ogawa T, Ouchi H, Hayashi M, and Awazu S. Differences in the Enhancing Effects of Sodium Caprate on Colonic and Jejunal Drug Absorption. Pharm Res. 1992; 9(5):648-653.

Tronde A, Norden B, Jeppsson AB, Brunmark P, Nilsson E, Lennernas H, and Bengtsson UH. Drug absorption from the isolated perfused rat lung-correlations with drug physicochemical properties and epithelial permeability. J Drug Target. 2003a; 11(1):61-74.

Tronde A, Nordén B, Marchner H, Wendel A-K, Lennernäs H, and Bengtsson UH. Pulmonary absorption rate and bioavailability of drugs in vivo in rats: Structure–absorption relationships and physicochemical profiling of inhaled drugs. J Pharm Sci. 2003b; 92(6):1216-1233.

Twentyman PR, Rhodes T, and Rayner S. A comparison of rhodamine 123 accumulation and efflux in cells with P-glycoprotein-mediated and MRP-associated multidrug resistance phenotypes. European Journal of Cancer. 1994; 30(9):1360-1369.

Uchenna Agu R, Ikechukwu Ugwoke M, Armand M, Kinget R, and Verbeke N. The lung as a route for systemic delivery of therapeutic proteins and peptides. Resp Res. 2001; 2(4):198 - 209.

Ulanova M, Gravelle S, and Barnes R. The Role of Epithelial Integrin Receptors in Recognition of Pulmonary Pathogens. Journal of Innate Immunity. 2009; 1(1):4-17.

Vårum KM, Myhr MM, Hjerde RJN, and Smidsrød O. In vitro degradation rates of partially N-acetylated chitosans in human serum. Carbohydrate Research. 1997; 299(1–2):99-101.

Vårum KM, Ottøy MH, and Smidsrød O. Acid hydrolysis of chitosans. Carbohydr Polym. 2001; 46(1):89-98.

Verheul RJ, Amidi M, van der Wal S, van Riet E, Jiskoot W, and Hennink WE. Synthesis, characterization and in vitro biological properties of O-methyl free N,N,N-trimethylated chitosan. Biomaterials. 2008; 29(27):3642-3649.

Verheul RJ, Amidi M, van Steenbergen MJ, van Riet E, Jiskoot W, and Hennink WE. Influence of the degree of acetylation on the enzymatic degradation and in vitro biological properties of trimethylated chitosans. Biomaterials. 2009; 30(18):3129-3135.

Vllasaliu D, Exposito-Harris R, Heras A, Casettari L, Garnett M, Illum L, and Stolnik S. Tight junction modulation by chitosan nanoparticles: Comparison with chitosan solution. International Journal of Pharmaceutics. 2010; 400(1–2):183-193.

Walters DV. Lung Lining Liquid – The Hidden Depths. Neonatology. 2002; 81(Suppl. 1):2-5.

Wan H, Winton H, Soeller C, Stewart G, Thompson P, Gruenert D, Cannell M, Garrod D, and Robinson C. Tight junction properties of the immortalized human bronchial epithelial cell lines Calu-3 and 16HBE14o. European Respiratory Journal. 2000; 15(6):1058-1068.

Watson CJ, Rowland M, and Warhurst G. Functional modeling of tight junctions in intestinal cell monolayers using polyethylene glycol oligomers. American Journal of Physiology-Cell Physiology. 2001; 281(2):C388-C397.

Wedmore I, McManus JG, Pusateri AE, and Holcomb JB. A special report on the chitosan-based hemostatic dressing: Experience in current combat operations. J Trauma. 2006; 60(3):655-658.

Weibel ER. Morphometry of the human lung: Academic Press; 1963.

Whitehead K, Karr N, and Mitragotri S. Safe and Effective Permeation Enhancers for Oral Drug Delivery. Pharm Res. 2008; 25(8):1782-1788.

Wuts PGW, and Greene TW. Protection for the Hydroxyl Group, Including 1,2- and 1,3-Diols. Greene's Protective Groups in Organic Synthesis. 4 ed. New Jersey: John Wiley & Sons, Inc.; 2007. p. 189-198.

Yamaya M, Finkbeiner WE, Chun SY, and Widdicombe JH. Differentiated structure and function of cultures from human tracheal epithelium. American Journal of Physiology - Lung Cellular and Molecular Physiology. 1992; 262(6):L713-L724.

Yeh T-H, Hsu L-W, Tseng MT, Lee P-L, Sonjae K, Ho Y-C, and Sung H-W. Mechanism and consequence of chitosan-mediated reversible epithelial tight junction opening. Biomaterials. 2011; 32(26):6164-6173.

Yu ASL, Enck AH, Lencer WI, and Schneeberger EE. Claudin-8 expression in Madin-Darby canine kidney cells augments the paracellular barrier to cation permeation. Journal of Biological Chemistry. 2003; 278(19):17350-17359.

Yu SY, Zhao Y, Wu FL, Zhang X, Lu WL, Zhang H, and Zhang Q. Nasal insulin delivery in the chitosan solution: in vitro and in vivo studies. Int J Pharm. 2004; 281(1-2):11-23.

Zabner J, Karp P, Seiler M, Phillips SL, Mitchell CJ, Saavedra M, Welsh M, and Klingelhutz AJ. Development of cystic fibrosis and noncystic fibrosis airway cell lines. American Journal of Physiology - Lung Cellular and Molecular Physiology. 2003; 284(5):L844-L854.

Zambito Y, Fogli S, Zaino C, Stefanelli F, Breschi MC, and Di Colo G. Synthesis, characterization and evaluation of thiolated quaternary ammonium-chitosan conjugates for enhanced intestinal drug permeation. Eur J Pharm Sci. 2009; 38(2):112-120.

Zheng Y, Cai Z, Song X, Yu B, Bi Y, Chen Q, Zhao D, Xu J, and Hou S. Receptor mediated gene delivery by folate conjugated N-trimethyl chitosan in vitro. Int J Pharm. 2009; 382(1–2):262-269.

Zhu J, Rogers AV, Burke-Gaffney A, Hellewell Pg, and Jeffery Pk. Cytokine-induced airway epithelial ICAM-1 upregulation: quantification by high-resolution scanning and transmission electron microscopy. European Respiratory Journal. 1999; 13(6):1318-1328.